European Commission

JRC TECHNICAL REPORT

EU harmonised protocols for testing of low temperature water electrolysers

G. Tsotridis, A. Pilenga

2021

Joint Research Centre

EUR 30752 EN

Contact information
Name: Alberto PILENGA
Address: European Commission, Joint Research Centre (JRC),
Westerduinweg, 3 1755 LE Petten, The Netherlands
Email: alberto.pilenga@ec.europa.eu
Tel.: +31 (0)224 565067

EU Science Hub
https://ec.europa.eu/jrc

JRC122565

EUR 30752 EN

PDF	ISBN 978-92-76-39266-8	ISSN 1831-9424	doi:10.2760/58880
Print	ISBN 978-92-76-39265-1	ISSN 1018-5593	doi:10.2760/502481

Luxembourg: Publications Office of the European Union, 2021

How to cite this report: Tsotridis, G. and Pilenga, A., *EU harmonised protocols for testing of low temperature water electrolysers*, EUR 30752 EN, Publications Office of the European Union, Luxembourg, 2021, ISBN 978-92-76-39266-8, doi:10.2760/58880, JRC122565.

CONTENTS

Acknowledgements

The protocols presented in this report are the result of a collaborative effort between industry partners and research organisations participating in a number of Fuel Cell and Hydrogen Joint Undertaking funded projects dealing with low-temperature electrolysis research and applications. In particular, we acknowledge the permission to use materials from deliverables of the projects ElectroHyPem (GA No. 300081) and QualyGridS (GA No. 735485).

We are very grateful to L. Abadía, S. A. Ansar, A. Aricò, Siu Fai Au, R. Backhouse, B. Bensmann, C. Bernäcker, J. Brauns, A. Gago, E. N. Gallego, D. Greenhalgh, C. Haegele, C. Harms, V. Gil Hernandez, C. Lamy, F. Marchal, P. Millet, R. Pérez, I. Radev, R.H. Rauschenbach, F. Razmjooei, P. Redon, R. Reißner, S. Stypka, M. Suermann, K. Therkildsen, I.G. Torregrosa, T. Turek, N. Valckx, P. Wagner, L. Wang, E. Wolf for their feedback on the previous versions of this document.

The authors would like to express their sincere gratitude to all participants and their respective organisations for their contributions in developing the harmonised testing protocols in this report (cited in organization's alphabetical order in the list below).

They would also like to thank the Fuel Cell and Hydrogen Joint Undertaking Programme Office for the continuous support and encouragement received throughout the different stages of this activity.

The authors would like to thank our colleagues at the Directorate for Energy, Transport and Climate of the Joint Research Centre for their continuous support throughout the different stages of this effort.

Last but not least we would like to acknowledge Marc Steen for his prolific contribution for the revision of the document.

List of contributors

Name	Organisation
Nick Valckx	Agfa-Gevaert NV
David Frimat	AirLiquide
Jessie Ponce	AirLiquide
Laurent Ferenczi	AirLiquide
Louis Sentis	AirLiquide
Nicolas Richet	AirLiquide
Esther Albertin	Aragon Hydrogen Foundation
Laura Abadia	Aragon Hydrogen Foundation
Pablo Marcuello Fernández	Aragon Hydrogen Foundation

Rodrigo Pérez	Aragon Hydrogen Foundation
Vanesa Gil Hernandez	Aragon Hydrogen Foundation
Fabien Auprêtre	AREVA H2Gen, Les Ulis
Frederic Fouda-Onana	CEA, Grenoble
Patrick Redon	Chemours company
Siu Fai Au	China Southern Power Grid
Aricò Antonino Salvatore	CNR-ITAE, Messina
Alexander Dyck	DLR, Oldenburg
Aldo Saul Gago Rodriguez	DLR, Stuttgart
Fatemeh Razmjooei	DLR, Stuttgart
Indro Biswas	DLR, Stuttgart
Li Wang	DLR, Stuttgart
Peter Wagner	DLR, Stuttgart
Regine Reißner	DLR, Stuttgart
Syed Asif Ansar	DLR, Stuttgard
Aziz Nechache	Engie
Pierre Olivier	Engie lab crigen - Hydrogen Lab
Madeleine Odgaard	EWII Fuel Cells A/S
Marcello Carmo	Forschungszentrum Jülich GmbH
Christian Immanuel Bernäcker	Fraunhofer IFAM, Dresden
Dominik Härle	Fraunhofer IMWS, Halle (Saale)
Tom Smolinka	Fraunhofer ISE, Freiburg
Bernd Bauer	FUMATECH BWT GmbH, Bietigheim-Bissingen
Tomas Klicpera	FUMATECH BWT GmbH, Bietigheim-Bissingen
Kasper Therkildsen	Green Hydrogen systems A/S
Africa Castro	H2B2 Electrolysis Technologies, S.L., Sevilla

Christian Haegele	Hitachi Zosen Inova ETOGAS GmbH
Denis Thomas	Hydrogenics Europe
Wouter Schutyser	Hydrogenics Europe
Michel Suermann	IfES-EES, Leibniz University Hannover (LUH)
Boris Bensmann	IfES, Leibniz Universität Hannover, Hannover
Richard Hanke-Rauschenbach	IfES, Leibniz Universität Hannover, Hannover
Manuel Romero	IMDEA
Franco Nodari	Industrie Haute Technologie S. A., Monthey
Andre Weber	Institut für Angewandte Materialien – Werkstoff der Elektrotechnik (IAM-WET), KIT, Karlsruhe
Stelios G. Neophytides	Institute of Chemical Engineering Sciences (ICE-HT), Forth, Patras
Laila Grahl-Madsen	IRD Fuel Cells A/S
Daniel Greenhalgh	ITM Power plc
Frederic A. L. Marchal	ITM Power plc
Marcus Newborough	ITM Power plc
Rachel Backhouse	ITM Power plc
Emilio Nieto Gallego	National Center for Hydrogen Technology Experiment and Fuel Cells (CNH2)
Marius Bornstein	NEL
Anders Søreng	NEL, Notodden
Corinna Harms	NEXT ENERGY
Graham Smith	NPL, Middlesex UK
Bruno G. Pollet	Norwegian University of Science and Technology (NTNU)
Graham Smith	NPL, Middlesex UK
Paolo Marocco	Politecnico Torino / Sintef
Nick van Dijk	PV3 Technologies, Launceston

Richard R. W. Wagner	Siemens
Erik Wolf	Siemens Gas and Power GmbH & Co. KG
Alejandro Oyarce Barnett'	Sintef Industry, Oslo
Magnus Skinlo Thomassen	Sintef Industry, Oslo
Jörn Brauns	Technische Universität Clausthal
Thomas Turek	Technische Universität Clausthal
Arend De Groot	TNO (ECN)
A. Paige Shirvanian	TNO (ECN)
Ivan Garcia Torregrosa	TNO (ECN)
Claude Lamy	Université de Montpellier
Deborah Jones	Université de Montpellier
Pierre Millet	Université Paris-Sud
Ivan Radev	ZBT GmbH, Duisburg
Sebastian Stypka	ZBT GmbH, Duisburg
Ludwig Jörissen	ZSW, Ulm

Abstract

This report is the outcome of a combined effort of experts active in water electrolysis related projects coordinated by FCH2JU. It considers all three technologies of low temperature water electrolysis: proton (PEMWE), anion exchange membrane (AEMWE) and alkaline water electrolysers (AWE). It consists of a set of harmonised operating conditions, testing protocols and procedures for assessing both performance and durability of low temperature water electrolysis devices at every level of aggregation, from materials to stacks, up to grid-coupled systems. For the operating conditions, a number of agreed reference settings are presented, covering a.o. temperature, pressure, gas flow rate and gas composition. System boundaries are defined for these conditions, within which the electrolyser cell or stack is expected to operate. The report also presents an approach for assessing the effect on electrolyser performance and degradation of the exposure to more challenging conditions, known as "stressor conditions". The grid balancing harmonised testing profiles are the result of the QualyGridS project N.735485.

Executive summary

The policy frame

Green hydrogen is expected to play a critical role in the transition to a future low carbon energy system characterised by high shares of variable renewables. Hydrogen has the potential to decarbonise those sectors that cannot be easily electrified, such as heavy transport and a range of industrial processes. Green hydrogen may also play a role in energy storage, contributing to ensuring availability and/or flexibility to energy services independently from external factors (weather, time or season, consumer behaviour, etc.). The critical component for any green hydrogen value chain is water electrolysis for the production of hydrogen from water by using renewable electricity sources.

The needs

There is an acknowledged need for objective assessment of the performance and durability of electrolysers under conditions representative of current and future applications. Such assessment should be based upon performance tests mimicking the conditions encountered in real life as closely as possible. For a successful adoption of these tests among research centres and industry, it is critical that they are jointly developed and agreed by all stakeholders. This implies reaching consensus on operating conditions, on testing protocols and procedures, as well as on load profiles: this is particularly challenging when simulating dynamic operating conditions for electrolysers connected to intermittent power sources such as wind or solar for off-grid applications, or subject to partial load operation for electricity grid balancing.

Moreover, the way how testing results are reported should be harmonised, to allow for their direct and unambiguous comparison and interpretation. To facilitate this task, the Fuel Cells and Hydrogen Joint Undertaking (FCH 2 JU) has developed and maintains the results database TRUST (Technology Reporting Using Structured Templates), where projects are required to report progress according to a common repository structure. The TRUST database consists of 'template questionnaires' dedicated to the various technologies and their technology readiness level [1]. Each questionnaire is divided into descriptive parameters and quantitative performance data, which, for low-temperature electrolysers, are the scope of this report.

The goals

The availability and the adoption of tests performed to agreed specifications contributes to the following goals:

- improving the repeatability and reproducibility of the generated test results, thereby enhancing their comparability,
- enhancing the representativeness of laboratory test results in simulating real-world conditions and applications,
- achieving coherency of data originating from different projects, and enabling a measurement of the progress towards meeting targets,
- assessing Key Performance Indicators (KPIs) for low temperature electrolysers and proposing improved or new indicators for their performance and durability.

The objective of the report *(Why was the work undertaken?)*

To address the needs identified above, the FCH 2 JU has set up a Working Group on Low Temperature Electrolysers Testing Harmonisation (LTWE), composed of European stakeholders from research and industry, including raw material suppliers, Original Equipment Manufacturers, (OEMs), electrolysis cell material manufacturers and various establishments active in Electrolysis Research & Development. The activities of the LTWE Working Group have been coordinated by the Joint Research Centre (JRC) of the European Commission and have profited of the results of several FCH 2 JU projects.

The objective of this group is not to replace currently existing testing practices used in various industries and research establishments, but rather to propose commonly agreed, '*harmonised*' testing protocols and procedures. This will enable an objective comparison between different projects and products and an evaluation of the progress achieved towards agreed technology performance targets.

The LTWE work followed a previous harmonisation effort on testing of low temperature PEM fuel cells [1] and used the harmonised terminology available in [2]. Three reports dedicated to specific harmonised test methods for electrolysers were already published in 2018: one on polarisation curves [7], one on cyclic voltammetry (CV) [8] and one on electrochemical impedance spectroscopy (EIS) [9].

1 Introduction

1.1 Background and purpose

There is an acknowledged need for objective comparative assessment of the behaviour of electrolyser components and devices under conditions foreseen in future applications. For such assessment to be reliable and trustworthy, a number of requirements have to be met.

First, the assessment should be based on tests according to specifications agreed by a broad range of stakeholders, covering both performance and durability aspects. Testing according to these agreed specifications will contribute to improving the repeatability and reproducibility of the generated test results, thereby enhancing their comparability.

Second, agreement on the operating conditions imposed during testing for assessing performance and durability under representative application conditions is required. This applies in particular for simulation of the dynamic operating conditions for electrolysers connected to fluctuating power sources such as wind or solar for off-grid applications, or subject to partial load operation for electricity grid balancing, or for supplying hydrogen to the gas grid or directly for power-to-gas applications, see Figure 1. This also requires agreement on the definition of appropriate electrolyser system boundaries.

Meeting the above set of requirements will improve the consistency between test results originating from different sources and enhance the representativeness of laboratory test results in simulating real-world applications.

Figure 1. Electrolyser system grid integration

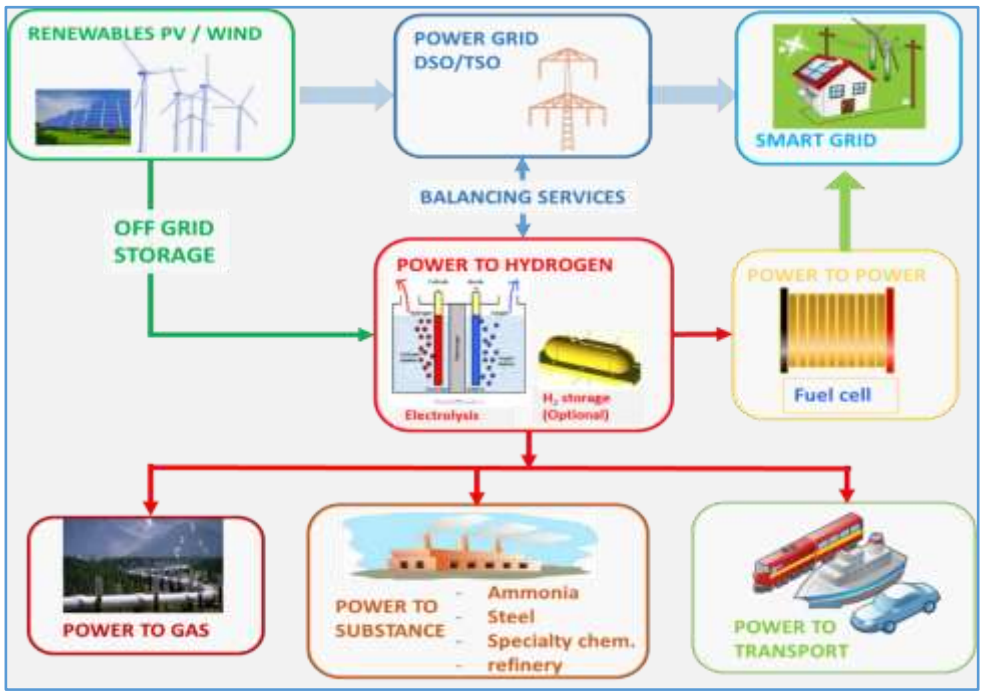

Source: JRC, 2020

This report addresses the above needs by presenting an agreed set of operating conditions and testing protocols for assessing both performance and durability of low temperature water electrolysers. It also suggests ways of graphically presenting the test results from

performance and durability testing, comparing them to the results obtained under the reference operating conditions ([1]). It does not intend to replace testing practices currently used in various industries and research establishments.

In addition to their primary use for enabling comparison, the results of the "harmonised" performance and durability tests presented in this report are expected to assist FCH2JU through enhanced coherency of data originating from various FCH2JU funded projects. The results obtained from harmonised tests can serve in assessing Key Performance Indicators (KPIs) for low temperature electrolysers and for proposing improved and/or new indicators for their performance and durability.

1.2 Content

The report first presents a set of protocols for determining the functional properties of materials used in electrolyser components. Additionally, it specifies testing conditions and protocols for assessing and evaluating performance of electrolyser cells/short stacks at the Beginning of Life (BoL) or Test (BoT) ([2]). It also describes loading profiles and protocols for durability assessment through intermittent performance evaluation before reaching the End of Life (EoL) or Test (EoT). This is followed by a description of accelerated testing at cell/short stack level to assess the capability of cell materials and components to withstand service loads and for evaluating the effect of improving materials and/or components on performance and durability. The report concludes by describing system-level testing as defined by the QualyGridS project in its project deliverables 2.4 and 2.5.

1.3 Methodology

The methodology adopted in this document reflects the successive stages in the efforts aimed at improving performance and durability of electrolysers in a number of applications. The development sequence usually consists of four distinct steps, namely: Development of Materials, of Single Cells and short stacks and of Systems as depicted in the following figure.

([1]) The graphical representation of test results is complementary to the mandatory reporting in TRUST

([2]) Throughout this report the terms Beginning of Test (BoT) and End of Test (EoT) refer to laboratory practices, i.e. Single Cell and Short Stack Testing, whereas Beginning of Life (BoL) and End of Life (EoL) refer to System Testing.

Figure 2. Schematic of the process chain for electrolyser development

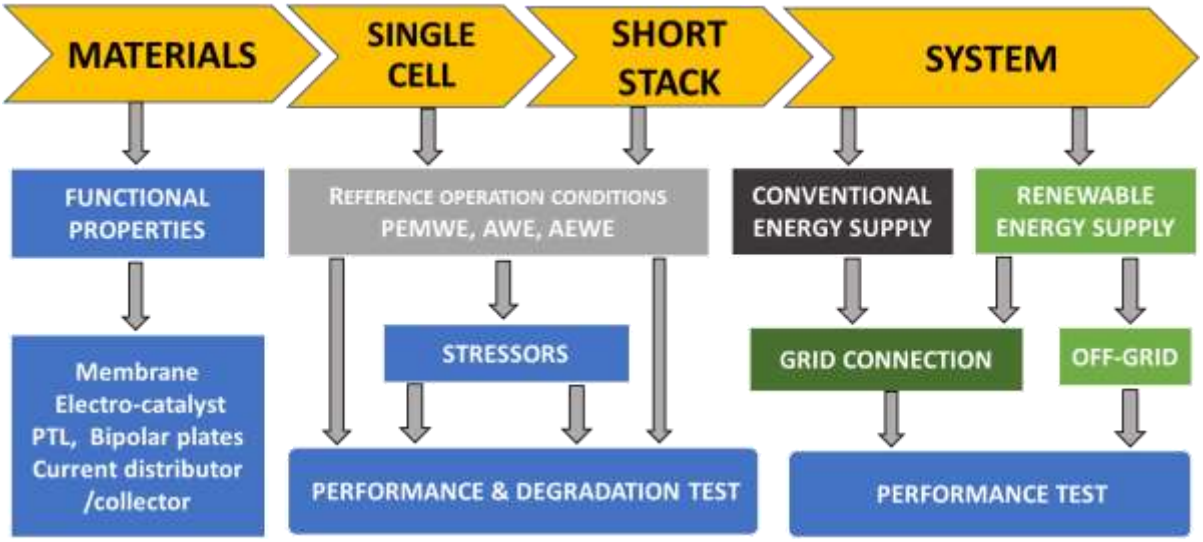

Source: JRC, 2020

The development of materials entails R&D for a range of components such as membranes and catalysts, using innovative methods, processes and manufacturing techniques. Once these new materials and components have been developed, they are "screened" *ex-situ* for their potential use as candidate materials for water electrolysis. When the *ex-situ* results meet the expectations, the materials are subsequently used for preparation of components such as Catalyst Coated Membranes (CCMs, when the catalyst layer is coated onto the membranes) or in Membrane Electrode Assemblies (MEAs, when the catalyst layer is coated on a Porous Transport Layer, PTL ([3])), bipolar plates, diaphragms, etc. These components are subsequently tested *in-situ,* in single cell configuration. Single cells with successful *in-situ* performance are considered as candidates for direct use or after scaling up to the required electrode geometric area for inclusion in short stacks and then the stacks are integrated with appropriate Balance of Plants (BoPs) to systems level.

This report is the result of a joint effort by several mainly European interested parties, including Original Equipment Manufacturers, (OEMs), electrolysis cell material manufacturers and various research establishments active in Electrolysis Research & Development who, on a voluntary basis, agreed on a set of operating conditions and testing protocols for characterization of Low Temperature Water Electrolysers at Single Cell, Stack and System levels.

([3]) The term MEA may also include CCMs with integrated anode and cathode PTLs

2 Overview of low-temperature water electrolysis technologies

2.1 Underlying electrochemistry

In low-temperature water electrolysis, two main parameters dictate technology differences, namely:

(i) the operating conditions: temperature and pressure (Figure 3a)

(ii) the ion conduction mechanism for the electrode separator and the pH of the electrolyte at the hydrogen evolution reaction (HER) and oxygen evolution reaction (OER) sites (Figure 3b).

2.1.1 Operating temperature

As shown in Figure 3a, electrolytic water dissociation is endothermic, i.e. it requires heat input in addition to electricity over the zero to 1,000 °C temperature range. The step change in the required amount of heat and hence in the total energy need (electricity + heat) at 100 °C is due to the water phase transition from liquid to gas. The heat required ($T \cdot \Delta S$) linearly increases with temperature T because the entropy change ΔS is assumed constant. Consequently, the Gibbs free energy change (ΔG) or electricity input required decreases with temperature, whereas the total energy need corresponding to the enthalpy change $\Delta H = \Delta G + T \cdot \Delta S$ only weakly depends upon temperature both below and above 100 °C.

According to Faraday's law, the change in Gibbs free energy for an electrochemical system in equilibrium is expressed as:

$$\Delta G = z\, F\, U_{rev}$$

with Faraday constant F = 96,485.33 C.mol^{-1} (coulomb.mole^{-1}) and z the number of electrons involved in the electrochemical reaction. U_{rev} represents the reversible cell voltage, which is the minimum voltage needed to drive the reaction. For water electrolysis, U_{rev} is the minimum voltage needed for water splitting. At lower cell voltage water electrolysis is not possible, whereas at higher cell voltage electrolysis is possible and heat is consumed in the reaction. Isothermal cell operation (i.e. reactant and reaction products at the same temperature) hence requires additional heat input from the environment.

However, cell operation generates heat by the irreversible processes associated to the electrochemical reactions (overvoltages) and by internal resistance as electric and ionic currents flow through the cell (ohmic resistance leading to Joule heating). This internally generated heat reduces the amount of heat to be supplied from the environment to the cell for maintaining thermal equilibrium. With increasing cell voltage, the internal heat generation by the Joule effect increases and at the thermoneutral voltage the internally generated heat equals the amount of heat $T \cdot \Delta S$ required for maintaining the reaction in thermal equilibrium. According to the above, the thermoneutral cell voltage U_{tn} given by:

$$\Delta H = z\, F\, U_{tn}$$

is the voltage required for electrolysis without withdrawing heat from the surroundings. In this case, ΔH represents the amount of *electric* energy required for electrolysis in the absence of external heat supply.

When the cell is operated at higher voltage than U_{tn}, the reaction becomes exothermic and heat needs to be removed for maintaining thermal equilibrium. In practice excess heat is generated because electrolysers are operated above the thermoneutral voltage to overcome losses incurred by inefficiencies of the electrochemical reactions and by electrical and ionic resistance as the current flows through the cell.

Because of the phase transition of water upon heating, two different regimes need to be considered for electrolysis of liquid water and for electrolysis of water in the gas phase (water vapour), respectively.

1) Liquid water electrolysis

When water is supplied to the electrolyser in the liquid phase, as applies for low-temperature electrolysis, the hydrogen production reaction reads:

$$\mathbf{2\ H_2O_{(l)} + \Delta G_{H2O(l)} + T\Delta S \rightarrow 2\ H_{2(g)} + O_{2(g)}} \quad \text{[Eq. 2.1]}$$

The reaction enthalpy is $\Delta H_{H2O(l)} = \Delta G_{H2O(l)} + T\Delta S = 237.16\ kJ.mol^{-1} + 48.68\ kJ.mol^{-1} = 285.84\ kJ.mol^{-1}$. The energy content of the produced hydrogen corresponds to the higher heating value of hydrogen (HHV).

The indicated values for ΔG, $T\Delta S$ and ΔH apply for a perfect cell operating in a thermodynamically reversible manner at standard conditions of temperature (25 °C) and pressure (1 bar). Under these conditions (z = 2 for hydrogen):

$$U_{rev,\ HHV} = \Delta G_{H2O(l)} / (z \cdot F) = \mathbf{1.229\ V} \quad \text{[Eq. 2.2]}$$

$$U_{tn,\ HHV} = \Delta H_{H2O(l)} / (z \cdot F) = \mathbf{1.481\ V} \quad \text{[Eq. 2.3]}$$

2) Water vapour electrolysis

When water is supplied to the electrolyser in the gas phase, the heat energy needed for water vaporization does not need to be provided and the reaction reads:

$$\mathbf{2\ H_2O_{(g)} + \Delta G_{H2O(g)} + T\Delta S \rightarrow 2\ H_{2(g)} + O_{2(g)}} \quad \text{[Eq. 2.4]}$$

In this case, the reaction enthalpy is $\Delta H_{H2O(g)} = \Delta G_{H2O(g)} + T\Delta S = 228.60\ kJ.mol^{-1} + 13.23\ kJ.mol^{-1} = 241.83\ kJ.mol^{-1}$ and the energy content of the produced hydrogen corresponds to its lower heating value (LHV). The difference between HHV and LHV originates from the latent heat of water evaporation. The thermoneutral and reversible cell voltages for water vapour electrolysis are:

$$U_{rev,\ LHV} = \Delta G_{H2O(g)} / (z \cdot F) = \mathbf{1.185\ V} \quad \text{[Eq. 2.5]}$$

$$U_{tn,\ LHV} = \Delta H_{H2O(g)} / (z \cdot F) = \mathbf{1.253\ V} \quad \text{[Eq. 2.6]}$$

For electrolysers operating at temperatures above the 100 °C boiling point of water, the use of LHV rather than HHV is relevant for the produced hydrogen.

3) Pressure and temperature effects on cell voltage

The effect of pressure arises from the change in Gibbs free energy [28]. Assuming dry and ideal gases are produced, the variation of the cell voltage, ΔU_{cell}, from the one at reference pressure, $U_{rev}(T,p^{\theta})$, as a function of pressure p (expressed in bar) is expressed by the equation:

$$\Delta U_{cell} = U_{rev}(T,p,I=0) - U_{rev}(T,p^{\theta}) = \frac{RT}{2F} ln\left[\left(\frac{p_{O2}}{p^{\theta}}\right)^{\frac{1}{2}}\left(\frac{p_{H2}}{p^{\theta}}\right)/\left(\frac{p_{H2O}}{p^{\theta}}\right)\right] \quad \text{[Eq. 2.7]}$$

with p^{θ} the reference pressure at the working temperature T, p_i the partial pressures of O_2, H_2, H_2O respectively and $p = \sum p_i = p_{O_2} + p_{H_2} + p_{H_2O}$ is the total pressure in each cell compartment. For LTWE the term $\frac{p_{H2O}}{p^{\theta}}$ is equal to 1.

The overall expression to calculate the equilibrium cell voltage, $U_{cell,I=0}$, as a function of temperature and pressure in respect to the standard cell voltage U^0_{rev} is:

$$U_{cell} = U^0_{rev} + \frac{RT}{2F} ln\left[(p_{O2})^{\frac{1}{2}}(p_{H2})/(p_{H2O})\right] \quad \text{[Eq. 2.8]}$$

Since the produced gasses are saturated with water vapour the following expression shall be used to calculate ΔU_{cell}:

$$\Delta U_{cell} = \frac{RT}{2F} ln\left[\left(\frac{p^A - p^{sat}_{H2O}}{p^{\theta}}\right)^{\frac{1}{2}}\left(\frac{p^C - p^{sat}_{H2O}}{p^{\theta}}\right)/\left(\frac{p^{sat}_{H2O}}{p^{\theta}}\right)\right] \quad \text{[Eq. 2.9]}$$

Where p^A is the total pressure of anodic semi-cell given by Oxygen, Hydrogen, if present due to leak or cross-over and water vapour. The cathodic pressure p^C is equal to p^A for equi-pressure operation or the additional pressure quantity, Δp, shall be added for differential pressure operation. p^{sat}_{H2O} is the water saturation pressure at the operation temperature *T.*

2.1.2 Electrolyte pH

The values for U_{rev} and U_{tn} quoted in the previous section apply for water electrolysis. Because of its low electric conductivity, electrolysis of pure water proceeds very slowly. By adding a water-soluble electrolyte, the ionic conductivity of water rises considerably. The Pourbaix-diagram in Figure 3b shows that by increasing the pH of the electrolyte, the half cell (H^+ aq / hydrogen and oxygen / water) redox potentials shift downwards to a potential range where conventional metals are usually passivated. This explains why water electrolysers have traditionally been using an alkaline aqueous solution as electrolyte. This has changed recently with the progress in acidic membrane water electrolysis technology in terms of production rate, gas purity and direct pressurised operations, while new research activities on alkaline membranes have started more recently. These three types of electrolyte lie at the basis of the three low-temperature electrolysis technologies included in this report, namely AWE, PEMWE and AEMWE respectively.

Figure 3. Water splitting characteristics

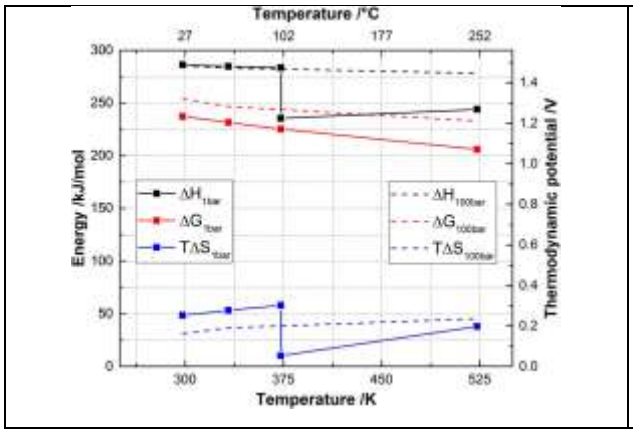

Figure 3a. The energy required to split water over a range of temperatures at 1 bar and at 100 bar.

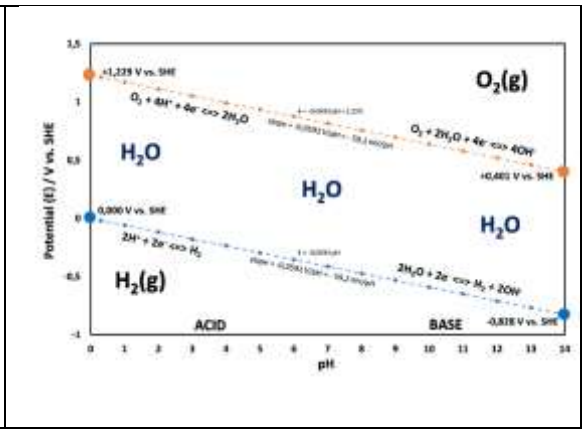

Figure 3b: Water electrolysis electrode potentials (E) variation with pH at standard conditions.(SHE: Standard Hydrogen Electrode potential)

 https://doi.org/10.1149/2.1441704jes

Source: B.G.Pollet, 2021

2.2 Low-temperature electrolysis technologies

Three different low temperature electrolysis technologies are currently available as commercial products or under development, namely Proton Exchange Membrane (PEM) that uses an acidic polymer membrane sheet as solid electrolyte, Alkaline Water Electrolysis (AWE) that uses a liquid electrolyte (usually an aqueous solution of an alkaline product, e.g. potassium hydroxide, KOH) and a diaphragm as separator, and more recently Anion Exchange Membrane (AEM) that uses a hydroxyl-ion conducting polymer membrane sheet as solid electrolyte. Relevant state-of-the-art data for these three technologies are summarized in Table 1.

A brief description of these low temperature liquid water electrolysis technologies is given in the sections below. Note that high temperature electrolysis (700–1,000 °C), such as Solid Oxide Water Electrolysis, is not considered in this report.

Table 1. State-of-the-art low temperature water electrolysis technologies

ELECTROLYSIS TYPE	PEMWE Proton Exchange Membrane	AWE Alkaline	AEMWE Anion Exchange Membrane
Charge carrier (1)	H^+	OH^-	OH^-
Reactant	Liquid Water	Liquid Water	Liquid Water
Electrolyte	Proton exchange membrane	NaOH or KOH 20-40 wt.% / water	Anion exchange membrane
Anode Electrode	IrO_2 IrO_2/Ti_4O_7 $Ir_xRu_yTa_zO_2$, Ir black	Co_3O_4, Fe, Co, Mn Mo, P, S, $NiFe(OH)_2$, Fe(Ni)OOH, oxides, hydroxides, borides, nitrides, carbide-based catalysts	IrO_x $Pb_2Ru_2O_{6.5}$, $Bi_{2.4}Ru_{1.6}O_7$, NiO_x, Ni-Fe, $Li_xCo_{3-x}O_4$, $Cu_{0.6}Mn_{0.3}Co_{0.21}O_4$, $CuCoO_x$
Cathode electrode	Pt/C	Raney®-Ni, Co, Cu, NiCu, NiCuCo, Ni-Co-W, Ni-Cu-Zn-B, Ni-Co, Ni-Fe, Ni-Co-Mo, NiCoZn, Raney®-Co, Ni-Mo, Ni-S, Ni-rare earth alloys	Raney®-Ni, NiO, Co based catalyst $Ni/(CeO_2\text{-}La_2O_3)/C$ Pt/C
Current density	0.2-8.0 A/cm^2	0.2-2.5 A/cm^2	0.2-0.8 A/cm^2
OperatingTemperature	20-80 °C (2)	40-90 °C	40-60 °C
Pressure H_2 out (3)	(10 –30)·10^5 Pa	(10 –30)·10^5 Pa	(10 –30)·10^5 Pa
Cathode reaction (H_2 evolution reaction HER) (4)	$4H^+(aq) + 4e^- \rightarrow 2H_2(g)$	$4H_2O(l) + 4e^- \rightarrow 2H_2(g) + OH^-(l)$	$4H_2O(l) + 4e^- \rightarrow H_2(g) + 4OH^-(aq)$
Anode reaction (O_2 evolution reaction OER)	$2H_2O(l) \rightarrow O_2(g) + 4H^+(aq) + 4e^-$	$4\ OH^-(aq) \rightarrow 2H_2O(l) + O_2(g) + 4e^-$	$4\ OH^-(aq) \rightarrow 2\ H_2O(l) + O_2(g) + 4e^-$

Source: JRC, 2020

(1) Conventional water ions notation is used
(2) Research efforts are targeting temperatures up to 150°C and 200°C with water vapour
(3) Higher hydrogen output pressure reduces the compression needs for storage or transport of hydrogen
(4) (aq), (l) & (g) refers to aqueous, liquid and gaseous state

The R&I activities are continuously improving the electrolyser's performances, therefore better data can be found in the latest research papers([4]).

([4]) For example, for PEMWE, the current density has been reported up to 20 A.cm-2 [18], or the outlet pressure up to 350 · 105 Pa [19]

2.3 Proton exchange membrane water electrolysis (PEMWE)

A PEM water electrolysis cell is a zero-gap cell, i.e. the electrodes are directly sandwiched or coated onto the membrane. Reaction gases (H_2 and O_2) are evolved at the rear of the catalytic layers, and not in the inter-polar gap. This compact design allows for high (in the several $A \cdot cm^{-2}$ range) current density operation. Figure 4 shows the cross-section of a PEM electrolysis cell. The elementary cell is delimited by two end plates usually made of titanium or of coated stainless steel - see Figure 5. The total cell thickness is typically 5-7 mm.

The central cell component is the proton conducting membrane {region 1} made of Perfluorosulfonic Acid (PFSA) or containing other chemical groups with similar behaviour, like for example hydrocarbon membranes which are a R&D topic. The membrane needs hydration to maintain conductivity, which limits the operating temperature, and is surface coated by two catalytic layers. Unsupported or carbon supported Pt nanoparticles are usually used at the cathode for the Hydrogen Evolution Reaction (HER) and supported or unsupported iridium dioxide (IrO_2) or alternative catalyst-based particles are used mostly at the anode for the Oxygen Evolution Reaction (OER) {regions 2 and 2', respectively}. Both catalytic layers are microscopically porous to allow gas evolution and contain a mixture of catalyst particles, support particles and ionomer which acts as a binder and provides a high ionic contact with the membrane. The electrochemical reactions take place at the three-phase boundary: ionic conductor (electrolyte), electric conductor (catalyst) and reactant.

The two catalytic layers are directly sprayed in form of ink on the membrane to form a so-called Catalyst Coated Membrane or CCM. The CCM is clamped between two Porous Transport Layers (PTL) {regions 4 and 4'} which are used for water distribution as well as for gas collection and removal. In some cases, the catalyst layer is coated directly on the PTLs and not on the membrane to form a catalyst coated electrode (CCE). CCM or CCE can be also referred as membrane electrode assembly (MEA). Whereas sintered titanium disks are usually used at the anode {region 3'}, carbonaceous PTLs are at the cathode {region 3}. PTLs can be subject to physicochemical degradation due to temperature gradients and hotspots, the presence of an acid environment [3], as well as to mechanical degradation caused by compression effects.

Cell spacers, meshes, grids can be placed between the end plates and porous transport layers. They offer an open space allowing water flux through the cell and gas removal from the cell. De-ionised liquid water is pumped through the anodic compartment to feed the electrolysis reaction and to remove heat (when the cell operates above the thermoneutral voltage). To assist in heat removal and maintaining temperature constant, in some cases water is also provided to the cathode compartment. The gaseous reaction products H_2 and O_2 need to be de-humidified and the captured water is recirculated to the water inlet.

During operation, protons migrate from the anode (where they are formed) through the membrane to the cathode (where they are reduced to hydrogen gas). During their migration, protons transport a number of water molecules from the anode to the cathode, a process known as electro-osmotic drag. The magnitude of this water flux depends upon the type of proton conducting polymer, temperature, pressure and electric current density used in the electrolysis process.

Figure 4. Cross section of a PEMWE cell

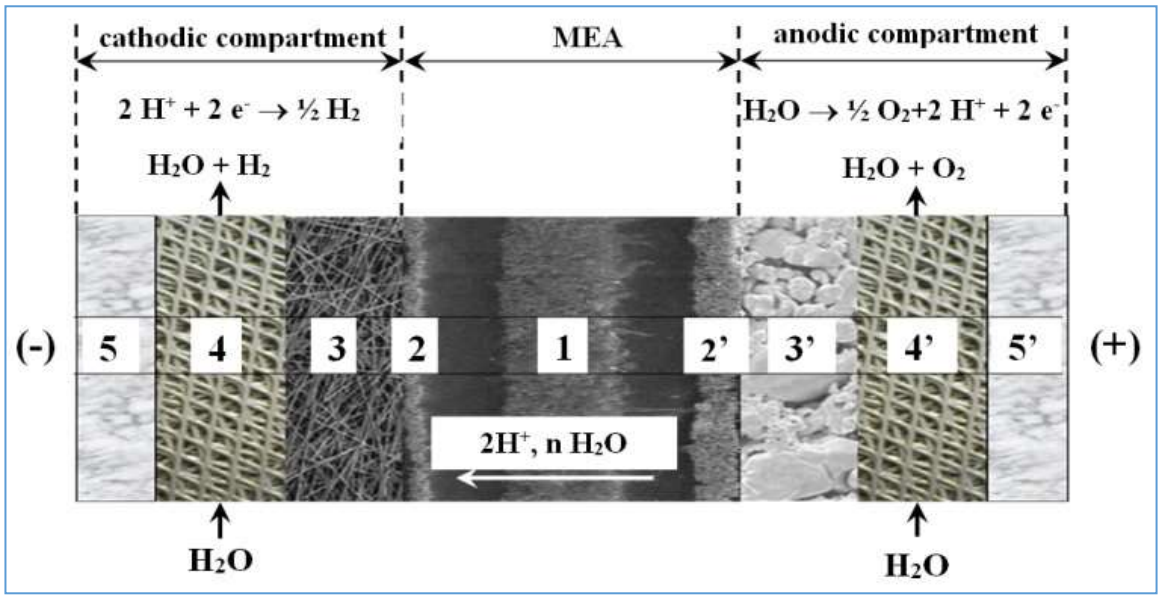

Source: [16]

Figure 5. Typical PEM water electrolysis cell components (highlights identify those components for which functional testing is discussed in this report)

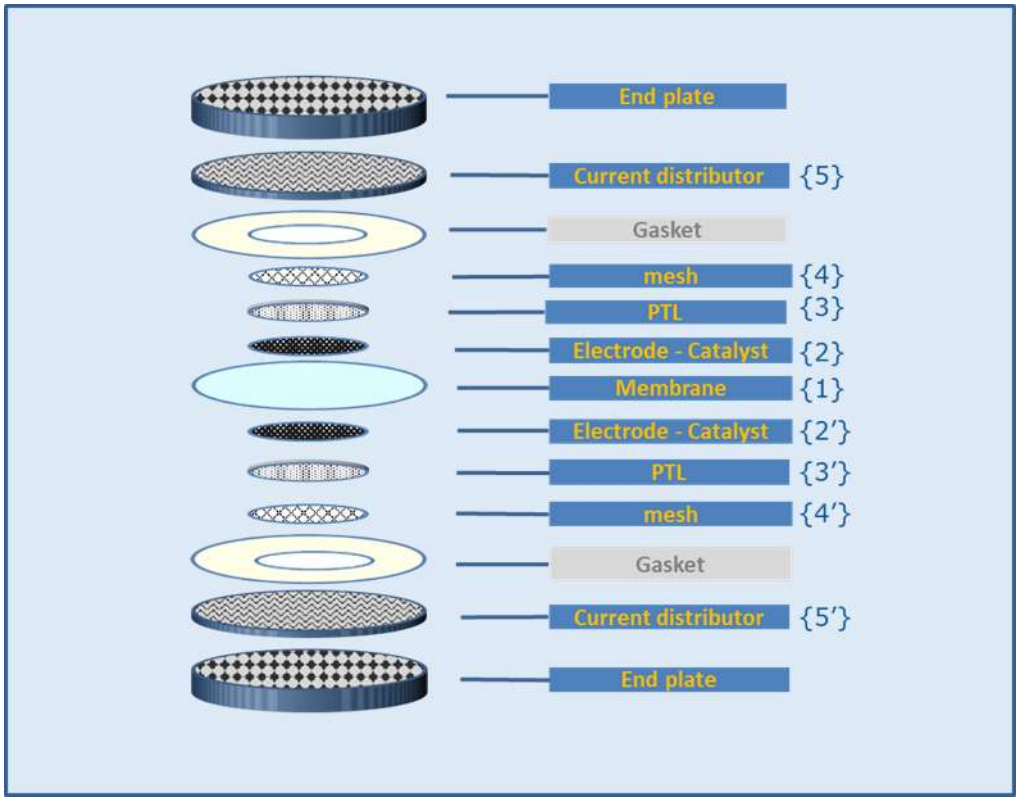

Source: JRC, 2020

To yield higher hydrogen production rates, several single cells, a set of components as shown in Figure 5, are connected electrically in series and hydraulically in parallel as a stack. A metallic plate separates two adjacent cells and simultaneously acts as anode of one cell and cathode of the adjacent cell, hence the term bipolar plate (BPP). Pressure plates fix the components of the cells and provide the clamping force by threaded bolts and nuts.

Industrial PEM electrolysers have a typical hydrogen discharge pressure of 10-30 bar. High pressure operation is possible in two modes: either with anode and cathode at the same pressure ("equibar"), or in differential mode with the hydrogen compartment at higher pressure. In the latter case, the balance of plant (BoP) of the oxygen compartment is simpler, but with the drawback of the additional stress on the MEA.

Compared to the main other low temperature electrolyser technology, alkaline electrolysis, a concentrated electrolytic solution is not required, and the advantages include high current density, smaller systems size and ease of gas separation in differential pressure operations mode. These advantages enable high performance and excellent load-following at a low safety risk. However, the acidic environment of PEM limits the materials of bipolar plates and current collectors, and in particular the catalysts, to expensive platinum-group metals (PGMs). Furthermore, durability related to catalyst loss and membrane lifetime is an issue.

Hydrogen and oxygen produced with this technique have a very low level of contaminants. In the hydrogen gas, the main other compounds are water that can be easily removed and oxygen due to gas crossover that also can easily be removed (e.g. with catalytic conversion). The final hydrogen purity can reach 99.99 %.

The power of PEM electrolysers ranges from a few kilowatts to several megawatts. The system power, for equal cell area and current density depends on the number of stacks contained in the system.

Water purification treatment at 1 MΩ·cm level, or above, is recommended to minimize negative impact of impurities on membrane and catalyst operation.

2.4 Alkaline water electrolysis (AWE)

Alkaline water electrolysis is a mature technology industrialised since the nineteenth century. In an alkaline water electrolyser (AWE), water molecules are decomposed electrochemically at the cathode to molecular hydrogen (H_2) and hydroxyl ions (OH^-); the latter diffuse through the alkaline electrolyte and a diaphragm (also called separator), and discharge at the anode releasing molecular oxygen (O_2).

The major components of an AWE single cell are the diaphragm and the two electrodes. The diaphragm has a microporous structure, allowing the alkaline electrolyte to seep through for sufficient ionic conductivity. The electrolyte is an aqueous solution containing either sodium hydroxide (NaOH) or potassium hydroxide (KOH). The latter is usually preferred for its higher OH- conductivity for the same molarities. The typical concentration of 20-40 wt.% corresponds to the highest conductivity; at higher concentrations the conductivity decreases due to Coulombic force interactions.

The electrolyte concentration can be expressed in wt.% or in molar unit [$mol.L^{-1}$] ≡ [M], In the Box 1 hereafter is presented a concentration table and formulas for their conversion for KOH electrolyte.

Box 1. KOH electrolyte concentration table and conversion formulas

KOH [M]	KOH [wt.%]
1	5,45
2	10,61
3	15,50
4	20,13
5	24,54
6	28,72
7	32,71
8	36,51
9	40,14
10	43,61
11	46,92
12	50,10

M - molar mass of KOH = 56.10564 $g.mol^{-1}$

ρ - density of dry KOH = 2.044 $g.cm^{-3}$

n - molarity of the KOH solution in water [M] ≡ $[mol \cdot L^{-1}]$

c - KOH concentration [wt.%]

m - mass of dry KOH for 1L KOH solution in water = M·n

$V_{KOH\ solution}$ = volume of KOH solution = M n / ρ

Formula for conversion from $mol.l^{-1}$ to wt.%:

$$c\ [wt.\%] = (M \cdot n) / (M \cdot n + (1000 - (M \cdot n / \rho)) \quad [Eq.\ 2.9]$$

Formula for conversion from wt.% to $mol.l^{-1}$:

$$M\ [mol.l^{-1}] = c\ (M \cdot n + (1000 - (M \cdot n / \rho)) / n \quad [Eq.\ 2.10]$$

Anode and cathode are separated into two compartments by the diaphragm. Two configurations exist: Figure 6a depicts the cross-section of a gap-cell, in which a void between electrodes and diaphragm is filled with electrolyte. Gases evolve on both sides of each electrode, especially in the inter-polar domain, resulting in ohmic losses. Figure 6b shows the cross-section of a zero-gap cell. Electrodes with latticed or porous structures (grids, meshes, fibre felts, porous sintered or foamed metals) are pressed against the central diaphragm. Gases evolve at the rear of both electrodes, leading to a reduction of ohmic losses caused by the gaps and gaseous films. The zero-gap design is widely used in modern alkaline water electrolysers. The thickness of commercial diaphragms (e.g. Zirfon®, Supor-200®), which is equal to the distance between two electrodes, is typically 0.5 mm for the former and 0.14 mm for the latter. Some manufacturers integrate the electrodes and the diaphragm into a single component to achieve a true zero gap. Recently launched advanced membranes based upon an open mesh polyphenylene sulphide fabric, which is symmetrically coated with a mixture of a polymer and zirconium oxide (Zirfon) show an efficiency improvement on the overall electrolysis process. The thinner membranes with thickness lower than 250 µm have demonstrated improvement on the overall process without losing the dynamic behaviour and gas purities level. Other types of low thickness membranes, less than 200 µm compared to 500 µm or more of diaphragms, e.g. PBI (poly(2,2-(m-phenylene)-5,5-bibenzimidazole) membranes, provide acceptable mechanical resistance and increased ionic conductivity.

The cathode catalyst typically is a Raney®-Ni catalyst coated on a porous substrate (mesh, foam) or perforated plate. The coated substrate is made of Nickel or stainless steel. Alternatives are Ni-Mo on a ZiO_2-TiO_2 support. The anode catalyst is usually made of pure Ni or Raney®-Ni (sometimes doped with transition metals), and other materials like Ni_2CoO_4, La-Sr-CoO_3 or Co_3O_4 are under evaluation. Current distributors are typically nickel

(the electrodes are directly pressed or welded onto the bipolar plates) with the main containment material being Ni-coated steel.

Alkaline electrolysers like PEM ones have a very wide range of rated power, from a few kilowatts (kW) to several megawatts (MW). The system power is a function on the number of stacks present in the system. Operation temperatures are within the range of 60-90 °C to ensure electrolyte conductivity and to promote reaction kinetics. Typical electrolysis pressure is in the range 10-30 bar. The current density is typically 200 to 400 $mA.cm^{-2}$. In the latest technology development, new diaphragm concepts and the use of membranes with lower ohmic resistance have resulted in current density increases up to 1.5 $A.cm^{-2}$ and even to 2.5 $A.cm^{-2}$. By improving the electrochemical active surface area of the electrode and by adjusting the stack geometry (zero-gap design) the corresponding cell voltage could also decrease below 2 V.

For AWE, water needs to be purified at ppm impurities level before use and the product gases must be dried before release. The purity level of hydrogen and oxygen can reach 99.9 and 99.7 vol. %, respectively, without auxiliary purification equipment.

Advantages of alkaline electrolysis are that it does not use expensive noble metal catalysts (e.g. PGM – Platinum Group Metals) and that it is stable over a long lifetime, often in excess of 100,000 hours. One disadvantage is that alkaline water electrolysers experience high ohmic losses across the diaphragm/separator and hence operate at relatively low current densities compared to PEM water electrolysers. Historically alkaline water electrolysis systems have been used in constant load mode. If operated under dynamic load, a limited power range can be applied. This occurs because separator materials are not very effective at preventing cross-diffusion of gases. Hydrogen crossing to the anode and oxygen crossing to the cathode lead to a lowering in efficiency (as they can be converted back to water) and to potential safety issues, particularly in low load scenarios. These challenges need to be overcome, and are currently object of some FCH2JU and other research projects, for the deployment of alkaline water electrolysers with renewable energy sources (RES) such as wind or solar PV.

Figure 6. Alkaline electrolysis cell

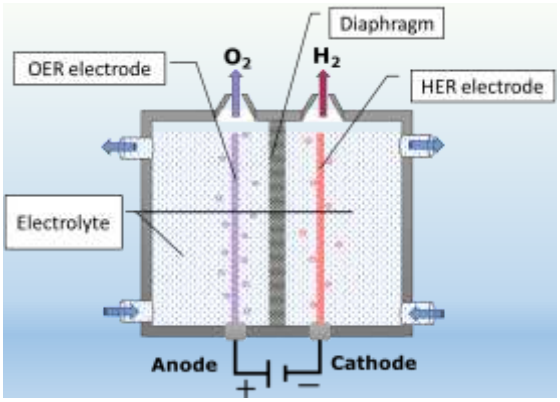

Figure 6a: Alkaline water electrolysis gap-cell.

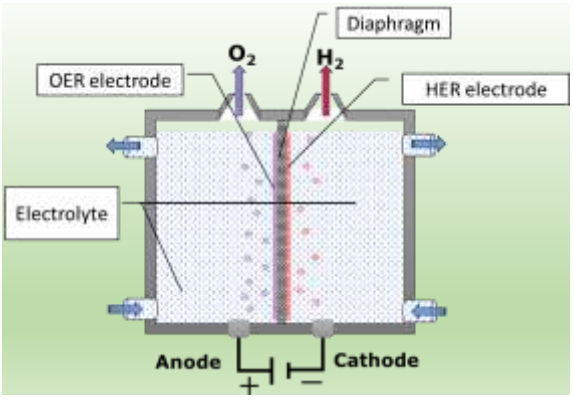

Figure 6b: Alkaline water electrolysis zero-gap-cell.

Source: JRC, 2020

2.5 Anion exchange membrane water electrolysis (AEMWE)

AEM (anion exchange membrane) water electrolysis is a technology still under development with the aim to use less noble and rare catalyst materials, and less expensive support materials thanks to the less corrosive conditions. The main difference with alkaline water electrolysis is the replacement of the diaphragm with a solid AEM, which allows the use of distilled water or of a low concentration alkaline solution as supporting electrolyte([5]), e.g. potassium carbonate (K_2CO_3), instead of concentrated KOH or NaOH. The membrane serves as solid electrolyte for conducting OH^- ions and as separator for hydrogen and oxygen gasses. Compared to PEM water electrolysis, switching the working condition from acidic to alkaline, relaxes the material restriction for the cell components. In particular, bipolar plates can be made from a cheaper material such as stainless steel, significantly reducing cost. In addition, alkaline conditions can enable the use of a lower amount of PGM catalyst, or even their substitution with PGM-free catalysts based upon lower cost transition metals (TM), such as Ni, Fe, Mo, Mn and Cu.
Figure 7 shows the schematic diagram of an anion exchange membrane (AEM) water electrolysis cell with a detail of ions transport and reactions.

Figure 7. Schematic diagram of an AEM water electrolysis cell

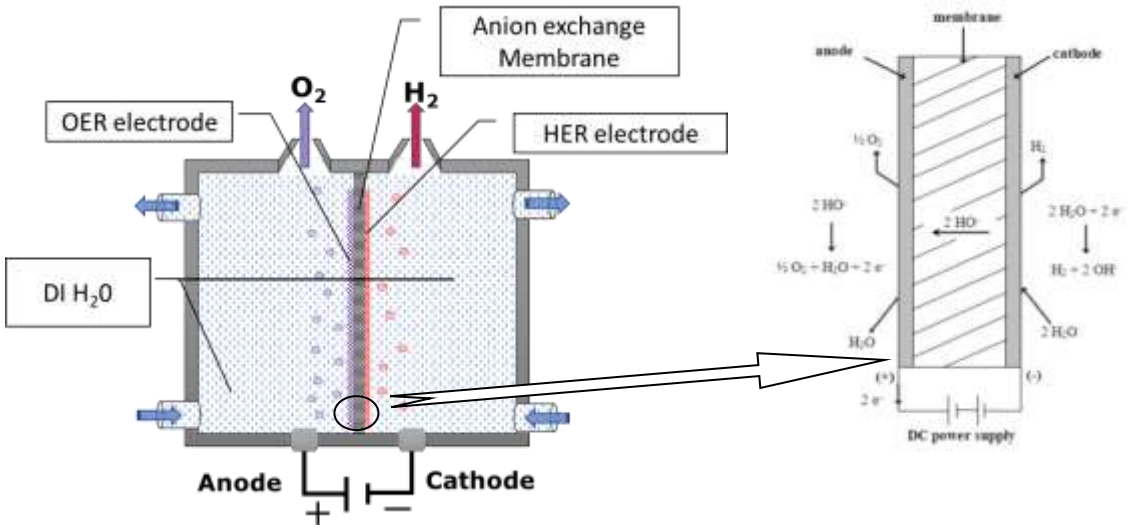

Source: JRC,2020

Water quality requirements for AEMWE are similar to those for PEM WE. As for PEM water electrolysis, the produced hydrogen can be easily pressurized. Because mechanical properties of the membrane and other components are almost the same for both PEM and AEM electrolysers, safe pressurized operation of an AEM electrolyser is expected to be possible. However, for pressurized operations, the increase in hydrogen cross-permeation through the membrane needs to be addressed as well as the mechanical resistance.

With a view to achieving commercially viable hydrogen production, AEM water electrolysis requires further improvements on both material and stack levels, specifically regarding efficiency, stability, robustness, catalyst development and cost reduction. One of the major

([5]) Solution with additional not electroactive constituents with high ionic strength thus increasing overall solution conductivity.

bottlenecks is the lack of highly ionic conductive and robust AEM as well as the related ionomer, which restrains the mass production and further commercialisation [20]. To date, the single stack of market available product only has a few kilowatts, systems with higher power of several hundred kilowatts or beyond are under development.

3 Materials testing for electrolyser applications

Improvement of properties of materials and of components for electrolyser application is based upon a number of innovative methods, processes and manufacturing techniques. In a first step, *"screening"* the functional properties of newly developed or improved materials making up the different cell components is needed. Such *"screening"* is performed by two testing approaches, namely *"ex-situ"* and *"in-situ",* as depicted in Figure 8. When performing screening tests, either *ex-situ* or *in-situ*, care must be taken that the test outcomes are not affected by experimental artefacts or biased measurements resulting from testing in different environments, from damages during preparation (cutting, crushing, etc.), storing and handling, or from unintended damages induced by the testing technique itself (e.g. rotating disc electrode - RDE - measurements [4]).

Figure 8. Flow chart for functional materials testing according to the two approaches

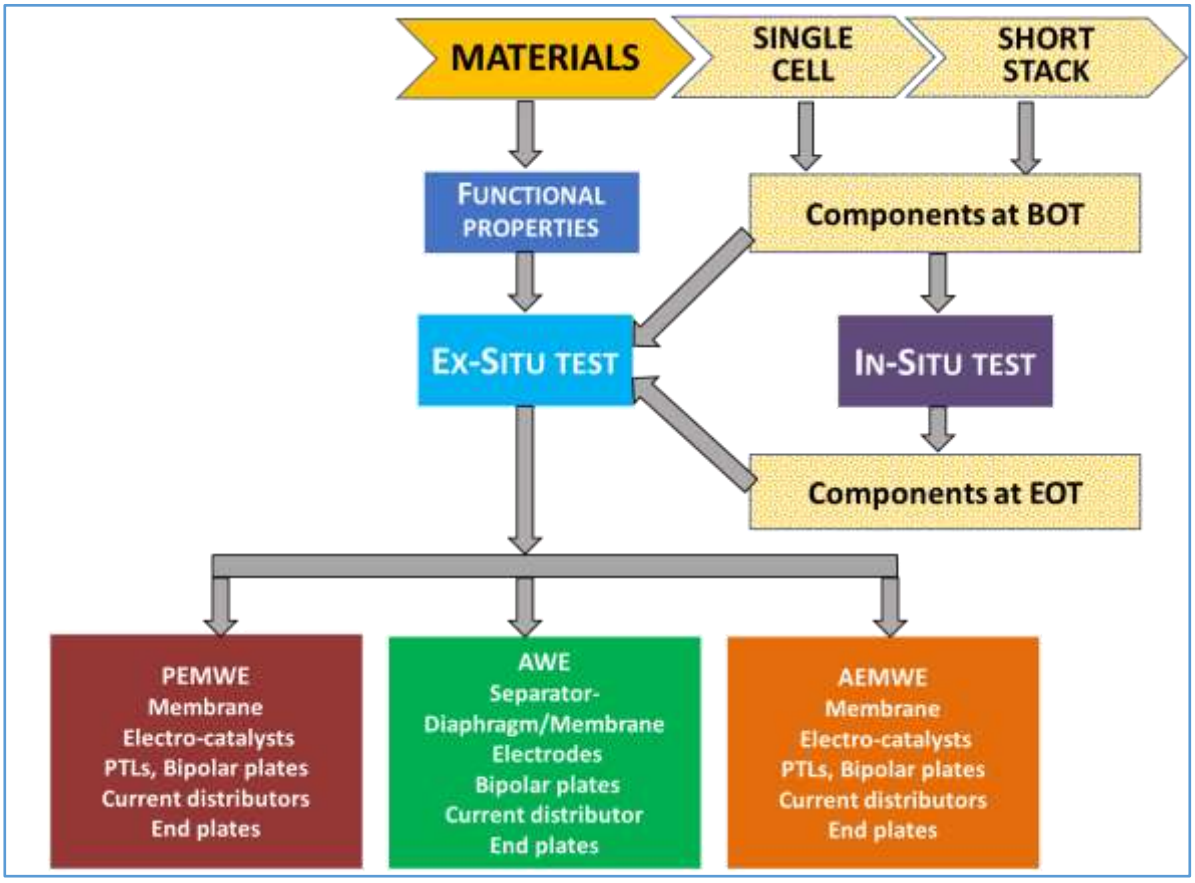

Source: JRC,2020

"*Ex-situ"* tests discussed in this chapter support the development or improvement of materials to better meet the requirements for use in low-temperature electrolysis cell components such as Catalyst Coated Membranes, CCMs, or Membrane Electrode Assemblies, MEAs. Such tests, in which materials under test are not integrated in an electrochemical cell, may also be performed on materials that have been previously assembled in the smallest functional electrochemical unit based on three electrode

arrangements or in a bipolar cell structure for *in-situ* testing (which will be discussed in Chapter 4)**.** In this case, *ex-situ* testing aims at evaluating the effects of material modifications that may result from electrolyser operation.

Ex-situ testing covers a wide range of analyses, aimed at assessing materials used in PEMWE, AWE and AEMWE components. The material properties to be characterised are those that affect cell performance. Table 2 provides a list of such relevant functional properties and identifies associated test methods.

Table 2. *Ex-situ* test methods

Property Classification	PROPERTY	*EX-SITU* TEST METHOD OR MEASUREMENT TOOL
PHYSICAL	Thickness	Micrometer screw gauge
	Ultimate tensile strength	Tensile Test
	Elongation at break	Tensile Test
	Young's Modulus	Tensile Test
	Permeability	Mercury intrusion method, Mercury porosimeter
		Potential sweep (H_2 crossover test)
	Hydrogen uptake and permeation	Potentiodynamic polarization test - ASTM G148 -97(2018)
	Porosity -pore size -pore size distribution	Bubble point pressure test
		Mercury intrusion method, Mercury porosimetry
		Gas Liquid porosimetry Pressure step/stability porosimeter
	Pore structure	Optical microscopy
	Tortuosity	Mercury intrusion method, Mercury porosimetry
		Gas Liquid Porometry Pressure step/stability porometry
	Mass loss in water (dissolution)	Hydrolytic stability test
	Water content	Water absorption test (ASTM D570)

Property Classification	PROPERTY	*EX-SITU* TEST METHOD OR MEASUREMENT TOOL
	Water uptake	Water absorption test (ASTM D570)
	Volumetric expansion (swelling)	Water absorption test (ASTM D756)
	Hydrophobicity/hydrophilicity	Water contact angle test
		Washburn method
	Surface roughness	Profilometer; Interferometer
PHYSICO-CHEMICAL	Bulk / surface chemical composition Material microstructure • Grain size • Crystallographic phases • Crystal Orientation	Cyclic voltammetry (CV)
		Electrochemical Impedance spectroscopy (EIS)
		Atomic emission spectroscopy (AES)
		Atomic force microscopy (AFM)
		Brunauer-Emmett-Teller (BET) surface area measurement
		Energy dispersive X-ray spectroscopy (EDX)
		Field emission gun-scanning electron microscopes energy dispersive X-Ray analysis (FEG SEM-EDX)
		Fourier transformed infrared analysis (FTIR)
		Neutron tomography
		Scanning electron microscopy (SEM)
		Secondary ion mass spectroscopy (SIMS)
		Transmission Electron Microscopy (TEM)
		Extended X-ray absorption fine structure (EXAFS)
		X-ray absorption near-edge structure (XANES)

Property Classification	PROPERTY	*EX-SITU* TEST METHOD OR MEASUREMENT TOOL
		X-ray diffraction (XRD)
		X-ray fluorescence (XRF)
		X-ray micro computed tomography (μ-CT)
		X-ray photoelectron spectroscopy (XPS)
ELECTRICAL	Electrical conductivity	In-plane/through-plane conductivity test
	Contact resistance	Four-wire Kelvin method
		Davies and Wang method [21]
	Ionic conductivity	In-Plane/through plane conductivity test
CHEMICAL	Reaction kinetics	Rotating disc electrode (RDE) electrochemical tests
	Oxidative stability (mass loss)	Fenton's reagent test
	Ion exchange capacity (IEC)	Chemical titration
	Equivalent weight (EW)	Chemical titration
	Metal dissolution	Inductively coupled plasma mass spectrometry (ICP-MS)
THERMAL	Thermal conductivity	Thermal conductivity measurement
	Thermal expansion	Thermal dilatometry measurement
	Glass transition temperature	Dynamic mechanical analysis DMA(T_g)
	Thermal decomposition	Thermogravimetric Analyser/Differential Scanning Calorimeter (TGA-DSC)

Source: JRC, 2020

Additional information on physico-chemical methods is presented in Annex A.

The cell components and functional property tests from the above table relevant for the individual low temperature electrolysis technologies are discussed in the following sections of this chapter.

Inputs to the test methods which are treated successively in the following sections have been gathered from literature or provided by the FCH-JU funded projects ELECTROHYPEM, HPEM2GAS, NEPTUNE, NEXPEL, NOVEL for PEMWE; ELYGRID, ELYNTEGRATION for AWE, ANIONE, CHANNEL and NEWELY for AEMWE.

3.1 PEMWE functional property testing

For PEMWE components *ex-situ* testing aims at establishing the functional properties of materials used in

- Membranes
- Electrodes and electrocatalysts layer
- Porous Transport Layers (PTLs)
- Current collectors, meshes, bipolar plates and separator plates
- End plates

3.1.1 PEMWE membrane materials

Key requirements for the membrane relate to its barrier effect to transfer electrons and gases between the anode and cathode compartments and its capacity of acting as electrolyte for ionic species. For the barrier effect gas transport properties are the most relevant, whereas the ionic resistance serves as a metric for electrolyte properties. The ionic resistance depends on:

- Ion exchange capacity (IEC, mmol ion·g^{-1} polymer) and equivalent weight (EW, g polymer per mol, IEC = 1000 / EW).
- Amount of water uptake
- Cross-permeation of gasses, which is affected by permeability and depends on the applied current density and the differential pressure between the anode and the cathode
- Thickness
- Geometrical surface area

The ionic resistance can be characterised by two parameters: area resistance [$\Omega.cm^2$], i.e. measured resistance [Ω] multiplied by the geometric surface area [cm^2], or resistivity [$\Omega.cm^2/cm$], i.e. area resistance divided by thickness.

A list of functional properties of membrane materials is presented in Table 3. The protocols for performing the associated *ex-situ* tests are identified in the table in Annex B. Because functional properties may depend on temperature and upon pressure, assessment of PEMWE membrane materials may require performing *ex-situ* tests over a wide range of temperatures or pressures.

Table 3. PEMWE membrane material *ex-situ* tests

MEMBRANE			
Property Classification	**PROPERTY**	***EX-SITU* TEST METHOD OR MEASUREMENT TOOL**	**Ann.**
PHYSICAL	Thickness	Micrometer screw gauge	B5
	Ultimate tensile strength	Tensile Test (ASTM D882-09, ASTM D638)	
	Elongation at break	Tensile Test	B9
	Young's Modulus	Tensile Test (ASTM D638 type V)	
	Permeability	Potential sweep (H_2 crossover test)	B7
	Mass loss in water (dissolution)	Hydrolytic stability test	B2
	Water content	Water absorption test (ASTM D570)	
	Water uptake	Water absorption (ASTM D570)	
	Volumetric expansion (swelling)	Water absorption test (ASTM D756) ➢ Thickness increase Δz in H_2O at specific T ➢ Machine direction (MD) thickness increase Δx in H_2O at specific T ➢ Transverse direction (TD) thickness increase Δy in H_2O at specific T	B6
	Surface roughness	Profilometer; interferometer	
ELECTRICAL	Electrical conductivity	In-plane/through-plane conductivity test (Four-electrode chronopotentiometry)	
	Contact resistance	Four-wire Kelvin method	
	Ionic Conductivity	In-plane/through plane conductivity test	B4
		EIS	
CHEMICAL	Oxidative Stability (mass loss)	Fenton's reagent test	B3
	Ion exchange capacity (IEC)	Chemical titration	B1
	Equivalent weight (EW)	Chemical titration	B1
THERMAL	Thermal conductivity	Thermal conductivity measurement	
	Glass transition temperature	Dynamic mechanical analysis DMA(T_g)	B8

MEMBRANE			
Property Classification	**PROPERTY**	***EX-SITU* TEST METHOD OR MEASUREMENT TOOL**	**Ann.**
	Thermal decomposition	Thermogravimetric analyser/differential scanning calorimeter (TGA-DSC)	B8

Source: JRC, 2020

3.1.2 PEMWE electrode and electrocatalysts

The function of an electrocatalyst is to increase the electrochemical reaction rate, in this case of water splitting, by reducing the activation energy. Pt nanoparticles are usually used at the cathode for the hydrogen evolution reaction while iridium dioxide (IrO_2) or alternative catalyst-based particles (see Table 1) are used mostly at the anode for the oxygen evolution reaction. When such precious materials are used as catalysts, it is important to maximise their use by increasing the electrochemical surface area (ECSA). For this reason, some porous supporting medium like porous titanium (Ti) or Magneli phase, is used for the anode electrode. Carbon fibres are suitable for the cathode only, because their corrosion resistance is too low in the anodic environment.

For functional property evaluation of electrocatalyst materials, *ex-situ* tests include determination of morphology, particle size and dispersion of the catalysts (see Table 4). For electrode materials, surface homogeneity, hydrophobicity/hydrophilicity, chemical resistance and electrical properties are the most relevant to be investigated.

Table 4. PEMWE electrode and electrocatalyst *ex-situ* tests

ELECTRODE AND ELECTROCATALYST		
Property Classification	**PROPERTY**	***EX-SITU* TEST METHOD OR MEASUREMENT TOOL**
PHYSICAL	Thickness	Micrometer screw gauge
	Hydrophobicity/hydrophilicity	Water contact angle test
		Washburn method
	Surface Roughness	Profilometer; interferometer
PHYSICO-CHEMICAL	Bulk / surface chemical composition Material microstructure • Grain size • Crystallographic phases • Crystal Orientation	Cyclic voltammetry (CV)
		Atomic emission spectroscopy (AES)
		Atomic force microscopy (AFM)
		Brunauer-Emmett-Teller (BET) surface area measurement
		Energy dispersive X-ray spectroscopy (EDX)

ELECTRODE AND ELECTROCATALYST		
Property Classification	**PROPERTY**	***EX-SITU* TEST METHOD OR MEASUREMENT TOOL**
		Field emission gun-scanning electron microscopes energy dispersive X-Ray analysis (FEG SEM-EDX)
		Fourier transformed infrared analysis (FTIR)
		Neutron tomography (NT)
		Scanning electron microscopy (SEM)
		Secondary ion mass spectroscopy (SIMS)
		Transmission Electron Microscopy (TEM)
		Extended X-ray absorption fine structure (EXAFS)
		X-ray absorption near-edge structure (XANES)
		X-ray diffraction (XRD)
		X-ray fluorescence (XRF)
		X-ray micro computed tomography (μ-CT)
		X-ray photoelectron spectroscopy (XPS)
ELECTRICAL	Electrical conductivity	In-plane/through-plane conductivity test
	Contact resistance	Four-wire Kelvin method
	Ionic conductivity	In-plane/through plane conductivity test
CHEMICAL	Reaction kinetics	Rotating disc electrode (RDE) electrochemical tests
	Metal dissolution	Inductively coupled plasma mass spectrometry (ICP-MS)
THERMAL	Thermal conductivity	Through-plane thermal conductivity measurement

Source: JRC, 2020

3.1.3 PEMWE porous transport layer materials

The porous transport layer (PTL) acts as electroconductive diffusion layer facilitating mass transport of reactants and removal of reaction products between the electrode and the bipolar plate (BPP). It is made of a porous medium or a combination of different porous media forming adjacent layers or a composite layer. The effectiveness of the PTLs, especially at high current density, could be improved by the adoption of an additional layer on the electrode side called micro-porous layer (MPL). Such additional MPL can greatly improve performance, durability, and stability. The MPL reduces the interfacial contact resistance and can protect the membrane from being punctured by PTL.

PTLs can be subjected to electrochemical degradation due the combination of thermal variation and presence of an acid environment [3], as well as some mechanical degradation due to the compression effects. When differential pressures are applied, the PTL has to provide also mechanical support for the membrane.

The properties of PTLs are measured with tests similar to those used for the bipolar plate materials (see Section 3.1.4). Additional characterization methods are as follows: gas/water permeation, mechanical tests, X-ray micro computed tomography, and neutron tomography for assessing water/gas presence.

A list of *ex-situ* tests used for PTL materials is provided in Table 5.

Table 5. PEMWE PTL *ex-situ* tests

POROUS TRANPORT LAYER		
Property Classification	**PROPERTY**	***EX-SITU* TEST METHOD OR MEASUREMENT TOOL**
PHYSICAL	Thickness	Micrometer screw gauge
	Ultimate tensile strength	Tensile Test
	Elongation at break	Tensile Test
	Young's Modulus	Tensile Test
	Permeability	Mercury intrusion method, Mercury porosimeter
	Hydrogen uptake and permeation	Potentiodynamic polarization test - ASTM G148 -97(2018)
	Porosity	Mercury intrusion method, Mercury porosimeter
	Tortuosity	Mercury intrusion method, Mercury porosimeter
	Pore size distribution	Mercury intrusion method, Mercury porosimeter
	Hydrophobicity/hydrophilicity	Water contact angle test
		Washburn method

POROUS TRANPORT LAYER		
Property Classification	**PROPERTY**	***EX-SITU* TEST METHOD OR MEASUREMENT TOOL**
	Surface roughness	Profilometer; interferometer
PHYSICO-CHEMICAL	Bulk / surface chemical composition	Neutron tomography (NT)
	Material microstructure • Grain size • Crystallographic phases	Scanning electron microscopy (SEM)
	Crystal orientation	X-ray micro computed tomography (μ-CT)
ELECTRICAL	Electrical conductivity	In-plane/through-plane conductivity test
	Contact resistance	Four-wire Kelvin method
CHEMICAL	Metal dissolution	Inductively coupled plasma mass spectrometry (ICP-MS)
THERMAL	Thermal conductivity	Thermal conductivity measurement

Source: JRC, 2020

3.1.4 PEMWE bipolar plates and current distributor materials

A BPP is an electrically conductive gastight plate separating individual cells in a stack. It distributes current and reagents flows and provides mechanical support for the electrodes or membrane electrode assembly (MEA). For BPP materials, the relevant functional properties include electrical/thermal conductivity, corrosion resistance and characterization of applied coating materials. A list of *ex-situ* tests used for bipolar plates and current distributor material is reported in Table 6.

BPPs should have sufficient electrical and thermal conductivity. Often a flow field based upon a channel structure, typically in the mm-range, is used to distribute the reactant water evenly over the active area and remove product gases and waste heat.The same function can be performed by an additional multilayer expanded metal.

Table 6. PEMWE BPPs and current distributor *ex-situ* tests

BPPs and current distributor		
Property Classification	**PROPERTY**	***EX-SITU* TEST METHOD OR MEASUREMENT TOOL**
PHYSICAL	Thickness	Micrometer screw gauge
	Ultimate tensile strength	Tensile test
	Elongation at break	Tensile test

BPPs and current distributor		
Property Classification	**PROPERTY**	***EX-SITU* TEST METHOD OR MEASUREMENT TOOL**
	Young's Modulus	Tensile test
	Hydrogen uptake and permeation	Potentiodynamic polarization test - ASTM G148 -97(2018)
	Hydrophobicity/hydrophilicity	Water contact angle test
	Surface Roughness	Profilometer; interferometer
PHYSICO-CHEMICAL	Bulk / surface chemical composition	Atomic force microscopy (AFM)
		Field emission gun-scanning electron microscopes energy dispersive X-Ray analysis (FEG SEM-EDX)
		Neutron tomography (NT)
		Scanning electron microscopy (SEM)
		X-ray diffraction (XRD)
		X-ray micro computed tomography (μ-CT)
		X-ray photoelectron spectroscopy (XPS)
ELECTRICAL	Electrical conductivity	In-plane/through-plane conductivity test
	Contact resistance	Four-wire Kelvin method
CHEMICAL	Metal dissolution	Inductively coupled plasma mass spectrometry (ICP-MS)
THERMAL	Thermal conductivity	Thermal conductivity measurement
	Thermal expansion	Thermal dilatometry measurement

Source: JRC, 2020

3.1.5 PEMWE end plate materials

End plates are components located on either end of the electrolyser cell/stack serving to transmit the required compression to the stacked cells. The end plates may comprise ports, ducts and manifolds for transporting fluids (reactants, coolant) to and from the stack.

For end plates components the mechanical and thermal properties are relevant. A list of *ex-situ* tests used for end plate material assessment is given in Table 7.

Table 7. PEMWE end plate *ex-situ* tests

END PLATE		
Property Classification	**PROPERTY**	***EX-SITU* TEST METHOD OR MEASUREMENT TOOL**
PHYSICAL	Thickness	Micrometer screw gauge
	Ultimate tensile strength	Tensile test
	Elongation at break	Tensile test
	Young's Modulus	Tensile test
	Surface roughness	Profilometer
THERMAL	Thermal conductivity	Thermal conductivity measurement
	Thermal expansion	Thermal dilatometry measurement

Source: JRC, 2020

3.2 AWE functional properties

For AWE systems, materials of the following components require functional testing:

- Diaphragm
- Membranes (for newer AWE technology)
- Electrodes
- Support plates

3.2.1 AWE diaphragm materials

The main requirements for the diaphragm are ionic conductivity and gas separation capability. Ionic conductivity should be high to minimise ohmic losses, and it depends upon material composition, porosity and wettability, as well as on thickness and assembly. Gas separation capability should also be high to withstand the anode-cathode differential pressure. Measures to increase gas separation normally negatively affect ionic conductivity.

Other relevant properties are mechanical form stability, flexibility and chemical resistance.

Table 8. AWE Diaphragm *ex-situ* tests

DIAPHRAGM		
Property Classification	**PROPERTY**	***EX-SITU* TEST METHOD OR MEASUREMENT TOOL**
PHYSICAL	Thickness	Micrometer screw gauge
	Ultimate tensile strength	Tensile test (ASTM D882-09, ASTM D638)
	Young's Modulus	Tensile test (ASTM D638 type V)
	Porosity -pore size -pore size distribution	Bubble point pressure test cell Gas Liquid Porometry Pressure step/stability porometer
	Tortuosity	Mercury intrusion method, Mercury porosimeter
	Surface roughness	Profilometer; interferometer
ELECTRICAL	Electrical conductivity	In-plane/through-plane conductivity test (four-electrode chronopotentiometry)
	Contact resistance	4-wire Kelvin method
	Ionic conductivity	In-plane/through plane conductivity test

Source: JRC, 2020

3.2.2 AWE membrane materials

With the latest technology developments polymeric membranes have been introduced in alkaline electrolysers to improve their efficiency.

For the applicable *ex-situ* tests see table 3.

3.2.3 AWE electrode materials

Electrodes are in contact with the electrolyte for the supply of electrical energy for the electrochemical reaction. Electrode materials normally consist of metal porous structures that exhibit high electrical conductivity,good electrocatalytic activity, high surface area and high corrosion resistance in the electrolyte caustic environment.

Table 9. AWE Electrode *ex-situ* tests

ELECTRODE		
Property Classification	**PROPERTY**	***EX-SITU* TEST METHOD OR MEASUREMENT TOOL**
PHYSICAL	Thickness	Micrometer screw gauge
	Ultimate tensile strength	Tensile test (ASTM D882-09, ASTM D638)
	Young's Modulus	Tensile test (ASTM D638 type V)
	Porosity	Bubble point pressure test cell
	channel structure	SEM cross section
	Tortuosity	Mercury intrusion method, Mercury porosimeter
	Hydrophobicity/hydrophilicity	Water contact angle test
		Washburn method
	Surface Roughness	Profilometer; interferometer
	Attachment of catalyst to the substrate	SEM cross section
		Optical microscopy
PHYSICO-CHEMICAL	Bulk / surface chemical composition Material microstructure • Grain size • Crystallographic phases • Crystal Orientation	Atomic emission spectroscopy (AES)
		Atomic force microscopy (AFM)
		Energy dispersive X-ray spectroscopy (EDX)
		Neutron tomography (NT)
		Scanning electron microscopy (SEM)
		X-ray diffraction (XRD)
		X-ray fluorescence (XRF)
		X-ray micro computed tomography (μ-CT)
		X-ray photoelectron spectroscopy (XPS)
	Electrical conductivity	In-plane/through-plane conductivity test

ELECTRODE		
Property Classification	**PROPERTY**	***EX-SITU* TEST METHOD OR MEASUREMENT TOOL**
ELECTRICAL	Contact resistance	Four-wire Kelvin method
	Ionic conductivity	In-plane/through plane conductivity test
CHEMICAL	Metal dissolution	Inductively coupled plasma mass spectrometry (ICP-MS)
THERMAL	Thermal conductivity	Thermal conductivity measurement

Source: JRC, 2020

3.2.4 AWE suppoer plate materials

Support plates or end plates have mainly a mechanical support function and are made of metals. For bipolar plates (BPP), considering that their electric conductivity is four orders of magnitude, or more, higher than that of the electrolyte, the electrical properties are not critical. Normally nickel (Ni) is used as it is easily available, cheap, stable and has low contact resistance. However, the use of passivating layers to protect against corrosion can significantly increase contact resistances which may become an important contributor to the total cell resistance. For the applicable *ex-situ* tests - see Table 6.

3.3 AEMWE functional properties

Notwithstanding the difference between PEMWE and AEMWE related to the use of an acidic and alkaline solid electrolyte respectively, the cells and stacks of both technologies contain similar components assembled in a similar way. Hence, the materials of interest, as well as the applicable *ex-situ* tests to establish their functional properties, are the same as for PEMWE (see 3.1).

4 *In-situ* tests

In *"in-situ"* tests the performance of materials is assessed by using measurement devices and sample connectors which are compatible with the operational environment that the materials are expected to experience in actual applications. These tests aim at evaluating performance under operating conditions in single cell or short stack arrangement, by measuring the electrochemical properties in terms of cell voltage, current and time. Test campaigns should only start after appropriate Cell/Stack Activation and Conditioning according to the manufacturer's instructions has been performed.

In-situ testing can be performed over a wide range of testing conditions and at different moments in time, as indicated schematically in Figure 9 below:

Testing conditions include static and dynamic operating conditions (the latter according to a given *load-versus-time* profile) imposed by the test hardware on the single cell or short stack. To be exhaustive, such conditions should cover normal and out-of-normal, or "stressor" operation for the cell or stack components. Hence, four dimensions apply for *in-situ* test conditions: static/dynamic/normal/stressor.

The time dimension enters because the performance determined from results of *in-situ* tests constitutes an instantaneous measure that depends upon the material properties of the components making up the single cell or short stack at a given time, as affected by their actual exposure history corresponding to a given *load-versus-time* profile. Interrupting the above-mentioned dynamic loading and subjecting a single cell or short stack to *in-situ* tests allows assessing the change of performance induced by a change in material properties ([6]). Execution of *in-situ* tests upon repeated interruption thus allows monitoring performance degradation or, in other words, assessing durability.

To reduce testing efforts and time required for assessing durability through performance degradation monitoring, the imposed load profiles may require adaptation to accelerate the induced degradation. This approach, known as accelerated *in-situ* testing, is based upon the assumption of an increase in the rate of degradation, with the mechanism(s) causing degradation in the accelerated tests remaining the same as in actual service. Confirmation of the assumption underlying the transferability of results obtained from accelerated *in-situ* testing to real life degradation still requires significant validation effort and is the subject of ongoing research. At present, the accelerated in-situ test methods and protocols proposed in this report are therefore provided to guide material development and improvement efforts for their use in components for electrolyser application.

([6]) Performing *ex-situ* tests (as described in chapter 3) allows measuring the functional material properties at any moment during their exposure history.

Figure 9. Schematic for in-situ single cell and short stack testing. Number labels to boxes refer to chapters in this report

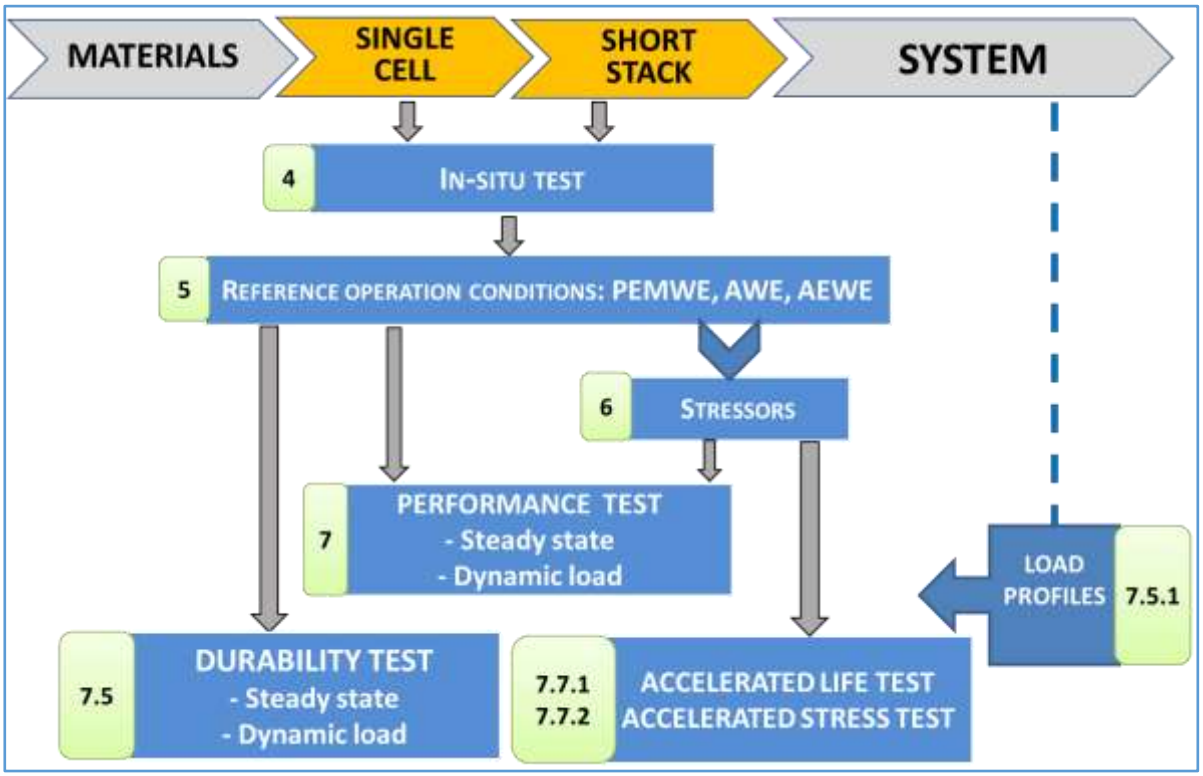

Source: JRC, 2020

In-situ cell or short stack tests enable evaluating performance in terms of a number of indicators derived from the test outcomes, either as a direct experimental result, or indirectly from an analysis of the test outcomes. The most frequently used *in-situ* tests are:

- **Polarization curve (I-V curve)** for the overall electrochemical performance evaluation
- **Electrochemical Impedance spectroscopy (EIS)** for separating the ohmic, activation and concentration losses and for the evaluation of reaction rates, diffusion coefficients, charge transfer resistance and double layer capacitance values.
- **Cyclic voltammetry (CV)** to measure reaction kinetics and for electrochemical active surface area (ECSA) determination

A detailed description of the associated test protocols is presented in JRC test reports for Polarisation Curve Measurements [7]; Cyclic Voltammetry [8] and Electrochemical Impedance Spectroscopy [9].

The *in-situ* test agreed approach is presented in the following table, where the last column shows the section of the present report in which this aspect is addressed.

The selection of test to be performed will depend on the actual development objectives.

Table 10. *In-situ* testing agreed assessment topics

***In-situ* test level**	**Subject of the assessment**	**Topic**	**Section**
Single cell/ short stack	Performance	Set of reference operating conditions	5
		Type and intensity of stressors	6
		Identification of performance indicators	7.1, Table 22
		Definitions for efficiency	7.2
		Performance assessment	7.3
	Durability (through monitoring of performance degradation)	Identification of durability indicators	7.4.1-3, Table 25
		Durability test protocol for steady state loading	7.5.1-2
		Durability test protocol for dynamic loading	7.5.3-4
	Accelerated testing	Protocol for accelerated life testing	7.7.1
		Protocol for accelerated stress testing	7.7.2
System	Performance	Identification of performance indicators	8.7, Table 47
		Grid-balancing fit for purpose test	8.4
		Harmonised grid services protocols	8.5
		Definitions for efficiency	8.6

Source: JRC, 2020

5 Reference operating conditions for testing of single cells and of short stacks

Electrolyser materials are subjected to a variety of operating conditions. The aim of establishing a set of Reference Operating Conditions is to be able to test and evaluate the Reference Performance of different materials *in-situ* in single cell or short stack configuration and to provide a means for objective comparison of test results. The reference operating conditions should be representative as far as possible of the current and future electrolyser applications.

The operating conditions selected as reference should ideally represent the centre of the window of normal operating conditions. However, in some cases, low-temperature water electrolysers are bound to operate under conditions outside of the normal operation window. Some of these conditions could be severe and act as stress factors to the cell and short stack materials. These stressor conditions are further elaborated in Chapter 6.

Operating conditions consist of two sets of parameters:

First, test parameters with a set-point value that can be controlled using a feedback loop within the test hardware are defined as **Test Input Parameters (TIP)**.

Second, non-adjustable parameters whose measured value depends on the values imposed by the TIPs are defined as **Test Output Parameters (TOP**).

Whereas the instrumentation for experimental measurement of TIPs (measurement and control) and TOPs (measurement only) should in principle be located as close as possible to the relevant position of interest in the cell, this is not always feasible in practice. Therefore, in the following sections TIPs and TOPs are identified for properties that are experimentally accessible at the level of the test bench and of the anode and cathode compartments ([7]). For test results to be valid, the values assumed by the TIPs have to fall within specific tolerances, independently or in combination with specific TOPs (see Table 14).

The following sections of this chapter list the agreed reference operating conditions (TIPs and TOPs) for the three considered low temperature electrolysis technologies.

([7]) In addition, electrical parameters current intensity (density) and cell voltage serve as TIP and TOP, respectively.

5.1 Reference operating conditions for PEMWE cells/short stack testing

5.1.1 Cell temperature *(TIP)*

Because cell temperature is one of the most important parameters affecting performance, it should be controlled as accurately as possible. Hence, to minimize temperature variations from the intended setting, cell temperature is controlled by a temperature control system incorporated in the recirculating water loop which is adequately insulated to minimize thermal losses to the environment.

The TIP cell temperature should be representative of the temperature of the MEA where the water electrolysis reaction occurs. The temperature sensor for monitoring and controlling cell temperature should hence be located as close as possible to the MEA. Depending upon test bench configuration, a number of cases can be differentiated for the location of the temperature sensor:

i. Temperature sensor located inside the anode and cathode bipolar plate close to the MEA
   - The cell temperature is that indicated by the sensor at the anode side.

For a temperature sensor placed in the water recirculation loop, two cases should be considered:

ii. The liquid water is fed to the anode compartment only:
   - The cell temperature is equal to the temperature of the water measured as close as possible to the cell inlet.

iii. The liquid water is fed to both anode and cathode compartments:
   - The cell temperature is equal to the average water temperature of the water measured at anode and cathode inlets.

For the latter two cases, the uniformity of the water temperature between inlet and outlet of the cell is important and the water temperature difference between outlet and inlet should be minimised.

5.1.2 Water quality *(TIP)*

The indicator used for the quality of the de-ionised water is its electrical conductivity measured at the cell inlet. Recirculation of the water may deteriorate the water quality because of possible accumulation of ions or impurities such as organic carbonaceous and non-conducting pollutants. Whereas the presence of such impurities may not show up in the results of electric conductivity measurements, cell performance/durability may nevertheless be affected. It is therefore recommended to fit a purification stage in the recirculation loop upstream of the cell inlet, and to measure water conductivity downstream of the purification system.

The water reacted is replenished in the recirculation loop through a de-ionisation water treatment system ("water make up" unit).

5.1.3 Anode conditions

These are split in two classes: TIPs and TOPs which are discussed consecutively.

Anode Test Input Parameters

i. Anode water quality

- See 5.1.2

ii. Anode water inlet temperature

The anode water inlet temperature serves as TIP when the cell temperature cannot be measured in the cell bipolar plate close to the MEA. The temperature in this case should be measured as close as possible at the inlet of the cell/stack (case ii, 5.1.1).

iii. Water inlet pressure

Pressure is normally controlled indirectly with a feed-back control loop based upon the gas outlet pressure that is adjusted from ambient to the maximum design pressure with a backpressure regulation valve.

iv. Water inlet Flow rate

The water inlet flow rate should in principle be set based upon the cell or short stack active area perpendicular to the direction of the current, corresponding to the geometrical electrode area in contact with the membrane.

However, next to serving as feedstock for the electrolysis reaction, water also contributes to heat management of the cell/short stack by removing or minimising heat produced by the electrolysis reaction, thereby maintaining the correct temperature at the reaction site of the MEA. The water flow rate is related to the temperature difference between cell input and output through the dimensionless Lambda factor λ_{H_2O} [5] defined as:

$$\lambda_{H_2O} = \frac{2F}{M_{H_2O}\, c_{p(H_2O)} \Delta T}\,(U_{cell} - U_{tn}) \qquad \text{[Eq. 5.1]}$$

where

- λ_{H_2O} = a dimensionless and time independent ratio of the actual water flow rate to that of the electrolysed water.
- F = Faraday constant (96,485.33 C.mol^{-1}).
- M_{H_2O} = molar weight of water.
- $c_{p(H_2O)}$ = specific heat capacity of liquid water at constant pressure.
- ΔT = water temperature difference between cell outlet and inlet.
- U_{cell}= cell voltage at operational T, p.
- U_{tn} = thermoneutral cell voltage at operational T, p.

The unit to be used for each of the parameters is that indicated in Table 48, Symbols.

Figure 10. Lambda plot for various cell voltages and temperature differences

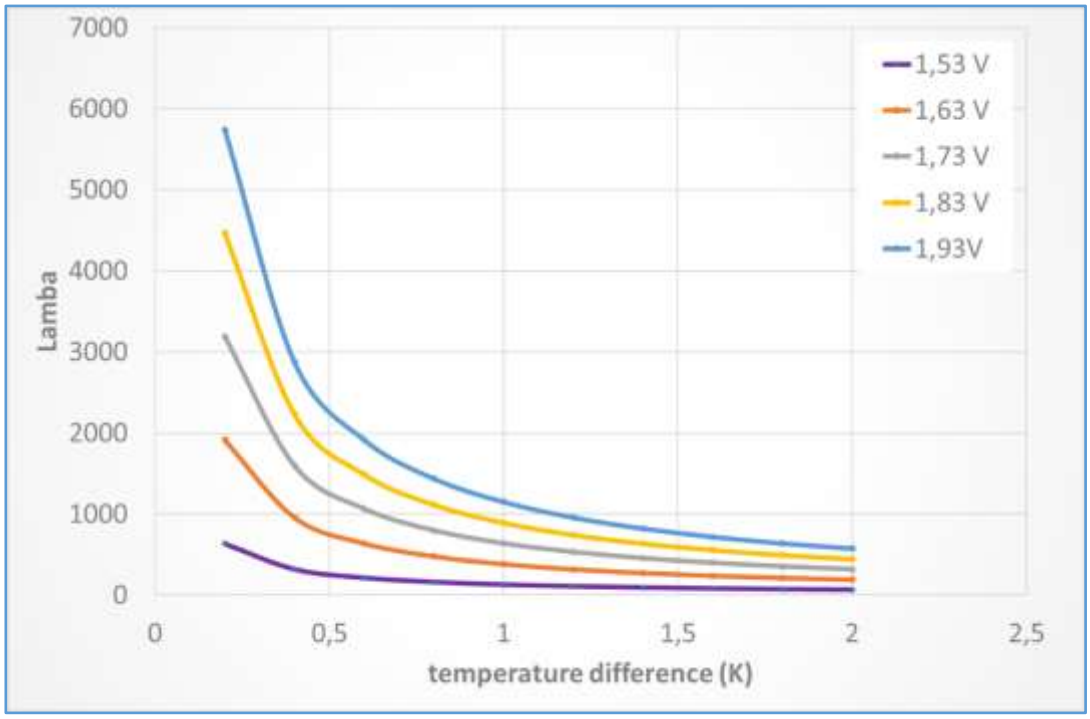

Source: JRC, 2020

As shown in Figure 10 lambda (λ_{H_2O}) increases with decreasing temperature difference and increasing operating voltage, indicating the need for higher water flow rates to maintain thermal equilibrium under these conditions.

Another parameter that can be used for determining an appropriate water inlet flow rate to minimise the temperature difference between inlet and outlet is the water utilization factor (UF_w). It is defined as the ratio of the water reacted at a given current and the corresponding water flow fed to the anode and calculated as follows:

The relationship between water reacted and total current for single cell (N=1) or short stack (N> 1), with current density *i*, active area A, is:

$$\dot{n}_{H2O,reacted} = \frac{i\,xA\;x\,N}{2F} = \dot{n}_{H2,out} \qquad \text{[Eq. 5.2]}$$

Therefore, with the specific feed water flowrate expressed in mL.min^{-1}.cm^{-2} of active area, UF_w can be calculated as:

$$UF_w = \left(\frac{i \times A \times N}{2F} \times M_{H2O} \times 60\right) / (specific\ feed\ water\ flow\ rate \times A \times N) \qquad \text{[Eq. 5.3]}$$

$$UF_w = \left(\frac{i}{96{,}485.33} \times 18.015 \times 30\right) / (Feed\ water\ flow\ rate) \qquad \text{[Eq. 5.4]}$$

$$UF_w = (i \times 0.0056) / (Feed\ water\ flow\ rate) \qquad \text{[Eq. 5.5]}$$

For typical water electrolysis operation, UF_w is commonly set at 0.5 %. As shown in Figure 11, this corresponds to specific feed flow rates higher than 2 $mL.min^{-1}.cm^{-2}$ for a typical current density, *i,* of 2 $A.cm^{-2}$. For operations at higher current density, a higher water utilisation factor is required for minimizing temperature difference while maintaining the reaction rate.

Figure 11. Water utilisation factor (UFw) evolution vs. current density and water inlet flowrate

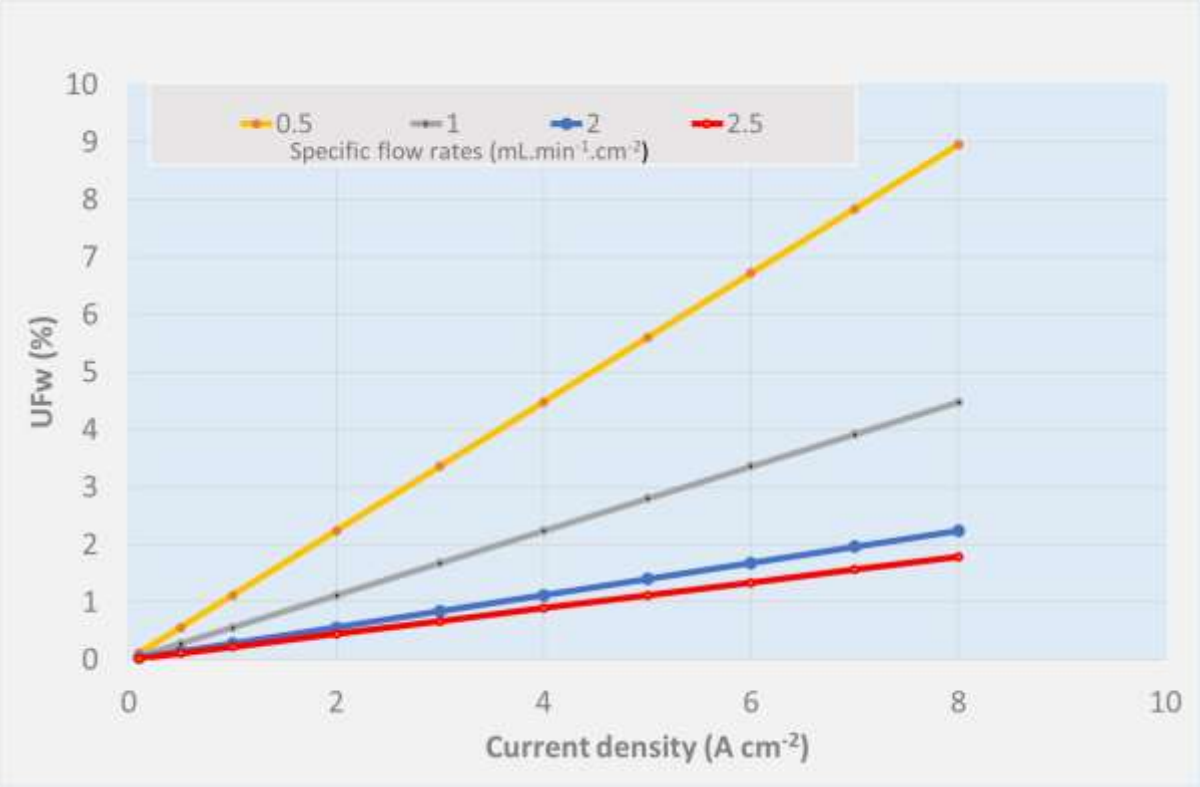

Source: JRC, 2020

In addition to the water flowrate requirements corresponding to the use of water as reactant and its contribution to heat management, water flow rate also affects gas bubble evolution and removal at the electrodes.

It should be noted that the water flow velocity that plays a role in the bubble's removal does not depend only on the flowrate but also upon the flow field pattern.

For the two above reasons, the water inlet flowrate is usually set considerably higher than that required for converting water into hydrogen and oxygen for a given active cell area and current density. Accordingly, the minimum specific feed flowrate in the water recirculation loop is set to 2 $mL.min^{-1}.cm^{-2}$ of active area.

v. Oxygen outlet pressure

Depending upon the anticipated use of the produced oxygen, its pressure may serve as a TIP. In this case, oxygen pressure should be measured at the outlet of the electrolysis cell/short stack, after the water removal components, and before the backpressure regulation valve. The measured oxygen pressure is then fed as a feedback control signal to the anodic water circulation pressure control loop.

In pressurized test hardware, anode and cathode half-cells can be designed to operate at the same or at different pressure; in the first case differential pressure effects on the MEA are minimized, while in the second case the oxygen line can be kept at lower (ambient) pressure, thereby reducing possible safety issues related to pressurised oxygen and simplifying BoP. The drawback is the increase of gas cross-over effects that can lead to other safety issues, especially at low load.

Anode Test Output Parameters

i. Water outlet temperature

The water outlet temperature depends upon the water inlet temperature, flowrates of water and of oxygen, heat transfer resulting from overvoltages and ohmic losses in the MEA, conductive heat losses from piping and from hardware surfaces.

The temperature difference between water outlet and inlet serves as a test validity criterion and should not exceed +/- 2 K (see Table 14). If the limit is exceeded the parameters of the temperature control loop of the test bench should be adjusted.

ii. Oxygen quality

When the produced oxygen is to be used as feedstock, its quality should be measured in real time at the cell or stack exit after water removal, according to the specifications for its use.

Due to the high diffusion coefficient of hydrogen, a certain amount of it is expected to be present in the oxygen gas stream. Experimental data shows that anodic hydrogen contamination decreases with increasing applied current density because the associated increase of oxygen evolution rate dilutes the permeating hydrogen, the amount of which is considered rather constant. The operating pressure is another important parameter affecting hydrogen concentration in the anodic compartment and is limited to approximately 30 bar.

In the absence of a real-time quality control system, for safety reason, it is recommended to monitor at least the presence of hydrogen in the oxygen outlet stream using a safety sensor to ensure that the hydrogen concentration does not reach the Lower Explosion Limit (LEL) of a hydrogen-oxygen gas mixture. LEL decreases with temperature and increases with pressure as shown in Table 11 and Figure 12, indicating that higher temperatures and lower pressures merit more attention from the LEL point of view [6]. In practice, when the hydrogen concentration exceeds 50 % of LEL, appropriate safety measures should be triggered. The higher safety issues are related to the high-pressure operation, in particular in differential mode due to the higher gas permeation and the operation at low currents.

Table 11. Influence of pressure on explosion limits of H_2-O_2 mixtures at room temperature, 25 °C and 80 °C [17]

Pressure in bar	LEL in mol% H_2		UEL* in mol% H_2	
	25°C	80°C	25°C	80°C
1	4.0	3.8	95.2	95.4
5	4.6	4.4	94.6	95.0
10	5.0	4.8	94.2	94.6
20	5.4	5.2	94.2	94.6
50	5.5	5.3	94.6	95.0
100	5.7	5.7	94.9	95.3
150	5.7	5.3	95.1	95.5
200	5.9	5.7	95.1	95.5

* UEL = upper explosion limit

Source: JRC, 2020

Figure 12. Pressure and temperature effect on LEL and UEL for H_2-O_2 mixture

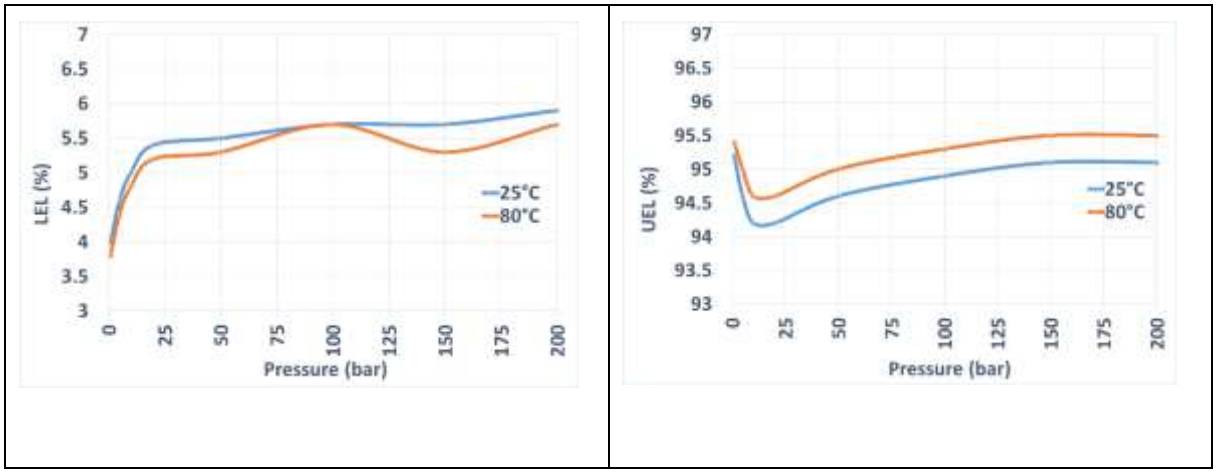

Source: JRC, 2020

iii. Oxygen production rate

The oxygen production rate is a direct consequence of the current applied with some loss depending on the overall system efficiency. Considering 100 % faradaic efficiency the oxygen production rate is:

$$\dot{n}_{O2,out} = \frac{I}{4F} \qquad \text{[Eq. 5.6]}$$

(with the number 4 in the denominator representing the number of electrons, z)

5.1.4 Cathode conditions

These are split in two classes: TIPs and TOPs which are discussed consecutively.

Cathode Test Input Parameters
For heat management purposes, liquid de-ionised water can also be fed to the cathode compartment, in parallel to the anode water feed. The related TIPs are identical to those for the anode water inlet (temperature, quality, pressure) discussed before. An additional TIP at cathode side is:

i. Hydrogen outlet pressure

The hydrogen pressure is measured at the outlet of the electrolysis cell/stack after the water mist and vapour removal components and before the backpressure regulation valve. The measured hydrogen pressure is fed as a feedback control signal to the water circulation pressure control loops for tests with the same pressure at anode and cathode sides. For differential operation mode, the hydrogen outlet pressure is the relevant TIP, because for safety reason oxygen outlet pressure is set at ambient or lower pressure.

Cathode Test Output Parameters
When optional cathode water feed is used for heat management purposes, the same TOPs apply as for the anode water feed. Additional TOPs at cathode side are:

i. Hydrogen purity

The hydrogen purity should be measured in real time at the exit of the cell or stack, after water removal (when the cathode operates under water flow) by techniques such as Gas Chromatography (GC), Mass Spectrometry (MS), Thermal Conductivity (TC) detector, or Galvanic Electrochemical Cell. The time interval between measurements is determined by the selected technique and the response characteristics of the method used. For research and characterization purposes, the composition of the hydrogen stream should be checked at least every 30 minutes.

Hydrogen purity levels not achievable directly by electrolysis can be increased by additional purification step(s). The main purification technologies available are Pressure Swing Absorption (PSA), Temperature swing absorption (TSA), cryogenic condensation, getter/palladium (Pd) membrane adsorption and deoxo-catalyst bed reactor.

The required hydrogen purity for commercial electrolyser systems depends upon its subsequent use. For example, for use in fuel cells, hydrogen purity should comply with the Fuel Quality Standards ISO 14687-2019 for fuel cell automotive applications and for fuel cell stationary applications. For all other industrial applications, the hydrogen purity level achieved by the electrolysis cell / stack should be mentioned.

In the absence of a real-time quality control system, for safety reason, it is recommended to monitor the presence of oxygen in the hydrogen outlet stream using a safety sensor to ensure that the hydrogen concentration does not drop below the Upper Explosion Limit (UEL) in a hydrogen-oxygen gas mixture. UEL increases with temperature and changes non-linearly with pressure as shown in Table 11. In practice, when the detected oxygen concentration exceeds 50 % of the (100-UEL) % difference, appropriate safety measures should be triggered.

ii. Hydrogen production rate

The hydrogen production rate is a direct consequence of the current applied with some loss depending on the overall system efficiency. With 100 % faradaic efficiency the hydrogen production rate is:

$$\dot{n}_{H2O,out} = \frac{I}{2F} = \dot{n}_{H2O,reacted} \qquad \text{[eq. 5.7]}$$

(z = 2 electrons)

5.1.5 Settings of TIPS for PEMWE reference operating conditions

The settings of the TIPs for the Reference Operating Conditions ("reference settings") for PEM Water Electrolysis for single cell and short stack are agreed as:

Table 12. Agreed reference settings for TIPs for PEMWE single cell and short stack testing

	Test Input Parameters	Unit	Reference Settings
Cell/short stack	Cell/Stack temperature	°C	60
	Water quality (conductivity) at recirculation loop ***inlet***	$\mu S.cm^{-1}$	≤1.0 ISO 3696 Grade 2 @ 25 °C
ANODE	Water inlet temperature	°C	60
	Water inlet pressure (absolute)	kPa; (bar)	100; (1)
	Water quality (conductivity) ***within recirculation loop***	$\mu S.cm^{-1}$	≤1.0 ISO 3696 Grade 2 @ 25 °C
	Minimum Water inlet flowrate	$mL.min^{-1}.cm^{-2}$	2.0
	Oxygen outlet pressure (absolute)	kPa; (bar)	100; (1)
CATHODE	Water inlet temperature	°C	60
	Minimum Water inlet flowrate (if applied)	$mL.min^{-1}.cm^{-2}$	2.0
	Hydrogen outlet pressure (abs)	kPa; (bar)	100; (1)

Source: JRC, 2020

5.1.6 Test hardware configuration and requirements for measurement devices of TIPs and TOPs for PEMWE cell/stack testing

To enable accurate control of the experimental conditions during cell and stack testing, the characteristics and location of the required instrumentation should be carefully considered. A general overall hardware configuration with location of TIPs and TOPs to be measured is schematically shown in Figure 13.

Figure 13. Scheme of PEM single cell/stack testing apparatus including position of the monitoring devices

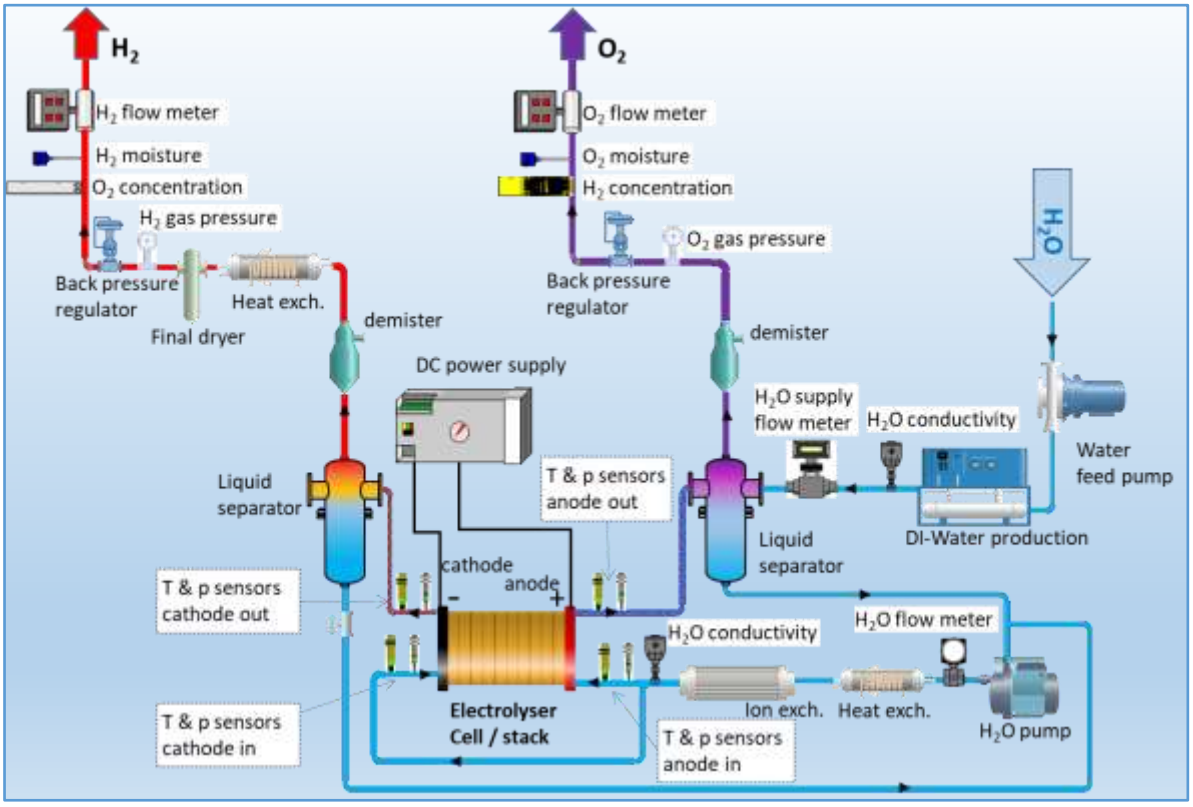

Source: JRC, 2020

Table 13 summarises the location of sensors or measuring devices (as in the figure above).

For testing apparatus with different configuration, the position and number of the sensor shall be given in the test results reporting.

Table 13. Sensor type/location for PEMWE cell/stack testing

INPUT /OUTPUT PARAMETER	TIP/TOP	POSITION OF SENSORS
Current intensity (or current density)	TIP	Power supply module
Cell/Stack voltage	TOP	Cell hardware, current collectors, voltage terminals
Temperatures		
Cell	TIP	Anode (TIP), and cathode BPPs, as close as possible to MEA
Water, anode inlet	TIP	As close as possible to cell/stack hardware inlet
Water, anode outlet	TOP	As close as possible to cell/stack hardware outlet
Water, cathode inlet (optional)	TIP	As close as possible to cell/stack hardware inlet
Water, cathode outlet (optional)	TOP	As close as possible to cell/stack hardware outlet
Pressures		
Water, anode inlet	TIP	As close as possible to cell/stack hardware inlet
Water, anode outlet	TOP	As close as possible to cell/stack hardware outlet
Water, cathode inlet (optional)	TIP	As close as possible to cell/stack hardware inlet, if in use
Water, cathode outlet (optional)	TOP	As close as possible to cell/stack hardware outlet
H_2, outlet	TIP	After liquid and vapour separation
O_2, outlet	TIP	After liquid and vapour separation
Flow rates		
Water feed to cell/stack	TIP	De-ionised water (DIW) cell inlet
Water make-up	TOP	Outlet de-ionised water (DIW) production
Hydrogen	TOP	After water knockout
Oxygen	TOP	After water knockout
Water quality		
Water conductivity	TIP	Outlet DIW production & recirculation loop
Gas safety sensors		
Hydrogen concentration	TOP	H_2 gas sensor in O_2 outlet
Oxygen concentration	TOP	O_2 gas sensor in H_2 outlet

Source: JRC, 2020

The type of measurement devices for the TIPs and TOPs should be selected based on the required range, accuracy, and sampling rate as indicated in Table 14. Measuring equipment should be regularly calibrated.

Table 14. Required measurement accuracy and sampling rate

Parameter to be measured	Unit	Required Measurement accuracy	Sampling rate Performance test	Sampling rate Durability test
Current	A	± 0.1 %	≥1 Hz	≥0.0166 Hz
Temperature	°C	± 2 K	≥1 Hz	≥0.0166 Hz
Cell voltage	*V*	± 1 mV	≥1 Hz	≥0.0166 Hz
stack voltage	*V*	± 0.5 %	≥1 Hz	≥0.0166 Hz
Pressure	kPa	± 2 %	≥1 Hz	≥0.0166 Hz
Water Flow rate	$L.min^{-1}$	± 2 %	≥1 Hz	≥0.0166 Hz
Gas Flow rate	$L.min^{-1}$	± 2 %	≥1 Hz	≥0.0166 Hz
Gas concentration	%	± 1 %	≥1 Hz	≥0.0166 Hz

Source: JRC, 2020

For the generation of valid results from *in-situ* tests the following conditions have to be met during the full test duration:

- As a minimum all the TIPs and TOPs listed in Table 13 shall be measured
- The measurement accuracy and sampling rate shall meet the specifications listed in Table 14
- The temperature difference between water outlet and water inlet shall not exceed +/- 2K.
- Any deviation from the suggested hardware configuration and/or from the location of measuring devices shall be reported

The incorporation of additional temperature sensors at appropriate locations in the test rig layout can provide supplementary information on performance in terms of efficiency of the cell/short stack (see Chapter 7). Depending upon the functional performance of its components and of the cell/short stack itself, efficiency may be affected, e.g. by recuperating heat by the introduction of exchangers at different locations.

5.2 Reference operating conditions for AWE cell/short stack testing

This subsection discusses TIPs and TOPs for *in-situ* testing of alkaline water electrolysis single cells and short stacks. Where possible and relevant, it refers back to those for PEMWE, while differences with PEMWE are elaborated specifically.

5.2.1 Cell temperature (TIP)

Depending upon the test bench configuration, a number of cases can be differentiated for the location of the temperature sensor:

i. Temperature sensor located close to the electrodes:
   - The cell temperature is that indicated by the sensor in the anode side.

ii. Temperature sensor located in the electrolyte circuit:
   - The cell temperature is equal to the average temperature of the electrolyte measured at anode and cathode inlets.

For the second case, the uniformity of the electrolyte temperature between inlet and outlet of the cell is important and the temperature difference between outlet and inlet should be minimised.

5.2.2 Water quality (TIP)

Considering the high alkalinity of the electrolyte it is important to reduce impurities in the replenishing water by a demineralisation treatment (or possibly de-ionisation for higher purity levels) to minimise the concentration of magnesium, iron and calcium ions in the feed water to avoid precipitation of their hydroxides, which may cause a performance reduction over time. The dissolution of carbon dioxide (CO_2) from the ambient air in the caustic electrolyte should also be minimised. Requirements at system level are given by the manufacturer (e.g. concentration for Ca/Mg/Fe, ions, Chloride ions (Cl^-), carbonate (CO_3^{2-}), sulphate ions (SO_4^{2-}), silicon (Si), etc.; for laboratory testing de-ionised water with 1 $\mu S.cm^{-1}$ conductivity has been agreed as the reference to be used.

5.2.3 Electrolyte TIPs

The circulation of the electrolyte can be implemented in two different ways, (i) mixed circuit and (ii) separated circuit:

i- mixed circuit: after separation of product gas from the electrolyte exiting each half-cell, both electrolyte streams are mixed, and the concentration is adjusted by water replenishment. As both electrolyte streams still contain remaining product gases soluble in the electrolyte solution, their mixing causes losses and higher gas impurities.

ii- separated circuit: the electrolyte streams are kept separated. Water formation on the anode side results in a decreased concentration, while water consumption on the cathode side increases the concentration. Occasional mixing of the two electrolyte streams is needed to re-establish the optimal concentration.

The TIPs below relate to the presence of an aqueous alkaline solution acting as liquid electrolyte and contributing to heat management.

i. Inlet temperature

One of the electrolyte temperature measured at anode and cathode inlets serves as TIP when the cell temperature cannot be measured in the bipolar plate. The temperature in this case should be measured as close as possible at the inlet of the cell/stack.

ii. Inlet pressure

Typically test benches have controlled back pressure valves positioned in the exhaust gas stream close to the cell outlet. Therefore, the pressure regulation is normally performed at cell outlet. Alkaline electrolysers are either operated with the same pressure (balanced pressure) on both compartments (sides), or with a very small differential pressure to limit cross-permeation of the electrolyte with its dissolved gases through the porous separator.

iii. Inlet concentration

The concentration of the aqueous solution electrolyte is measured at the inlet of the cell and adjusted to the set value with fresh de-mineralised water replenishment to maintain the correct specific conductivity of the electrolyte. Examples of the specific conductivity change with electrolyte concentration for NaOH and KOH are given in Figure 14. The ionic conductivity increases with electrolyte concentration up to a value beyond which Coulombic force interactions between ions result in a reduction of the conductivity.

Figure 14. Specific electrolyte conductivity as a function of the electrolyte concentration and temperature

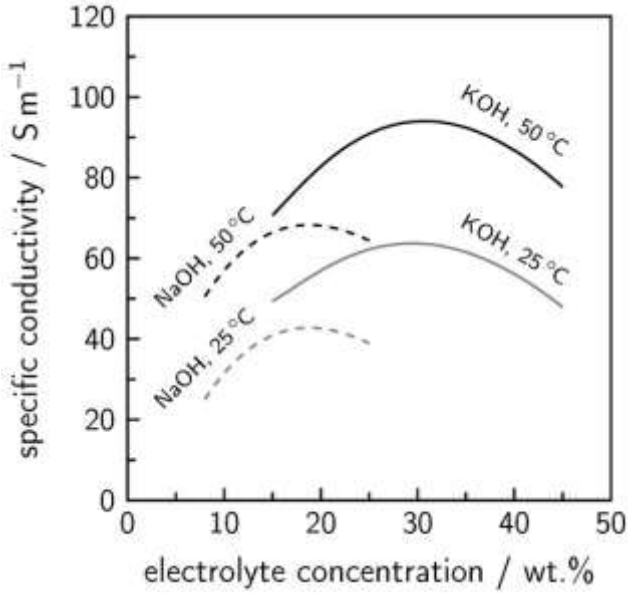

 Processes 2020, 8(2), 248; https://doi.org/10.3390/pr8020248

iv. Inlet Flow rate

Electrolyte flow operation can be done without pump aid through natural convection. The associated savings of the reduced BOPs are counter-balanced by the risk of increasing the gas coverage of electrodes, hence requiring a higher operation cell voltage. Nevertheless, for optimal process control the electrolyte is constantly pumped through the cell to maintain the electrolysis reaction and contribute to heat management. The circulation flowrate is hence set to minimise both the concentration difference and the temperature difference between inlet and outlet.

5.2.4 Anode conditions

i. Oxygen outlet pressure *(TIP)*

In pressure balanced operation mode, the oxygen outlet pressure equals the hydrogen outlet pressure TIP. High outlet pressures increase the concentration of H_2 in O_2 at anode outlet and O_2 in H_2 and at cathode outlet and thereby the risk of explosion, as shown in figure 15 for the anode side. The concentration does not depend only upon current density but other operating conditions like pressure as shown, temperature, separator material and design.

Figure 15. Anodic gas impurity (H_2 in O_2) in relation to current density at different pressure levels for (a) separated and (b) mixed electrolyte cycles

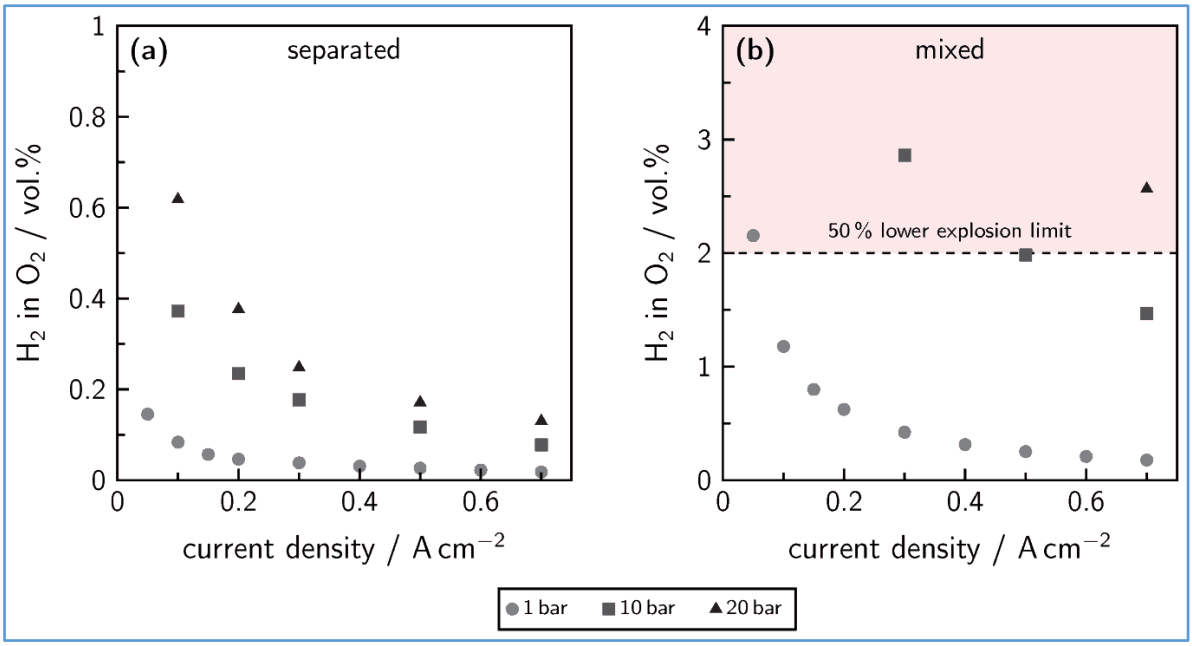

Processes 2020, 8(2), 248; https://doi.org/10.3390/pr8020248

ii. Oxygen quality *(TOP)*

The typical oxygen purity is in the range 99.0 to 99.5 vol %. The most relevant impurity is hydrogen crossing the separator. The gas crossover is mainly due to gas dissolution in the electrolyte and diffusion through the separator, and hence depends upon pressure (*p*), current density (*i*) and electrolyte circulation configuration, either with separate or mixed cycle. With increasing pressure, more molecular hydrogen is dissolved in the electrolyte and therefore more hydrogen can reach the other half-cell. Increasing current density results in higher hydrogen generation and considering that current does not affect the amount of gas crossing the separator, higher dilution of the crossing hydrogen. Operation with mixed electrolyte circulation increases the level of contamination.

An example of hydrogen concentration in the oxygen outlet stream by changing pressure, current density and electrolyte flow segregation is given in Figure 15 for a 32 % concentrated electrolyte at 60 °C and 0.35 $L.min^{-1}$ flow rate.

iii. Oxygen production rate *(TOP)*

See 5.1.3.

iv. Electrolyte concentration at anode outlet *(TOP)*

The concentration difference between electrolyte outlet and inlet serves as a test validity criterion and should not exceed +/- 5 wt. % (see Table 15).

v. Electrolyte temperature at anode outlet *(TOP)*

The temperature difference between electrolyte outlet and inlet serves as a test validity criterion and should not exceed +/- 2 K (see Table 15).

5.2.5 Cathode conditions

i. Hydrogen outlet pressure *(TIP)*

See 5.2.4 i.

TOPs at cathode side are:

ii. Hydrogen quality *(TOP)*

See 5.1.4

iii. Hydrogen production rate *(TOP)*

See 5.1.4

5.2.6 Setting of TIPs for AWE reference operating conditions

The settings of the TIPs for the Reference Operating Conditions ("reference settings") for alkaline water electrolysis for single cell and short stack are agreed as:

Table 15. Agreed reference settings for TIPs for AWE single cell and short stack testing

	Test input parameters	Unit	Reference Settings
cell / short stack	Cell / stack temperature	°C	80
	Conductivity of water used for electrolyte preparation and supply to electrolyser	$\mu S.cm^{-1}$	≤1, ISO 3696 Grade 2 @ 25 °C
ANODE	Electrolyte inlet temperature	°C	80
	Electrolyte inlet pressure	kPa; (bar)	100; (1)
	Electrolyte inlet concentration	KOH wt.%	30
	Minimum electrolyte inlet flow rate	$mL.cm^{-2}.min^{-1}$	1
	Oxygen outlet pressure (absolute)	kPa; (bar)	500, (5)
CATHODE	Electrolyte inlet temperature	°C	80
	Electrolyte inlet pressure	kPa, (bar)	100, (1)
	Electrolyte inlet concentration	KOH wt.%	30
	Minimum electrolyte inlet flow rate	$mL.cm^{-2}.min^{-1}$	1
	Hydrogen outlet pressure (absolute)	kPa; (bar)	500; (5)

Source: JRC, 2020

5.2.7 Test hardware configuration and requirements for measurement devices of TIPs and TOPs

Figure 16 shows a scheme with the location of the instrument measuring points for an alkaline water electrolysis experimental set-up. Selection of the sensors shall consider the caustic corrosion effects due to the electrolyte.

Figure 16. Scheme of AW Electrolyser with the position of monitoring devices

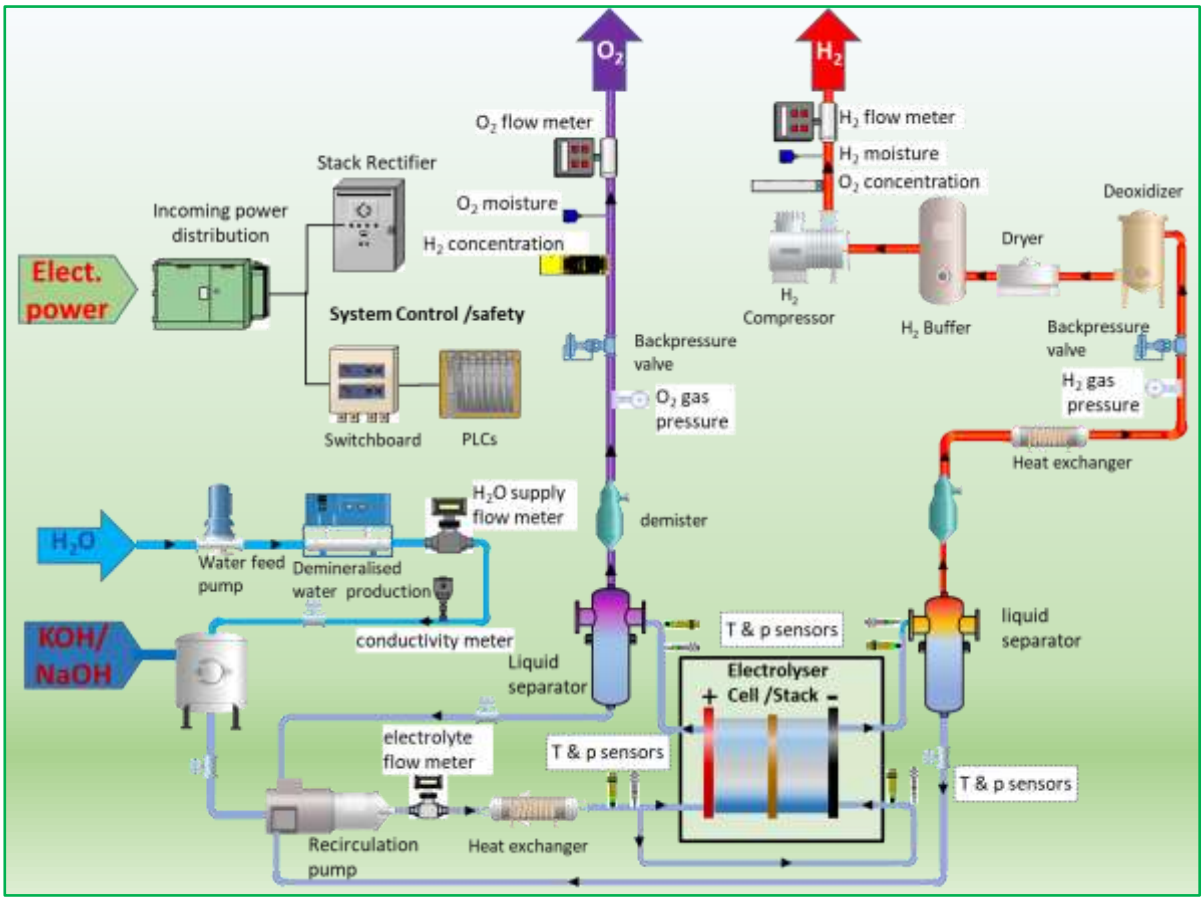

Source: JRC, 2020

Table 16 summarises the location of sensors or measuring devices (as in the figure above).

The incorporation of additional temperature sensors at appropriate locations in the test rig layout can provide supplementary information on performance in terms of efficiency of the cell/short stack (see Chapter 7). Depending upon the functional performance of its components and of the cell/short stack itself, efficiency may be affected, e.g. by recuperating heat by the introduction of exchangers at different locations.

Table 16. Sensor type/location for AWE cell/stack testing

INPUT / OUTPUT PARAMETER	TIP/TOP	LOCATION OF SENSOR
Current intensity (or current density)	TIP	Power supply module
Cell/Stack voltage	TOP	Cell hardware, current collectors, voltage terminals
Temperatures		
Cell Temperature	TIP	Close to electrodes, TIP uses anode as reference
Anode inlet	TIP	As close as possible to cell/stack hardware inlet
Anode outlet	TOP	As close as possible to cell/stack hardware outlet
Cathode inlet	TIP	As close as possible to cell/stack hardware inlet
Cathode outlet	TOP	As close as possible to cell/stack hardware outlet
Pressures		
Electrolyte Anode inlet	TIP	As close as possible to cell/stack hardware inlet
Electrolyte Anode outlet	TOP	As close as possible to cell/stack hardware outlet
Electrolyte Cathode inlet	TIP	As close as possible to cell/stack hardware inlet
Electrolyte Cathode outlet	TOP	As close as possible to cell/stack hardware outlet
H_2 outlet	TIP	After liquid and vapour separation
O_2 outlet	TIP	After liquid and vapour separation
Flow rates		
Electrolyte recirculation	TIP	Recirculation loop
Water make-up	TOP	Outlet demineralised/DI water production
Hydrogen	TOP	Mass Flow Meter after water knockout
Oxygen	TOP	Mass Flow Meter after water knockout
Water quality		
Water conductivity	TIP	Outlet demineralised water/DI production & recirculation loop
Gas safety sensor		
Hydrogen concentration	TOP	H_2 gas sensor in O_2 outlet
Oxygen concentration	TOP	O_2 gas sensor in H_2 outlet

Source: JRC, 2020

For the generation of valid results from *in-situ* tests the following conditions have to be met during the full test duration:

- As a minimum all the TIPs and TOPs listed in Table 15 shall be measured

- The measurement accuracy and sampling rate shall meet the specifications listed in Table 14
- The temperature difference between electrolyte outlet and electrolyte inlet shall not exceed +/- 2 K.
- The concentration difference between electrolyte outlet and electrolyte inlet shall not exceed +/- 5 wt.%.
- Any deviation from the suggested hardware configuration and/or from the location of measuring devices shall be reported.

5.3 AEMWE reference operating conditions

Because of the similarities between PEMWE and AEMWE, the same set of 'Reference Operating Conditions' as those for PEMWE can be used for AEMWE for both single cells and short stacks.

5.3.1 Cell temperature

See 5.1.1

5.3.2 Water quality

See 5.1.2

In case of anion exchange membranes (AEM) operated under alkaline conditions. the dissolved carbon dioxide (CO_2) should be monitored and controlled to minimise the negative effects of bicarbonates and carbonates ions.

5.3.3 Anode operating conditions

See 5.1.3

5.3.4 Cathode operating conditions

See 5.1.4

5.3.5 Settings of TIPs for AEMWE reference operating conditions

The settings of the TIPs for the Reference Operating Conditions ("reference settings") for Anion Exchange Membrane Water Electrolysis for single cell and short stack are agreed as shown in Table 17.

For further testing in alkaline environment, it is possible to replace water as electrolyte using a KOH solution with molarity comprised between 0.20 M or 1.00 M or alternatively a 1.00 M potassium carbonate (K_2CO_3) solution.

Table 17. Agreed reference settings for TIPs for AEMWE single cell and short stack testing

	Test Input Parameters	Unit	Reference Settings
Cell/short stack	Cell / stack temperature	°C	50
	Water quality (conductivity) at recirculation loop ***inlet***	$\mu S.cm^{-1}$	≤1.0 ISO 3696 Grade 2 @ 25 °C
ANODE	Water inlet temperature	°C	50
	Water inlet pressure (absolute)	kPa; (bar)	100; (1)
	Water quality (conductivity) ***within recirculation loop***	$\mu S.cm^{-1}$	<1.0 ISO 3696 Grade 2 @ 25 °C
	Minimum Water inlet flowrate	$mL.min^{-1}.cm^{-2}$	2.0
	Oxygen outlet pressure	kPa; (bar)	100; (1)
CATHODE	Water inlet temperature	°C	50
	Water inlet pressure (absolute)	kPa; (bar)	100; (1)
	Water quality	$\mu S{\cdot}cm^{-1}$	<1.0 ISO 3696 Grade 2 @ 25 °C
	Minimum Water inlet flowrate	$mL.min^{-1}.cm^{-2}$	2.0
	Hydrogen outlet pressure (absolute)	kPa; (bar)	100; (1)

Source: JRC, 2020

5.3.6 Test hardware configuration and requirements for measurement devices of TIPs and TOPs

Figure 17 shows a scheme with the location of the instrument measuring points for an AEM water electrolysis experimental set-up.

Figure 17. Scheme of AEMW electrolyser with the position of monitoring devices

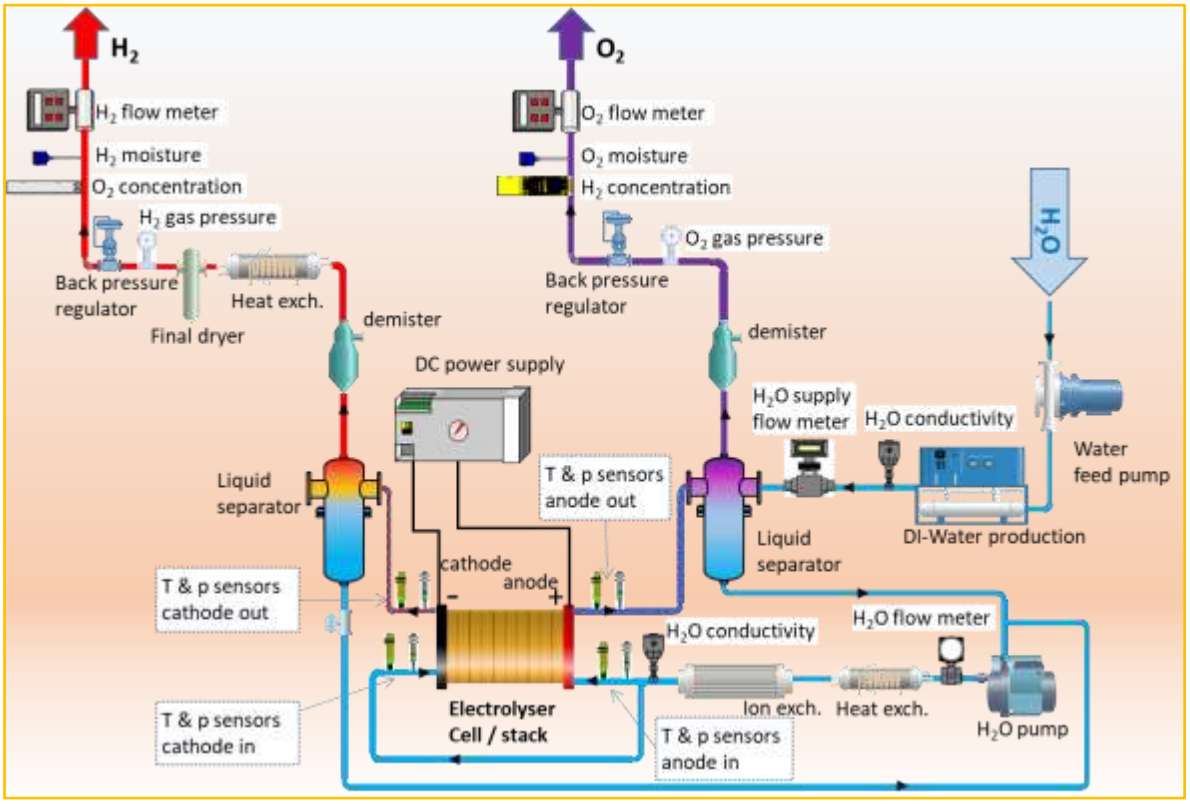

Source: JRC, 2020

For the generation of valid results from *in-situ* tests the following conditions have to be met during the full test duration:

- Considering the similarity with PEMWE the minimum set of TIPs and TOPs listed in Table 13 shall be measured
- The measurement accuracy and sampling rate shall meet the specifications listed in Table 14
- The temperature difference between water outlet and water inlet shall not exceed +/- 2 K.
- Any deviation from the suggested hardware configuration and/or from the location of measuring devices shall be reported.

The incorporation of additional temperature sensors at appropriate locations in the test rig layout can provide supplementary information on performance in terms of efficiency of the cell/short stack (see Chapter 7). Depending upon the functional performance of its components and of the cell/short stack itself, efficiency may be affected, e.g. by recuperating heat by the introduction of exchangers at different locations.

6 Stressor conditions for single cell and short stack testing

6.1 Approach

In this chapter a methodology has been established for examining the relative influence that TIPs deviating from the reference operating conditions (Chapter 5) exert on the performance and durability of single cells and short stacks. The methodology is also applied to investigate the effects of a number of important factors which may cause deviation from normal operation. The factors causing such deviation are hereafter called "stressors".

Investigating the effects of the identified stressors on cell and stack performance and durability, requires a systematic approach that consists of two consecutive stages. First the relevant types of stressors affecting behaviour at cell and stack level are identified (Section 6.2). Following this identification of relevant stressor types, the second element in this approach is to investigate how cells and stacks behave under the identified stressor conditions, which consists of quantifying the effects of the considered stressors on cell and short stack performance and durability, by performing *in-situ* tests. In these tests, different settings from those corresponding to the reference operation conditions are used for the TIPs identified in Chapter 5.

6.2 Types of stressors for single cells and short stacks

Table 18 identifies the types of stressors which are briefly discussed below. The first two stressor types are extensively covered in the following parts of this report, whereas the other four are not further considered.

Table 18. Categories of stressors

1	**STRESSORS DUE TO OPERATING CONDITIONS**
2	**STRESSORS DUE TO LOAD CYCLING**
3	**STRESSORS DUE TO MECHANICAL EFFECTS**
4	**STRESSORS DUE TO SEAL LEAKAGE**
5	**STRESSORS DUE TO WATER QUALITY**
6	**STRESSORS DUE TO ENVIRONMENTAL CONDITIONS**

Source: JRC, 2020

6.2.1 Stressors due to operating conditions

These stressors cover both higher and lower settings of the TIPs considered in Chapter 5. Because different TIPs apply for the three considered low-temperature electrolysis technologies, different sets of operational stressor conditions are used for each technology in sections 6.4 to 6.6 below.

6.2.2 Load cycling

Load cycling is applied in cell and stack testing to simulate the variable operating conditions, including transients associated to 'start-up and stop' sequences that electrolyser systems experience in practice and that affect performance and durability. Durability is evaluated through endurance testing by applying a repetitive load profile and measuring performance degradation rate in terms of cell/stack voltage increase rate as function of operating hours (see Chapter 7). To assess degradation rate, a representative dynamic load profile is required. Such load profiles are derived from the Real-World Degradation (RWD) profiles which represent a simplification of the load profiles that electrolyser systems are expected to encounter in a number of service applications.

6.2.3 Mechanical stressors

These include, e.g. the compression force applied to the cell (in single cell or short stack configuration), which is however fixed at the beginning of the test and not expected to change during *in-situ* testing; hence it will not be further considered in this report. Mechanical effects may also arise from variations in environmental conditions (pressure, temperature) as well as from acceleration and deceleration forces. Because these variations rather affect the performance and durability at system than at cell and short stack level, they are not considered here. Other mechanical stressors are vibrations induced by Balance of Plant (BoP) components like pumps, PSA, compressors, etc. These effects are also not considered in this document.

6.2.4 Seal leakage

Leakage of seals can cause mechanical degradation of gaskets, particularly in the presence of pressure cycling, which may result in gas leakage. This represents more a safety than a performance issue and is therefore not covered in this report. However, the occurrence of possible leakages should be monitored using a leak test apparatus.

6.2.5 Water quality

The tolerance of cells/stacks to water impurity level is an important factor. However, because of experimental difficulties/limitations to actively control water impurity level (decrease and/or increase of contaminants) in most test bench hardwares, this stressor is considered in this report as optional, when feasible. A commonly used method for characterising water quality is through electrical conductivity measurement which reflects the total amount of ions present but does not allow differentiating between chemical species. When relevant for the experimental campaign, ion selective sensors (i.e. fluoride, magnesium, calcium, etc.) or other type of sensors can be added in the circulation loop for continuous monitoring, or water can be sampled and analysed with other type of chemical analysis for *ad hoc* monitoring.

6.2.6 Environmental conditions

Environmental conditions are mostly relevant at system level, such as cold start and freeze when the system is exposed to sub-zero temperatures. For single cell and stack applications this stressor is not applicable and is not addressed within this document.

6.3 Operating condition stressors for single cell and short stack testing

The reference settings for the TIPs identified in Chapter 5 in principle correspond to the centre of the normal operation window. Stressors due to operating conditions relate to operation of the cell or stack at TIP settings falling outside of this operation window.

In principle *in-situ* tests under operation stressor conditions should enable to determine the effects of stressors associated to a specific TIP separately from the effect caused by other stressors. However, because performance in *in-situ* tests depends upon a number of factors, and is therefore affected by a number of TIPs, such discrimination between the effects of the considered operation stressors may not be possible. For that reason, and for limiting the test effort, operation stressors are identified for a reduced number of TIPs than those considered in Chapter 5, by selecting the ones that are more sensitive to process variation and that are adjustable within the majority of laboratory test benches, and for each of these stressors two settings are presented, one higher and one lower than the reference setting, respectively.

For each operation stressor, the expected effect of increase or of decrease of its setting compared to the reference settings agreed in Chapter 5 is discussed.

Because similarly to the reference settings identified in Chapter 5, settings for operating condition stressors differ for the different electrolysis technologies, the effects of operation stressors specific for each technology are discussed separately.

6.4 Effects of operation stressors for PEMWE

6.4.1 PEMWE anode stressors

i. Cell temperature stressor – water temperature stressor

Higher operating temperatures generally have a positive effect due to better electrochemical performance caused by increase of reaction kinetics and the reduction of membrane potential drop, resulting then in a higher current density at the same operating voltage or higher hydrogen production rate at the same efficiency.

Lower operating temperatures generally have a negative effect on performance but may result in a lower degradation rate, provided that the cell/stack is not operated above nominal voltage to compensate for lower reaction kinetics to maintain the hydrogen production rate.

ii. Water quality stressor

Water quality can have an important immediate or short-term effect (in minutes to hour scale) on performance, e.g. through poisoning the electrolyte and/or the electrodes, or by catalysing the formation of products, e.g. hydrogen peroxide, causing membrane degradation. The sensitivity of performance to water quality is usually expressed in terms of increase in ohmic resistance and electrode overpotential.

iii. Water inlet flow rate stressor

Too low water inlet flowrate may result in insufficient wetting, with risk of creating dry active area hot spots. It may also decrease the removal rate of gas bubbles from the membrane surface, resulting in hotspots or increased overvoltage (e.g. bubble overpotential).

When the water inlet flowrate is too high, the increased speed and pressure can accelerate catalyst loss due to dissolution/erosion effects.

iv. Oxygen outlet pressure stressor

Oxygen pressure increases the oxygen crossover, which might result in explosive gas mixtures. However, a lot of permeated oxygen will recombine with evolved hydrogen at the cathodic Pt-particles. During this reaction, radicals are formed which can lead to ionomer degradation in the membrane.

Oxygen outlet pressure stressor test is recommended to be performed only if proper safety measures related to oxygen use are implemented.

v. Water inlet pressure stressor

Water pressure could be relevant for temperature near or above 100 °C due to the effect on the two-phase liquid water/vapour ratio. As the stressor test conditions (Table 19) are limited to 80 °C, this stressor is not considered.

6.4.2 PEMWE cathode stressors

i. Water temperature stressor

When water circulation is implemented at the cathode side, water temperature is assumed to be the same of the anode one.

ii. Hydrogen outlet pressure stressor

Hydrogen pressure affects both hydrogen cross-over and leakage to the exterior and is affected by the electrolyser operation mode, balanced (same pressure applied at the anode and cathode side) or differential mode (different pressure in the two compartments creating additional mechanical stress on the MEA).

From a thermodynamic point of view, increasing hydrogen pressure is expected to increase the cell voltage. Experimental data shows that this effect is not so evident, which is likely due to the beneficial effects of pressure increase on kinetic and mass transport overvoltages. The kinetic effect may result from improved water circulation into the porous structure of the catalyst layer, while a reduction of vapour contribution in the two-phase flow, reduced viscosity and surface tension for liquid phase may be beneficial to the mass transport.

6.4.3 Settings of operation stressors for PEMWE

Table 19 shows the agreed reference, low and high settings for operation stressors for PEMWE single cells and short stacks. As indicated in the table, a total number of 8 tests is proposed for comparing the effect of operation stressors on the performance of PEMWE cells and short stacks with the performance obtained under reference operating conditions. The parameters modified for the specific stressor test are indicated by red font in Tables 19, 20 and 21.

Table 19. Agreed settings of operation stressors for PEMWE single cell and short stack testing

	Parameters	Unit	Reference Setting	Cell Temperature Stressor settings		Hydrogen Pressure Stressor settings ([9])	Oxygen Pressure Stressor settings([9])	Water quality (conductivity) at the *recirculation loop* Stressor setting		Water inlet minimum flowrate cell/stack (with recirculation) stressor setting	
				Test 1	Test 2	Test 3	Test 4	Test 5	Test 6	Test 7	Test 8
	Cell / stack temperature	°C	60	40	90	60	60	60	60	60	60
ANODE	Water inlet temperature	°C	60	40	90	60	60	60	60	60	60
ANODE	Water quality (conductivity) at the *recirculation loop*([8])	$\mu S.cm^{-1}$	≤1.0	≤1.0	≤1.0	≤1.0	≤1.0	≤0.1	≤5.0	≤1.0	≤1.0
ANODE	Minimum Water inlet flowrate cell/stack (with recirculation)	$mL.min^{-1}.cm^{-2}$	2.0	2.0	2.0	2.0	2.0	2.0	2.0	0.5	2.5
ANODE	Oxygen outlet pressure (absolute)	kPa	100	100	100	100	3,000[9]	100	100	100	100
CATHODE	Water inlet temperature	°C	60	40	90	60	60	60	60	60	60
CATHODE	Hydrogen outlet pressure (absolute)	kPa	100	100	100	3,000([9])	3,000([9])	100	100	100	100

Source: JRC, 2020

([8]) Optional test to be done only if feasible with test bench

([9]) In case of equipment/safety limitation a pressure limited to 500 kPa should be used as testing point.

6.5 Effects of operation stressors for AWE

For *in-situ* testing of AWE cells and short stacks, the effects of the operation stressors at anode and cathode are qualitatively similar to those considered for PEMWE.

6.5.1 AWE anode stressors

i. Cell temperature stressor – electrolyte temperature stressor

For AWE the temperature has a direct effect on the electrolyte conductivity as shown in Figure 14. The higher the temperature the lower is the viscosity, which increases ion mobility and hence conductivity. This conductivity increase at higher temperatures has a positive effect on performance because the ohmic overvoltage is reduced. In addition, higher operating temperature generally positively affects performance due to increased reaction kinetics.

A negative effect of higher temperature could be on the durability of components in contact with the caustic/alkaline environment.

ii. Water quality stressor

Water quality can have an important immediate or short-term effect (in minutes to hour scale) on performance, e.g. through poisoning the electrolyte and/or the electrodes. As previously mentioned, presence of magnesium, iron and calcium cations forming low soluble hydroxides may affect electrolyte performance.

iii. Electrolyte inlet flow rate stressor

Electrolyte inlet flow rate has an important effect on the thermal balance of the electrolysis cell. Additionally, through its effect on gas bubble formation, it affects cell ohmic resistance through two mechanisms: (i) the barrier effect on the electrode surface and (ii) the void fraction in the electrolyte. Higher flowrate has in general a positive effect because it facilitates the removal of gas bubbles from the reacting surfaces and from the electrolyte solution. The inlet flow rate also affects the concentration of the electrolyte at electrolyser output, with higher flowrate resulting in smaller concentration difference.

A negative effect of higher electrolyte inlet flowrate can arise from increased erosion that can contribute to reducing cell durability. A higher inlet flow rate also increases power need, reducing overall efficiency.

iv. Oxygen outlet pressure stressor

Oxygen outlet pressure stressor test is not considered for this technology for safety considerations.

6.5.2 AWE cathode stressors

i. Hydrogen outlet pressure stressor

Hydrogen pressure affects both hydrogen cross-over and leakage to the exterior.

ii. Water quality stressor

See 6.5.1.ii

6.5.3 Settings of operation stressors for AWE

Table 20 shows the agreed reference, low and high settings for operation stressors for AWE single cells and short stacks. As indicated in the table, a total number of 5 tests is proposed for comparing the effects of operation stressors on the performance of AWE cells and short stacks with the performance obtained under reference operating conditions.

Electrolyte concentration is not included in the set of operation stressors because of the experimental difficulty associated to varying it in a well-controlled manner, as also applies for the operational stressor on water feed quality.

Table 20. Agreed settings of AWE stressorsfor AWE single cell and short stack testing

	PARAMETERS	UNIT	REFERENCE Setting	Cell Temperature Stressor settings		H2 Pressure Stressor settings	Electrolyte Inlet Flowrate Stressor settings	
				Test 1	Test 2	Test 3	Test 4	Test 5
	Cell/stack temperature	°C	80	50	100	80	80	80
ANODE	Electrolyte inlet temperature	°C	80	50	100	80	80	80
ANODE	Minimum Electrolyte inlet flowrate	$mL.cm^{-2}.min^{-1}$	1	1	1	1	0.25	2
CATHODE	Electrolyte inlet temperature	°C	80	50	100	80	80	80
CATHODE	Minimum Electrolyte inlet flowrate	$mL.cm^{-2}.min^{-1}$	1	1	1	1	0.25	2
CATHODE	Hydrogen outlet pressure	kPa	500	500	500	3,000([10])	500	500

Source: JRC, 2020

([10]) In case of equipment/safety limitation a pressure limited to 1000 kPa or the maximum allowed by the test set-up should be used as TIP.

6.6 Effect pf operation stressors for AEMWE

For *in-situ* testing of AEMWE cells and short stacks, the effects of the identified operation stressors are qualitatively similar to those considered for PEMWE but considering the different role of anode and cathode.

6.6.1 Settings of operation stressors for AEMWE

Table 21 shows the agreed reference, low and high settings for operation stressors for AEMWE single cells and short stacks. As indicated in the table, a total number of 7 tests is proposed for comparing the effect of operation stressors on the performance of AEMWE cells and stacks with the performance obtained under reference operating conditions.

Table 21. Agreed settings of stressors for AEMWE single cell and short stack testing

	Parameters	Unit	Reference setting	Cell Temperature Stressor settings		Hydrogen Pressure Stressor settings	Water quality (conductivity) at the *recirculation loop* Stressor setting		Water inlet flowrate cell/stack (with recirculation) stressor setting	
				Test 1	Test 2	Test 3	Test 4	Test 5	Test 6	Test 7
	Cell/stack temperature	°C	50	30	65	50	50	50	50	50
ANODE	Water inlet temperature	°C	50	30	65	50	50	50	50	50
ANODE	Minimum Water inlet flowrate (with recirculation)	$mL.min^{-1}.cm^{-2}$	1	1	1	1	1	1	0.5	1.5
CATHODE	Water inlet temperature	°C	50	30	65	50	50	50	50	50
CATHODE	Water quality (conductivity) at the *recirculation loop*([11])	$\mu S.cm^{-1}$	<1	<1	<1	<1	<0.1	<5	<1	<1
CATHODE	Minimum Water inlet flowrate (with recirculation)	$mL.min^{-1}.cm^{-2}$	2	2	2	2	2	2	0.5	2.5
CATHODE	Hydrogen outlet pressure (absolute)	kPa	100	100	100	3,000([12])	100	100	100	100

Source: JRC, 2020

([11]) Optional test to be done only if feasible with test bench.

([12]) In case of equipment/safety limitation a pressure limited to 500 kPa should be used as testing point.

7 *In-situ* testing of sinle cells and short stacks

Testing of single cells and short stacks aims at characterising the performance and the durability of their constituent materials and components under experimental conditions that can provide relevant information about their behaviour when incorporated in electrolyser systems. As introduced in Chapter 4, such testing requires covering experimental conditions which simulate operation under reference conditions (Chapter 5) as well as under stressor conditions (Chapter 6), covering both static and dynamic loading conditions (Chapter 7). Results of these tests provide information on the performance of the cells and short stacks at a given moment in time.

Durability is a measure of the capability of a single cell/short stack to maintain its performance over a period of time. The measured performance is usually compared that established at BoT.

The sections in this chapter sequentially discuss aspects pertaining to both characteristics, performance and durability.

7.1 Performance indicators

The performance indicators for tests under Reference Operating Conditions and Stressor Conditions are presented in Table 22 for the three different low temperature water electrolysis technologies.

Table 22. LTWE Performance indicators

	Indicator	
1	**Cell/short stack voltage U measured at current densities *j***	• **PEMWE: 1.0 A/cm², 2.0 A/cm², and when feasible, *j* = 3.0 A/cm² and 6.0 A/cm²** • **AWE: 0.3 A/cm², 0.5 A/cm², 1.0 A/cm²** • **AEMWE: 0.4 A/cm², 0.8 A/cm², 1.0 A/cm²**
2	**Energy efficiency ε at covered current densities *j***	• **Eq. 7.2 cell;** • **Eq. 7.3 stack**
3	**Current efficiency η_I at covered current densities *j***	• **Eq. 7.6 cell;** • **Eq. 7.7 stack**
4	**Total efficiency η_ω at current densities *j***	• **Eq. 7.8 cell;** • **Eq. 7.9 stack**
5	**Hydrogen production efficiency $\eta^{(HHVorLHV)}$ at covered current densities *j***	• **Eq. 7.11**

Source: JRC, 2020

7.2 Efficiency calculation for single cell, short stack

In the literature there is currently a lack of uniformity on the definition and on methods used for evaluating efficiency of single cells and short stacks. A detailed discussion on efficiency metrics and the underlying assumptions is presented in [2]. Following a summary of the different efficiency metrics discussed there, this section presents a harmonised approach for evaluating efficiency at single cell and short stack level.

7.2.1 Energy efficiency (ideal efficiency, thermodynamic approach)

The energy efficiency ε_{cell} of an electrolysis cell is defined as the ratio of the amount of total energy required for splitting one mole of water under reversible conditions to the actual total amount of energy (electricity and heat) used in the process, i.e. including the energy to overcome irreversibilities.

$$\varepsilon_{cell} = \frac{energy\ requirement\ in\ reversible\ conditions}{energy\ requirement\ in\ irreversible\ conditions} = \frac{W_{rev}(J.mol^{-1})}{W_{irrev}(J.mol^{-1})} = \frac{\Delta H_{rev}}{\Delta H_{irrev}} \qquad \text{[Eq.7.1]}$$

with $\Delta H_{irrev} = \Delta H_{rev} + zF\,\eta_{loss} = zF\,U_{cell} + \Delta Q_{rev}$ with $\eta_{loss} = (U_{cell} - U_{rev}) = (\Sigma|\eta_i| + R_eI)$ associated to irreversibilities coming from the overvoltages η_i and ohmic drop R_eI and the reversible heat $\Delta Q_{rev} = T\Delta S$ associated with the entropy change ([13]).

The efficiency of a single cell can thus be expressed as:

$$\varepsilon_{cell} = \frac{\Delta H_{rev}}{\Delta H_{rev} + zF\eta_{loss}} = \frac{\Delta G_{rev} + \Delta Q_{rev}}{zFU_{cell} + \Delta Q_{rev}} = \frac{U_{tn}}{U_{tn} + U_{cell} - U_{rev}} \qquad \text{[Eq. 7.2]}$$

Another parameter relevant to the temperature control of the cell/stack is the thermal balance $\Delta Q_{rev} = T\Delta S - zF\,\eta_{loss} = zF\,(U_{tn} - U_{cell})$ between the reversible heat provided by the surrounding and the irreversible energy losses due to overvoltages and ohmic drop.

For cell voltages exceeding U_{tn}, the electrolysis reaction is exothermic and excess heat must be evacuated with a cooling system to maintain T constant. For lower operating voltage, electrolysis is endothermic and heat from an external source has to be provided for isothermal cell operation.

For a short stack, energy efficiency is calculated as for a single cell by accounting for the number N of single cells connected in series in the stack.

$$\varepsilon_{stack} = \frac{N \cdot z \cdot F \cdot U_{tn}}{N \cdot z \cdot F \cdot U_{cell} + \Delta Q_{rev\,stack}} \qquad \text{[Eq. 7.3]}$$

When reporting the efficiency value calculated according to Eq. 7.2 or 7.3, it should be clearly indicated whether the heat supplied has been measured or not.

([13]) U_{cell} is composed of the sum of the reversible cell voltage and of the voltage contributions from ohmic drop (electic cell resistance R_e), and irreversibilities of the electrochemical processes (overvoltages associated to charge transfer and diffusion limitations).

7.2.2 Current efficiency (or Faraday efficiency)

In an electrochemical reaction, current efficiency, η_I, is defined as the fraction of the electric current passing through an electrochemical cell, which accomplishes the chemical reaction.

For water electrolysis it is expressed as:

$$\eta_I(T,p,I) = \frac{I-I_{loss}}{I} = 1 - \frac{I_{loss}}{I} = 1 - \frac{2\cdot F\cdot\left[\dot{n}_{H_2\text{loss}}(T,p,I) + 2\,\dot{n}_{O_2\text{loss}}(T,p,I)\right]}{I}. \quad \text{[Eq. 7.4]}$$

where $I_{loss} = 2\cdot F\cdot\left[\dot{n}_{H_2\text{loss}}(T,p,I) + 2\,\dot{n}_{O_2\text{loss}}(T,p,I)\right]$ [Eq. 7.5]

i.e. I_{loss} is proportional to the sum of the flow rates of H_2 and O_2 permeated through the gas separator.

In an ideal cell, $\dot{n}_{H_2 loss} = \dot{n}_{O_2 loss} = 0$, leading to $\eta_I(T,p,I) = 1$, independently of operating conditions (T, p, I).
In a real cell, $\dot{n}_{H_2 loss} \neq \dot{n}_{O_2 loss} \neq 0$, resulting in $\eta_I(T,p,I) < 1$.

Because loss flow rates are small and impractical to measure, the current efficiency is usually expressed in terms of the flow rates of hydrogen and of oxygen measured at the exit of the cell. When only considering hydrogen production, the current efficiency at single cell level is calculated as:

$$\eta_I^{H_2} = \frac{2\cdot F\cdot \dot{n}_{H_2\,measured}}{I} \quad \text{[Eq. 7.6]}$$

For a short stack the current efficiency for hydrogen production only is given by eq. 7.7, with N representing the number of cells in the stack:

$$\eta_{I,stack}^{H2} = \frac{2\cdot F\cdot \dot{n}_{H_2,\text{stack}}}{I\cdot N} \quad \text{[Eq. 7.7]}$$

Considering that hydrogen production rate without loss corresponds to current efficiency $\eta_I = 1$, another interpretation of the current efficiency η_I is that it represents the ratio between the actual hydrogen production rate and the theoretical maximum hydrogen production rate, or the ratio of the actually produced amount of hydrogen and the theoretically maximum possible amount.

7.2.3 Total efficiency

The total efficiency, η_ω, is defined as the product of energy efficiency with the current efficiency.

For a single cell the total efficiency is given by:

$$\eta_{\omega,cell} = \varepsilon_{cell}\cdot\eta_{I,cell} \quad \text{[Eq. 7.8]}$$

For a short stack the total efficiency is given by:

$$\eta_{\omega,stack} = \varepsilon_{stack}\cdot\eta_{I,stack} \quad \text{[Eq. 7.9]}$$

7.2.4 Hydrogen production efficiency

In an alternative energy efficiency definition, mostly used in the industry, the numerator of Eq. 7.1, namely the energy requirement for reversible reaction conditions, is replaced by the energy content of the reaction products. The denominator does not change and represents the total energy required for the reaction (electricity and heat):

$$Efficiency = \frac{energy\ content\ of\ the\ reaction\ products}{total\ energy\ required} \qquad \text{[Eq. 7.10]}$$

When only hydrogen is considered as useful reaction product, the numerator only contains the energy content of the hydrogen, i.e. the generated amount of hydrogen multiplied by its specific energy content, either HHV or LHV. Because in practice, the flow rate of the produced hydrogen, $\dot{n}_{H2}$, is measured, the above equation can be written as:

$$\eta^{(HHV\ or\ LHV)} = \frac{HHV\ or\ LHV}{P_{therm}+P_{elec}} \cdot \dot{n}_{H_2} \qquad \text{[Eq. 7.11]}$$

with P_{therm} and P_{elec} representing respectively the thermal power and electric power provided.

$\eta^{(HHV\ or\ LHV)}$ is known as the (instantaneous) hydrogen production efficiency.

The total energy required to produce ΔN_{H_2} mole of H_2 during electrolysis time Δt can be calculated by integration of [Eq. 7.11] over time Δt, as follows:

$$W_{total} = \int_0^{\Delta t} \eta^{(HHV\ or\ LHV)}\,(P_{therm} + P_{elec})\,dt = \Delta H^{(HHV\ or\ LHV)} \cdot \Delta N_{H_2}$$

which under stationary conditions leads to:

$$\varepsilon_{indus}^{HHV} = \frac{(HHV\ or\ LHV)\,\dot{n}_{H_2}\Delta t}{W_{elec}+\Delta Q_{rev}+\Delta Q_{H2O}} = \frac{(HHV\ or\ LHV)\,\Delta N_{H_2}}{W_{elec}+\Delta Q_{rev}+\Delta Q_{H2O}} = \frac{\Delta H_{rev}\,\Delta N_{H_2}}{W_{irrev}} \qquad \text{[Eq. 7.12]}$$

with ΔQ_{H20} is the thermal energy input of an additional heat exchanger (external to the system) for further water heat up.
This last expression of energy efficiency is exactly the same as that given for the ideal energy efficiency of a cell [Eq. 7.1], but for the production of ΔN_{H_2} mole of H_2 in the stack.

When determining hydrogen production efficiency, specification of the higher or lower heating value is clearly relevant. For operating temperatures above 100 °C, LHV is to be used, as explained earlier. For low-temperature electrolysis, generally HHV is used in efficiency calculations, based upon the consideration that irrespective of the use that is made of the hydrogen, it may be possible to exploit the excess heat produced when operating the electrolyser at voltages higher than the thermoneutral voltage. Accordingly, efficiency targets for low temperature electrolysis in the FCH2JU programme are expressed in terms of HHV ([14]).

([14]) For electrolysis, efficiency calculated on the basis of HHV results in a higher value than that based upon LHV. The opposite applies for fuel cells.

It should be noted that some authors argue that the use of LHV or of HHV in determining efficiency values for low temperature electrolysis should be decided based upon the use of the produced hydrogen [15]:

- When the hydrogen is considered as a feedstock for the chemical industry, the higher heating value HHV is used.
- When, on the other hand, the generated hydrogen is used for energy production purposes, the lower heating value LHV is relevant, because it accounts for the energy contained in the produced hydrogen that can effectively be used in subsequent conversion steps to mechanical, electrical or thermal energy. Indeed, in the case of low-temperature electrolysis without use of an external heat source, the excess heat generated when operating at voltages higher than the thermoneutral voltage is mostly not exploited and is lost to the environment. It hence does not make sense to include a heat-related component in the specific energy content of the produced hydrogen, and LHV represents the practically relevant value. This approach is followed in the USA Department of Energy (DoE) programme.

The above considerations apply to efficiency at single cell or short stack level. Efficiency of electrolysis *at system level* can also be expressed in terms of the total energy required for producing a normal cubic meter or a kilogram of hydrogen. Using the specific electricity consumption to characterize electrolyser performance sidesteps the issue of using HHV or LHV. However, when experimentally determined values of specific electricity consumption are to be related to the theoretically minimum achievable value (or when having to set targets for it), identification of HHV or LHV is again required as comparison basis. For low-temperature electrolysis when water is fed at ambient temperature (25 °C) and pressure (1 atm) to the system and all energy input is provided in the form of electricity, the minimum specific electricity consumption on HHV-basis equals 3.54 $kWh \cdot Nm_{H2}^{-3}$, i.e. 39.40 kWh/kg_{H2}. When water is supplied as vapour, the values on LHV-basis equal 2.99 $kWh \cdot Nm_{H2}^{-3}$, i.e. 33.32 kWh/kg_{H2}. Higher system efficiencies corresponding to specific energy consumption below these values (lower electrical energy input needs) can be attained by providing heat energy to the system. State-of-the-art low temperature systems can reach electrical energy inputs around 50 kWh/kg_{H2}, corresponding to efficiency of 79 % on HHV-basis.

7.3 Performance assessment: presentation of test results

The set of performance indicators identified in Table 22 are determined through tests performed under reference and under stressor operation conditions. The indicator values or test results obtained for the latter are normalized according to equation 7.12:

$$\text{Normalised performance output} = 1 - \frac{test\ output\ under\ stressor\ conditions}{test\ output\ under\ \text{reference}\ conditions} \quad \text{[Eq. 7.12]}$$

A normalised performance output equal to zero indicates that the stressor condition applied does not affect performance. Non-zero normalised performance outputs imply that the considered stressor does have an impact performance, with negative normalised outputs corresponding to an increased test output and positive ones to a decreased test output. Whether an increase or a decrease in normalised performance output corresponds to performance enhancement or performance degradation, depends upon the indicator considered. However, it should be noted that a positive effect by a stressor on *performance* may have a negative effect on *durability*.

The normalised performance outputs are presented in a radar chart where each of the axes corresponds to a specific performance indicator (Table 22). Figure 18 shows an example for test results obtained on a PEMWE cell, with the ordinate on each axis representing the normalised output for a given PEMWE stressor condition (Table 19). In Figure 18 the blue polygon with ordinate value equal to zero corresponds to PEMWE Reference Operating Conditions (Table 12).

Figure 18. Spider plot illustration of representing normalised performance outputs for PEMWE.

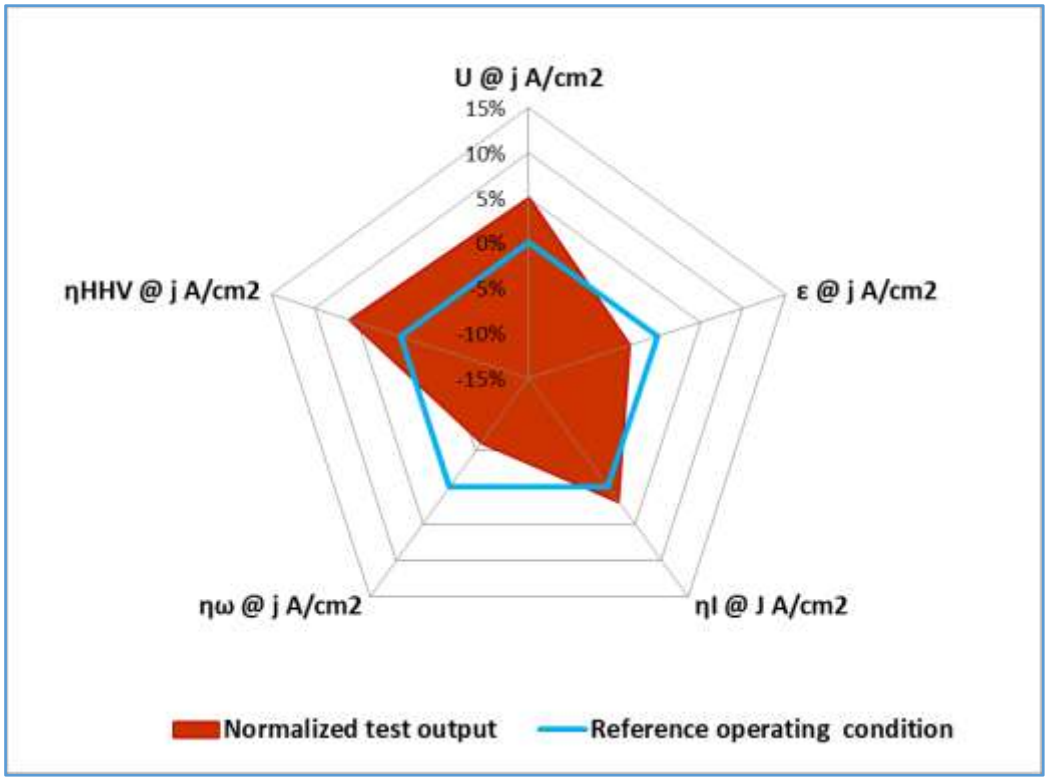

Source: JRC, 2020

7.4 Durability assessment

Successful operation of an electrolysis device depends not only upon its performance but also upon its capability to maintain performance over a period of time, known as durability. Such capability is affected by a number of factors, including cell design, manufacturing and assembly procedures, but also by the preceding operating history.

7.4.1 Selection of durability indicator for *in-situ* testing

Durability [2] is related to the loss of performance of the electrolysis device over a given time period. The lifespan of the device is expressed as its total number of hours of operation, irrespective of the actual nature of this operation (e.g. steady state, transient, cyclic, etc.). As such, durability is a concept that applies at system level.

In order to address durability through tests on single cells or short stacks, there is a need for a parameter that can be derived from performing tests at cell and short stack level. Such a parameter is the degradation rate, defined as the rate at which performance – characterised by one of the performance indicators listed in Table 22 – changes with time from its initial value.

Because a number of indicators can be used to characterise performance of an electrolysis cell or short stack (see 7.1), consideration should be given to which performance indicator among those listed in Table 22 is most suited for assessing durability through degradation rate. The performance indicator most frequently used in practice to assess degradation rate (and hence durability) is cell or short stack voltage (U) at reference operating conditions (*T,p,I*, see Table 22). Because cell/short stack voltage at reference operating conditions tends to increase as a function of time, the degradation rate represented by voltage rate is positive.

The use of cell/stack voltage increase rate as durability indicator is explained in the following section.

7.4.2 Cell/stack voltage increase rate as durability indicator

Cell/stack voltage increase rate is experimentally determined by monitoring voltage in a number of test blocks interspersed by rest periods. To obtain a meaningful value of cell/stack voltage increase, the loading profile (steady or dynamic) used in each block should be identical.

Part of the overall cell/stack voltage increase observed from one test block to the next may be recovered upon shutdown and consecutive restart. Also, shutdown and restart may lead to reduced overall cell/stack voltage increase compared to uninterrupted (steady or dynamic) operation. Both observations suggest that cell/stack voltage increase is composed of reversible and irreversible contributions, as shown in Figure 19 and Figure 20.

Figure 19. Reversible and irreversible cell/stack voltage increase during consecutive in-situ test cycles

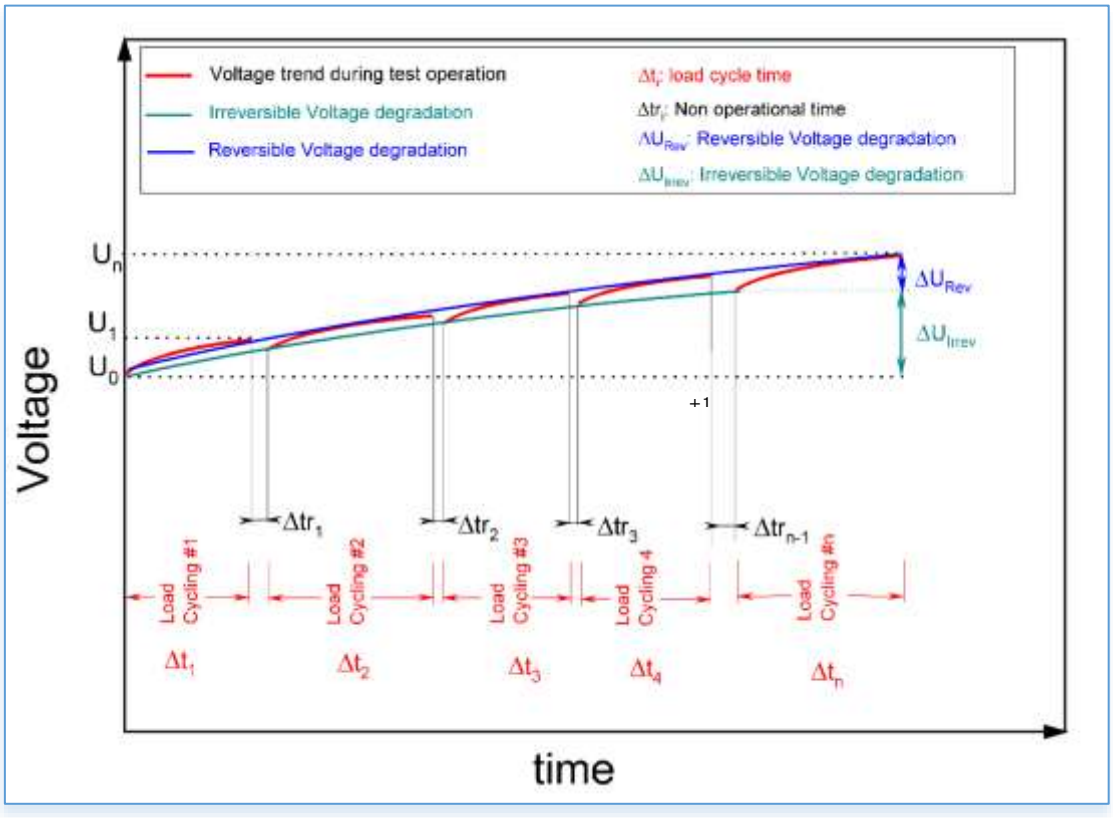

Source: JRC, 2020

Figure 20. Reversible and irreversible cell/stack voltage increase, graphical definition

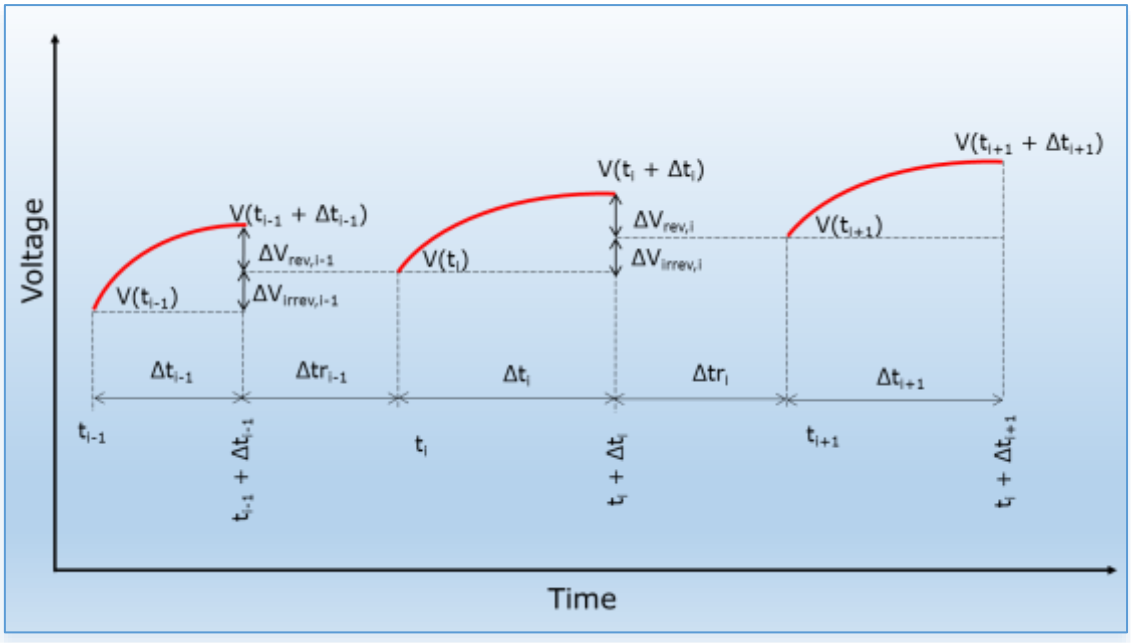

Source: JRC, 2020

The reversible cell/stack voltage increase ΔU_{rev} corresponds to the recoverable part of the overall cell voltage increase. For a typical test block in which the cell or stack is operated (either in steady state mode or in dynamic operation) for a time Δt_i between a start-up and a shut-down, the reversible cell/stack voltage increase $\Delta U_{rev,I}$ is the difference between the cell/stack voltage $U(t_{i+1})$ at the start time t_{i+1} of the test block $i+1$ and the voltage $U(t_i + \Delta t_i)$ at the end time $t_i + \Delta t_i$ of the test block i:

$$\Delta U_{rev,i} = U(t_i + \Delta t_i) - U(t_{i+1}) \quad \text{[Eq. 7.13]}$$

The total reversible cell/stack voltage increase $\Delta U_{rev,1\rightarrow N}$ upon performing N test blocks in total is the sum of all reversible voltage increments:

$$\Delta U_{rev,1\rightarrow N} = \sum_{i=1}^{N} \Delta U_{rev,\,I} \quad \text{[Eq. 7.14]}$$

The total reversible voltage increase rate $\dot{U}_{rev,1\rightarrow N}$ of all N test blocks is the ratio of $\Delta U_{rev,1\rightarrow N}$ to the sum of the duration of all N test blocks:

$$\dot{U}_{rev,1\rightarrow N} = \frac{\Delta U_{rev,1\rightarrow N}}{\sum_{i=1}^{N} \Delta t_i} \quad \text{[Eq.7.15]}$$

The irreversible cell/stack voltage increase due to a test block i is defined as the difference between the cell/stack voltage $U(t_i)$ at starting time t_i of the test block i and the voltage $U(t_{i+1})$ at the ending time t_{i+1} of the recovery period Δtr_i (i.e. the cell/stack voltage at starting time t_{i+1} of test block i+1):

$$\Delta U_{irrev,i} = U(t_{i+1}) - U(t_i) \quad \text{[Eq. 7.16]}$$

The total irreversible cell/stack voltage increase $\Delta U_{irrev,1\rightarrow N}$ upon performing N test blocks is the sum of all irreversible voltage losses:

$$\Delta U_{irrev,1\rightarrow N} = \sum_{i=1}^{N} \Delta U_{irrev,\,I} \quad \text{[Eq. 7.17]}$$

The total irreversible cell/stack voltage increase rate $\dot{U}_{irrev,1\rightarrow N}$ of all N test blocks is the ratio of $\Delta U_{irrev,1\rightarrow N}$ to the sum of the duration of all N test blocks:

$$\dot{U}_{irrev,1\rightarrow N} = \frac{\Delta U_{irrev,1\rightarrow N}}{\sum_{i=1}^{N} \Delta t_i} \quad \text{[Eq.7.18]}$$

The sum of reversible and irreversible cell/stack voltage increase rate is the overall degradation rate:

$$\dot{U} = \dot{U}_{rev} + \dot{U}_{irrev} \quad \text{[Eq.7.19]}$$

As implied in eq. 7.15, 7.18 and 7.19, the degradation rate is reported in terms of cell/stack, j voltage increase *versus* time, at a given current density.

7.4.3 Additional durability indicator

Evaluation of degradation rate through cell/stack voltage increase rate only partially addresses durability because it does not consider another relevant factor in this respect, namely initial cell/stack voltage. Indeed, for the same degradation rate at a given current density, starting from a lower initial voltage results in a lower cumulative voltage. This widens the voltage range under which the cell/short stack can operate and may hence extend its life.

A parameter that considers both degradation rate and initial cell/stack voltage at a given current density j is the stability factor SF_j, defined as the inverse product of cell/stack voltage increase rate, $\dot{U}_j$, and the initial cell/stack voltage deviation ($\Delta U_{cell/stack,j}$).The initial voltage deviation at BoL is defined as the voltage deviation after activation and conditioning:

Initial cell/stack voltage deviation, j $= \Delta U_{cell/stack,j} = U(j) - U^{tn}$

$(SF)_j = 1 / (\dot{U}_j \cdot \Delta U_{cell/stack,j})$ [Eq.7.20]

7.5 Durability testing

7.5.1 Identification of load versus time profiles for durability testing

To assess durability by *in-situ* testing of single cells and short stacks, the operation history that the electrolyser system experiences in actual service needs to be "translated" into load-versus-time profiles to be imposed in the *in-situ* tests. Such translation involves a number of sequential steps:

- Identification of operational conditions experienced during actual service
- appropriate simulation of these as operation conditions to be imposed in *in-situ* tests on cell or short stack
- establishing the degradation rate (corresponding to the selected performance indicator, usually cell/short stack voltage) through *in-situ* testing
    - by continuous monitoring of the performance indicator during testing to establish its instantaneous degradation rate, or
    - by executing performance tests at BoT and at different stages after interruption of the simulated service conditions, to establish average degradation rates ([14])

To simplify execution of *in-situ* testing for the second step, actual service conditions are usually simulated by imposing two types of time-profiles for the electric power supply, namely operation at steady state and dynamic operation according to pre-defined profiles that are representative of transients and dynamic conditions. These are discussed in Sections 7.5.2 and 7.5.3, respectively.

To enable "translating" service operating conditions into load profiles to be used in *in-situ* tests, the electric power inputs to an electrolyser system need conversion into inputs of electrical current density. For this purpose, the maximum current density, $j_{max,}$ to be imposed during *in-situ* testing is proposed as that corresponding to a given cell/stack voltage on the polarisation curve at the Beginning of Test (BoT), while reaching a (higher) voltage at the same current density is proposed as End of Test (EoT) criterion. As an example, for PEMWE the respective voltages at cell level are proposed as 1.8 V and 2.0 V, respectively ([15]) (Figure 21). A similar approach, with adapted values for the cell voltages to be decided, is proposed for AWE and AEMWE.

([14]) Next to performing *in-situ* tests, ex-situ testing can provide complementary information on degradation mechanism(s) causing the change in performance induced by the simulated operation conditions.

([15]) Values proposed and used in Electrohypem project.

Figure 21. Illustration of determination of j_{max} and of EoT criterion for PEMWE

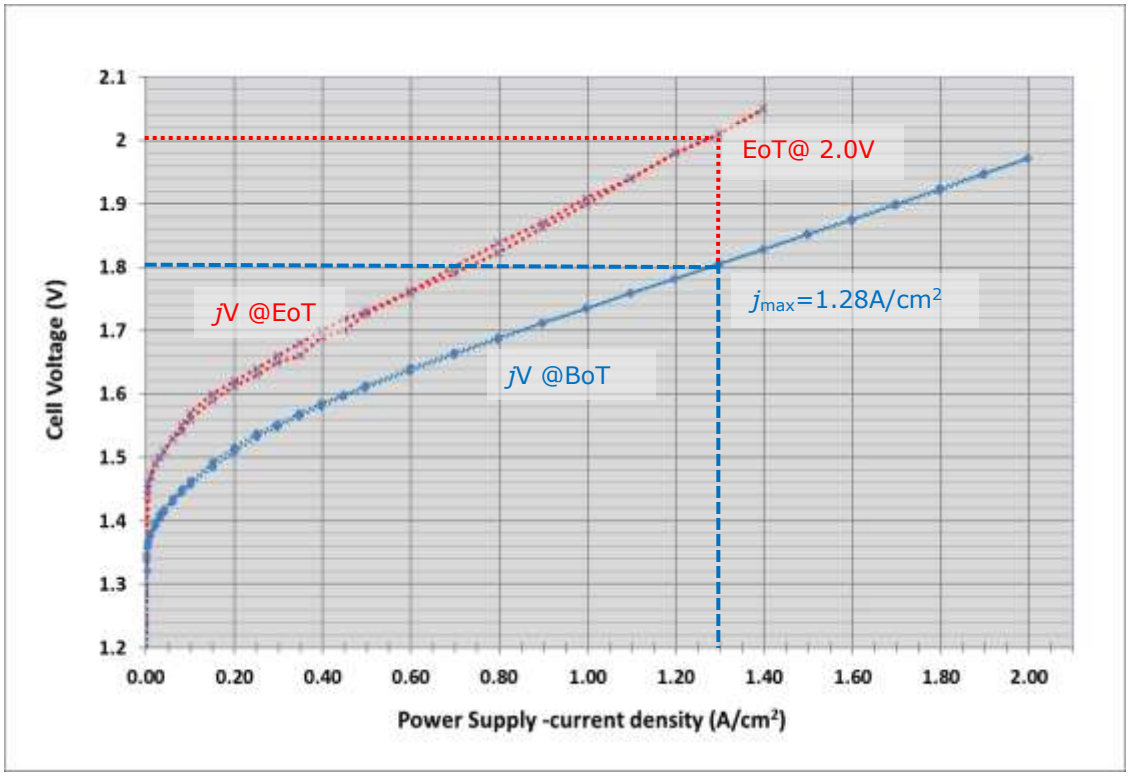

Source: JRC *Source:* JRC, 2020

7.5.2 Steady state loading

Degradation rate under steady state loading is identified as the cell/stack voltage increase rate calculated according to equation 7.19.

The time period considered for determining voltage increase and calculating voltage increase rate should exclude the initial conditioning period, where the cell potentials may decrease with time due to artefacts (e.g. change of the oxidation state of the anode catalyst, *in-situ* membrane purification). It should also exclude time periods during which microstructural instabilities caused by pre-exposure may affect the value and evolution of cell voltage with time. To enable reliable evaluation of a representative cell/stack voltage increase rate, the time period for its determination should only start when the average value of $\dot{U}=(\Delta U/\Delta t)$ calculated over the preceding two-hour period is equal or greater than zero.

The protocol agreed for assessing degradation rate under steady-state loading for PEMWE, AWE and AEMWE is presented in Table 23.

Table 23. Agreed Protocol for assessing steady state degradation rate for *in-situ* cell and short stack testing of PEMWE, AWE and AEMWE

STEADY STATE DEGRADATION TEST PROTOCOL	
STEP	**DESCRIPTION**
1	Perform activation and conditioning according to cell/stack manufacturer specifications. In the absence of such specification, common laboratory practice shall be adopted.
2	Set the test input conditions (TIPs) according to reference operating conditions (Chapter 5, Table 12, 15 and 17).
3	Perform a BoT polarization curve [7] and record cell/stack voltage at the corresponding current density *j*, $U(t_1)$.
4	Operate the cell/short stack at constant TIPs for 1,000 hours.
5	Perform a polarization curve and record cell/stack voltage at same j, representative of $U(t_1 + \Delta t_1)$ (or $U(t_i + \Delta t_i)$ *for subsequent iterations).*
6	Disconnect the current supply and leave the testing set-up under Open Circuit Potential (OCP) conditions for 60 minutes maintaining the water recirculation flowrate and test temperature.
7	Re-apply the TIPs of step 1 and let cell/stack voltage stabilise for 120 min. If ΔU/Δt calculated over this period is equal or greater than zero, go to next step, otherwise extend the stabilisation period for another 60 minutes until reaching a positive ΔU/Δt over the preceding 120 min.
8	Perform a polarization curve and record cell/stack voltage at same j, representative of *U(ti)*.
9	Repeat steps 3 to 7. The test ends with step 8 after 3,000 hours of steady state operation or when EoT criterion is reached.
Note	Total test duration can be extended when deemed useful.

Source: JRC, 2020

Test validity criteria are met when measurement accuracy given in Table 14 are fulfilled.

The quality of the result strictly depends upon the measurement accuracy of the test parameters concerned.

Depending upon the test hardware available, additional relevant information may be obtained from performing EIS or HFR tests ([16]) in steps 3, 5 and 8. Also performing *ex-situ* tests on component materials retrieved from intermittent *in-situ* tests can provide

([16]) EIS is used for assessing degradation impact on ohmic resistance, anode and cathode charge transfer resistances, diffusion resistance. If EIS is not available, HFR should be used to determine ohmic resistance and calculate IR free cell voltage.

qualitative / semi-quantitative information of the underlying mechanisms causing the observed degradation.

7.5.3 Dynamic load profiles

The conventional approach for assessing degradation rate and hence durability under dynamic loading conditions differentiates between system level and cell/short stack level:

- At system level Real-World Degradation (RWD) is considered, with a load versus time profile based upon actual operating conditions experienced in different electrolysis systems applications.
- At single cell and short stack level, Laboratory-World Degradation (LWD) is normally considered, in which the load versus time profile is derived from, yet differs from that experienced in actual service. One factor causing the difference between RWD and LWD is the load that may be induced by BoP components which form part of the system but are not present at cell/short stack level. Moreover, for reducing the expenditure and experimental effort for *in-situ* testing, LWD load profiles may be further simplified from those considered under RWD. Hence, LWD load versus time profiles imposed in *in-situ* testing of cells and stacks serve as simplified simulation in a laboratory environment of actual service loads, excluding those induced by BoP.

However, to avoid the inherent conservatism associated with subjecting cells/short stacks to LWD load profiles that do not include those arising from BoP and are simplified from those of RWD, the approach in this report stipulates that the dynamic load profiles to be applied in laboratory testing of single cells and short stacks are identical to those experienced by the electrolysis system in actual service, i.e. RWD load profiles rather than LWD profiles are imposed.

Hence, the Real-World Degradation load profiles which electrolyser systems are expected to be subjected to in a number of service applications presented in Chapter 8, are directly applicable to testing of single cells/short stacks.

7.5.4 Protocol for assessing degradation rate (durability) under dynamic loading

The aqreed protocol for assessing degradation rate under dynamic loading for PEMWE, AWE and AEMWE is described in Table 24 which is valid for a given imposed load profile, an example of which is shown in Figure 22.

Figure 22. Example of dynamic load degradation test protocol

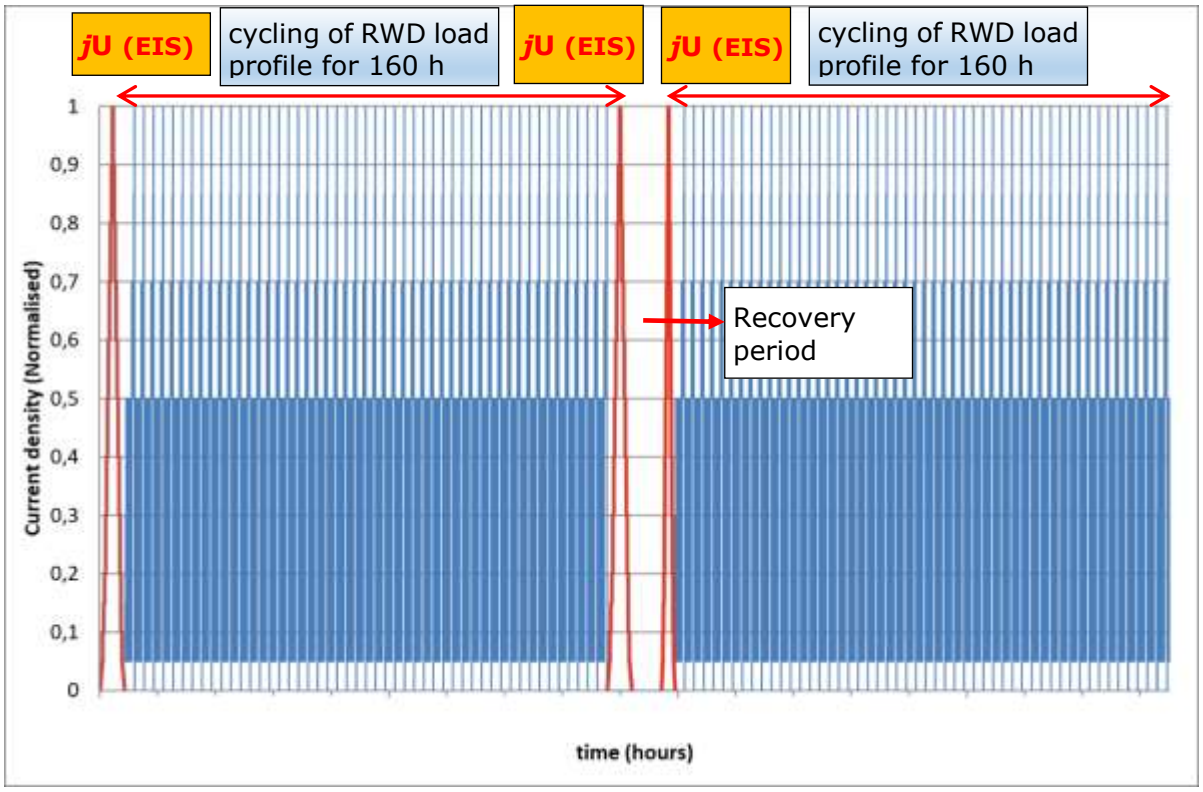

Source: JRC, 2020

Table 24. Agreed protocol for assessing dynamic load degradation rate for *in-situ* cell and short stack testing of PEMWE, AWE and AEMWE

DYNAMIC LOAD DEGRADATION TEST PROTOCOL	
1	Perform activation and conditioning according to cell / stack manufacturer specifications. In the absence of such specification, common laboratory practice shall be adopted.
2	Set the test input conditions (TIPs) according to reference operating conditions (Chapter 5, Table 12, Table 15, Table 17).
3	Perform a polarization curve [7] and record cell/stack voltage at the corresponding j, representative of $U(t_1)$.
4	Operate the cell/short stack at the selected RWD load versus time profile for N cycles equivalent to 160 hours (with N rounded to the closest integer).
5	Perform a polarization curve record cell/stack voltage at same j, representative of $U(t_1 + \Delta t_1)$ (or $U(t_i + \Delta t_i)$ *for subsequent iterations).*
6	Disconnect current supply and leave under OCP for 60 minutes maintaining the water recirculation flowrate and test temperature.([17])

([17]) OCP time shall be kept as uniform as possible to minimize the Open-circuit potential (OCP) or potential inversion, that happens when the potential of the cathode drifts to more anodic potentials during downtimes or

DYNAMIC LOAD DEGRADATION TEST PROTOCOL	
7	Re-apply the TIPs of step 1 and let cell/stack voltage stabilise for 120 min. If ΔU/Δt calculated over this period is equal or greater than zero, go to next step, otherwise extend the stabilisation period for another 60 minutes until reaching a positive ΔU/Δt over the preceding 120 min.
8	Perform a polarization curve and record cell/stack voltage at same j, representative of *U(ti)*.
9	Repeat steps 4 to 8. The test ends at step 7 after 10 loops for a total of 1,600 hours, or earlier upon reaching one of the EoT criteria.
Note	Total test duration can be extended when deemed useful.

Source: JRC, 2020

Test validity criteria are met when measurement accuracy given in Table 14 are fulfilled.

The quality of the result strictly depends upon the measurement accuracy of the test parameters concerned.

Depending upon the test hardware available, additional relevant information may be obtained from performing EIS or HFR tests ([18]) in steps 3, 5 and 8. Also performing *ex-situ* tests on component materials retrieved from intermittent *in-situ* tests can provide elements of clarification on the degradation mechanisms.

An exhaustive durability assessment exercise usually requires execution of this protocol for a number of load profiles considered relevant.

maintenance, can lead to electrode degradation not only for alteration of the active catalyst species but also for mechanical stress reasons [27].

([18]) EIS is usedfor assessing degradation impact on ohmic resistance, anode and cathode charge transfer resistances, diffusion resistance. If EIS is not available, HFR should be used to determine ohmic resistance and calculate iR free cell voltage.

7.6 Durability assessment: presentation of results

There are two methods of presenting the results of durability assessment. The first consists of using a normalised spider graph (Figure 23 below) where each axis corresponds to one of the performance indicators listed in Table 22. The axis ordinate represents the normalised performance determined according to eq. 7.21:

$$\text{Normalised performance} = \frac{Performance\ indicator\ at\ EoT\ @\ j}{Performance\ indicator\ at\ BoT\ @\ j} \qquad \text{[Eq. 7.21]}$$

in which the numerator represents the value for the considered performance indicator observed/calculated according to Sections 7.1 and 7.2, after submitting the cell/short stack to a loading profile according to one of the protocols described in Sections 7.5.2 and 7.5.4. The denominator represents the value of the same performance indicator obtained/calculated at BoT.

BoT and EoT values shall represent data averages recorded over 30 minutes.

Figure 23. Illustration of durability test results on a PEMWE cell under steady and under a specific RWD load profile.

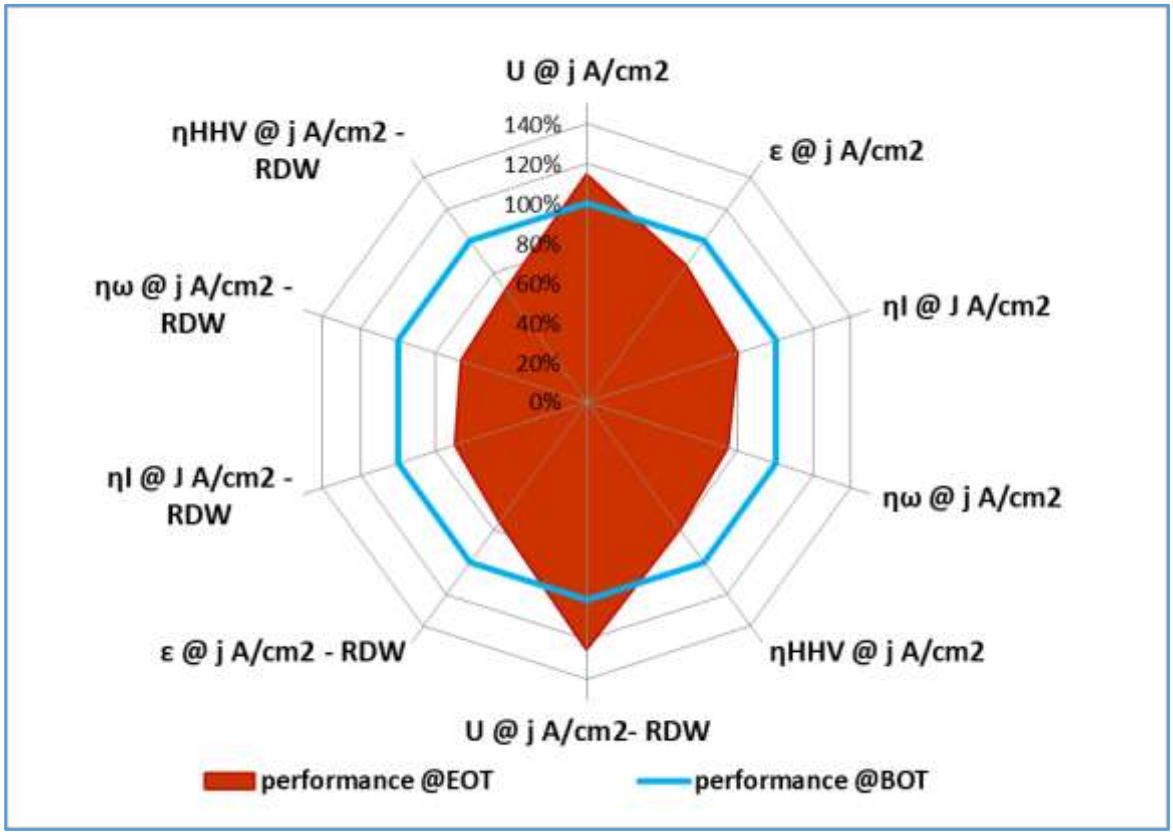

Source: JRC, 2020

The blue polygon represents the performance indicators obtained under PEMWE Reference Operating Conditions (Table 12).

The second way of representing the results of durability tests is through the use of the cell/short stack cell voltage increase rate as the metric for degradation rate. In this case the indicators listed in Figure 24 and 25 are used, which apply at a given current density at which the cell/stack voltage is measured under either steady state (Table 23) or a specific RDW load profile (table 24).

Table 25. Degradation Indicators

INDICATOR	SYMBOL	UNIT	REFERENCE
Total cell/stack voltage increase rate	$\dot{U}$	µV/h	Eq. 7.19
Reversible cell/stack voltage increase rate	$\dot{U}_{rev}$	µV/h	Eq. 7.15
Irreversible cell/stack voltage increase rate	$\dot{U}_{irrev}$	µV/h	Eq. 7.18
Stability factor	SF	$h \cdot V^{-2}$	Eq. 7.20

Source: JRC, 2020

The results for cell/stack voltage increase rate can be shown in a bar chart:

Figure 24. Bar chart showing degradation indicators under steady state and under one RWD load profile for PEMWE

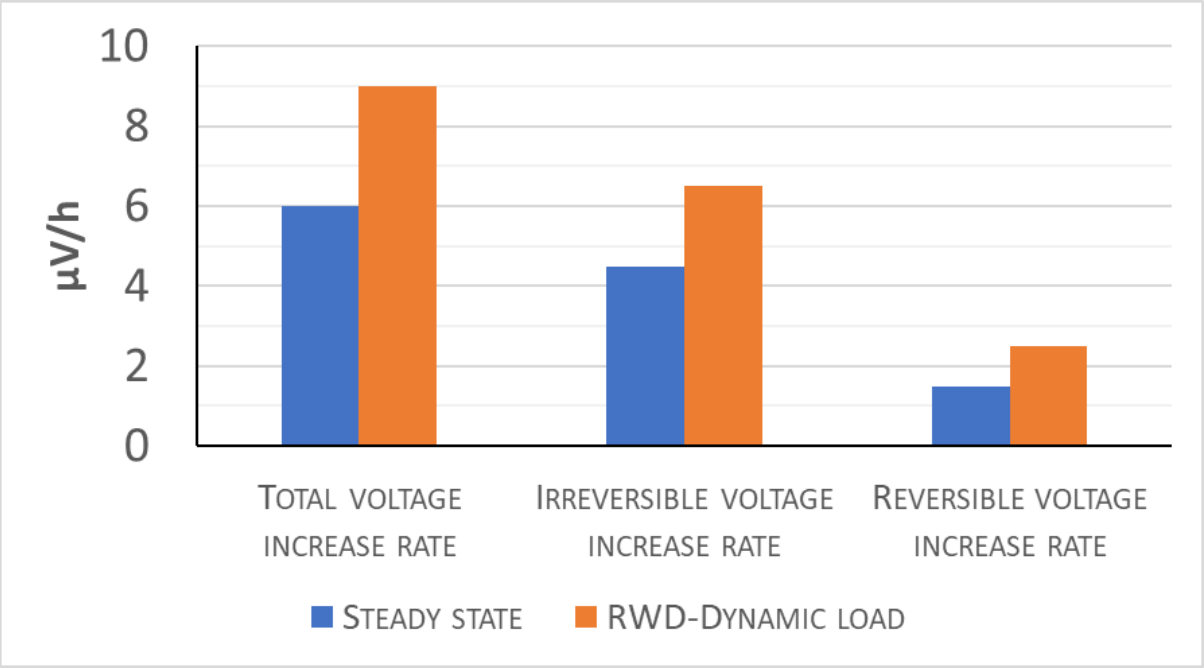

Source: JRC, 2020

7.7 Accelerated life and accelerated stress testing

Considering that the lifetime of an electrolyser system can easily reach many years, it is important when selecting new or improved materials or when assessing durability, to be able to evaluate degradation in a short(er) period of time. "Accelerated testing" is used for that purpose. In such testing, materials and components are subjected to operating conditions outside the normal operation window to trigger similar degradation as expected under actual service conditions but at a faster rate, thus shortening the required testing time.

The approach towards accelerated testing of single cells and short stacks presented in this report differentiates between two types of accelerated tests, each of which serves a specific purpose:

- Accelerated Life Tests (ALT) to be used for investigating the capability of electrolyser component materials to withstand service loads
- Accelerated Stress Test (AST) to assist in fast development of new and improved electrolyser materials

7.7.1 Protocols for accelerated life tests (ALT)

To investigate the capability of electrolyser materials to withstand service loads, Accelerated Life Tests aim at mimicking failures under Real World Degradation (RWD) conditions. The ALT protocols are similar to those for dynamic durability tests presented in Section 7.5.4, and achieve the acceleration by subjecting the materials during *in-situ* tests to stressor operating conditions (Chapter 6), rather than to reference operating conditions (Chapter 5). This requires selection of the appropriate "high" or "low" setting for the stressor triggering performance degradation.

Accelerated Life Tests (ALT) for single cells and short stacks are hence arranged as follows:

- Operating Conditions

  Stressor Operating Conditions for Single Cell and Short Stack Testing for PEMWE, AWE and AEMWE, Table 19, Table 20 and Table 21 respectively for the type of stressor effect that is subject of the evaluation.

- Test Protocol

  Dynamic load degradation test protocol for Single Cell and Short Stack, with RWD load profile from Chapter 8, Table 39 ([19]), 8.5.1 FREQUENCY CONTAINMENT RESERVES (FCR) test protocol, considered as the most demanding.

ALT results are analysed and presented as described in Section 7.6.

7.7.2 Protocols for accelerated stress tests (AST)

For material development and improvement purpose the ALT approach is not suitable because identification of stressor types and their associated settings for selective

([19]) As for dynamic load degradation testing, the power input settings from RWD profiles at system level have to be translated into current density input settings.

degradation of specific materials under conditions representative of actual service, is an as yet unresolved research issue. The absence of scientific consensus on load profiles and stressors able to selectively target degradation of materials for specific cell components hence warrants a different methodology for AST than for ALT.

The approach followed here builds upon that adopted for durability testing (see 7.5). The acceleration is realised by increasing the severity of a selected RWD profile. Such an increased severity may be achieved by

- using operation stressors
- and/or by increasing (the absolute value of) current ramp rates
- and/or by increasing frequency in the considered RWD profile.

This modified profile is then imposed as dynamic load profile in the durability test. The overall AST protocol consists of including such a profile as step 4 in the dynamic load degradation test protocol of Table 24.

Table 26 presents two agreed load profiles which are considered to represent the most stringent requirements for using electrolysers in a grid balancing application. In future, other load profiles, once validated, can be benchmarked against and possibly update and/or replace this set ([20]).

Table 26. Agreed AST load profile

STEPS	AST load profiles
1	**Flexibility**
2	**Reactivity**

Source: JRC, 2020

These load profiles are individually described in the sections below. As for dynamic load degradation testing, the power input settings from RWD profiles at system level have to be translated into current density input settings.

7.7.3 Flexibility load profile

This profile is a simplified version of the RWD profile as defined in Section 8.5, but aiming at an overall increase of the test severity by imposing high current ramp rate and by being applied also with the settings for the stressor operating conditions to simulate applications where the system is expected to experience frequent periods of load variations. Two load cases are considered, stepwise increase to 100% and to 200% of the nominal current density (left axis in Figure 25, and Figure 26, respectively).

([20]) such alternative AST profiles have been proposed within a number of FCH2JU projects.

Table 27. Agreed flexibility load profile

FLEXIBILITY LOAD PROFILE	
Step	**DESCRIPTION**
1	Increase the current setting by 25 % using a ramp-up profile with a ramp rate **+N** (A/s) and then maintain constant current for 15 minutes
2	Repeat step 1 up to 100 % or 200 % of nominal operating current
3	Decrease the current setting by 25 % using a ramp-down profile with a ramp rate of **-N** (A/s) and then maintain constant current for 15 minutes
4	Repeat step 3 until reaching 25 % of nominal current
Note	Ramp rate **N,** in A/s**,** is defined as the change of 25% of maximum design operating current, I, per second. This implies that each ramp is executed in one second.

Source: JRC, 2020

Figure 25. 100 % of nominal current flexibility profile

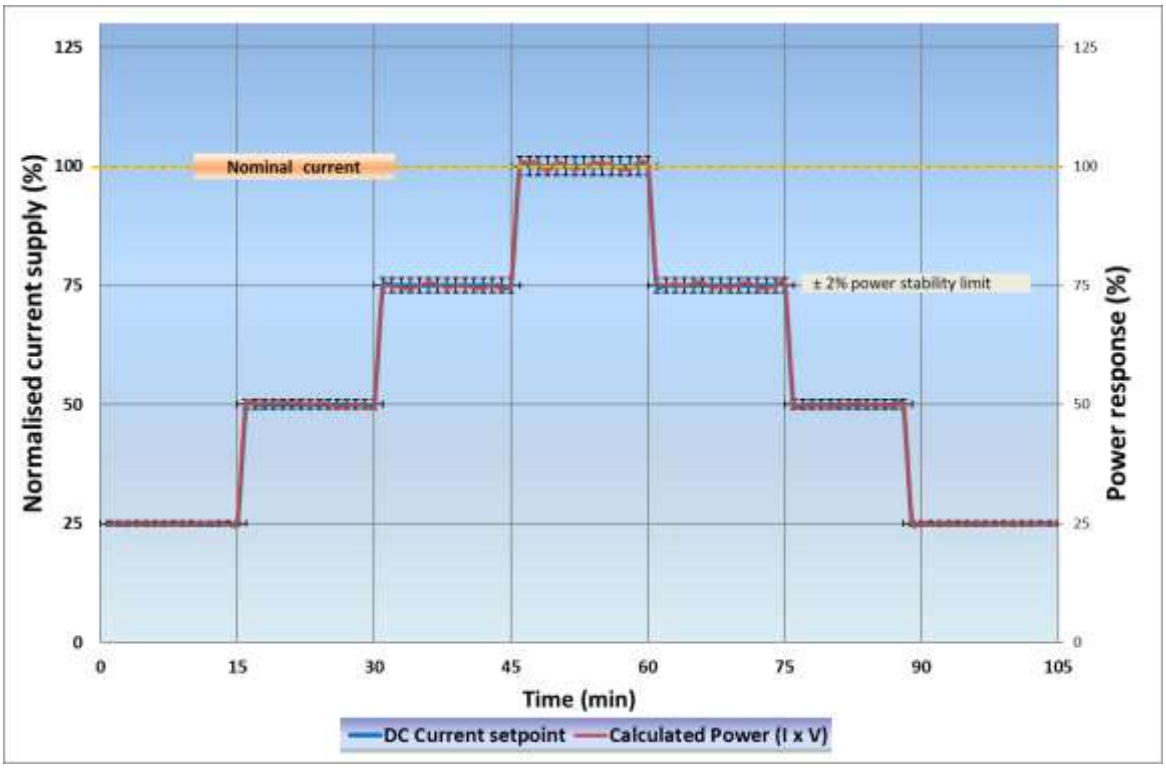

Source: JRC, 2020

When using the flexibility profile in AST according to the protocol described in Table 24, the variation of the power at each current setting (i.e. the product of the imposed current and the measured cell/stack cell voltage, right axis in Figures. 25 and 26) shall be smaller than +/- 2 %. The parameters to be determined from ALT using this profile and their derivation for each time the profile is imposed are given in Section 8.5.1.

Figure 26. 200 % of nominal current flexibility profile

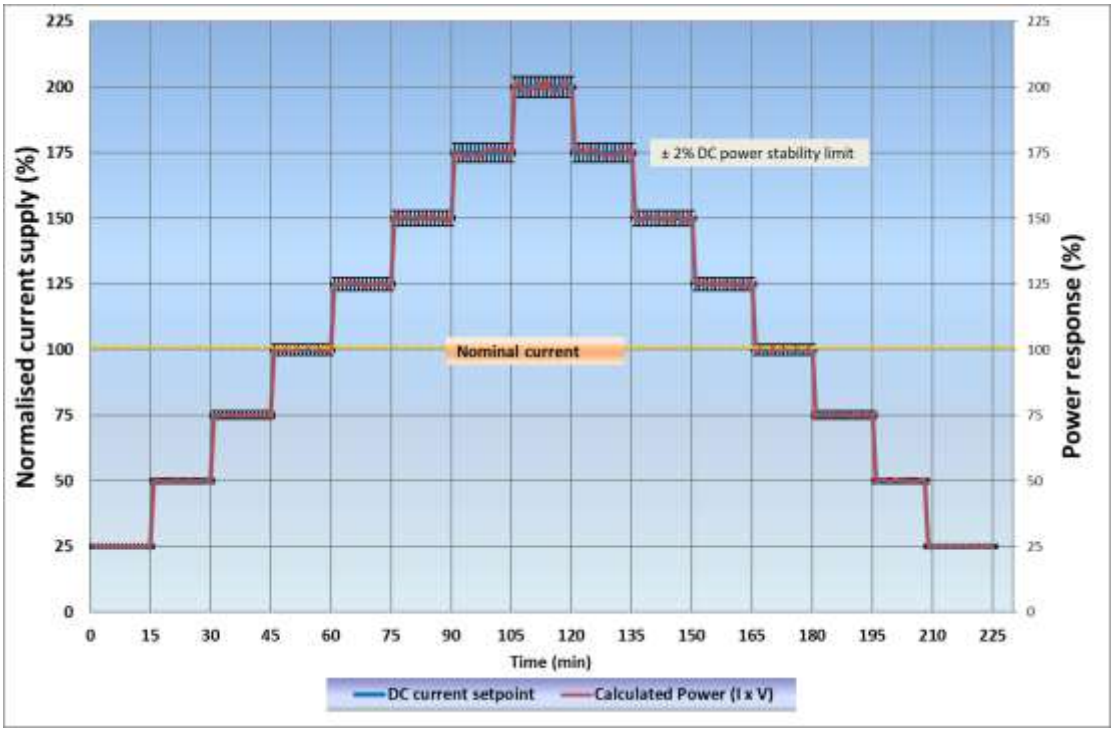

Source: JRC, 2020

The results of an AST test with the flexibility load profile are analysed and presented as described in Section 7.6.

7.7.4 Reactivity load profile

The reactivity load profile is derived from FCR RWD profile (8.5.1), with more severe conditions in terms of ramp rate and of frequency of current change. This is achieved by two factors: limiting the constant current step to 60 seconds instead of 15 minutes and using different magnitudes for the step variation, corresponding to 25 %, 50 %, 75 % and 100 % of the current range.

Table 28. Agreed reactivity load profile

REACTIVITY LOAD profile	
1	Set the current input to 100 % of nominal current
2	Perform 7 consecutive current cycles, each of 60 s total duration, with stepwise increasing amplitude of 25 % of the rated design operating current at a current ramp rate of ± N (A/s)
Note	Ramp rate N, in A/s, is defined as the change of 25% of nominal operating current, I, per second. This implies that each ramp is executed in one, two, three or four seconds, which is anyway faster than FCR test requirement. (see Table 40)

Source: JRC, 2020

Figure 27. Reactivity profile

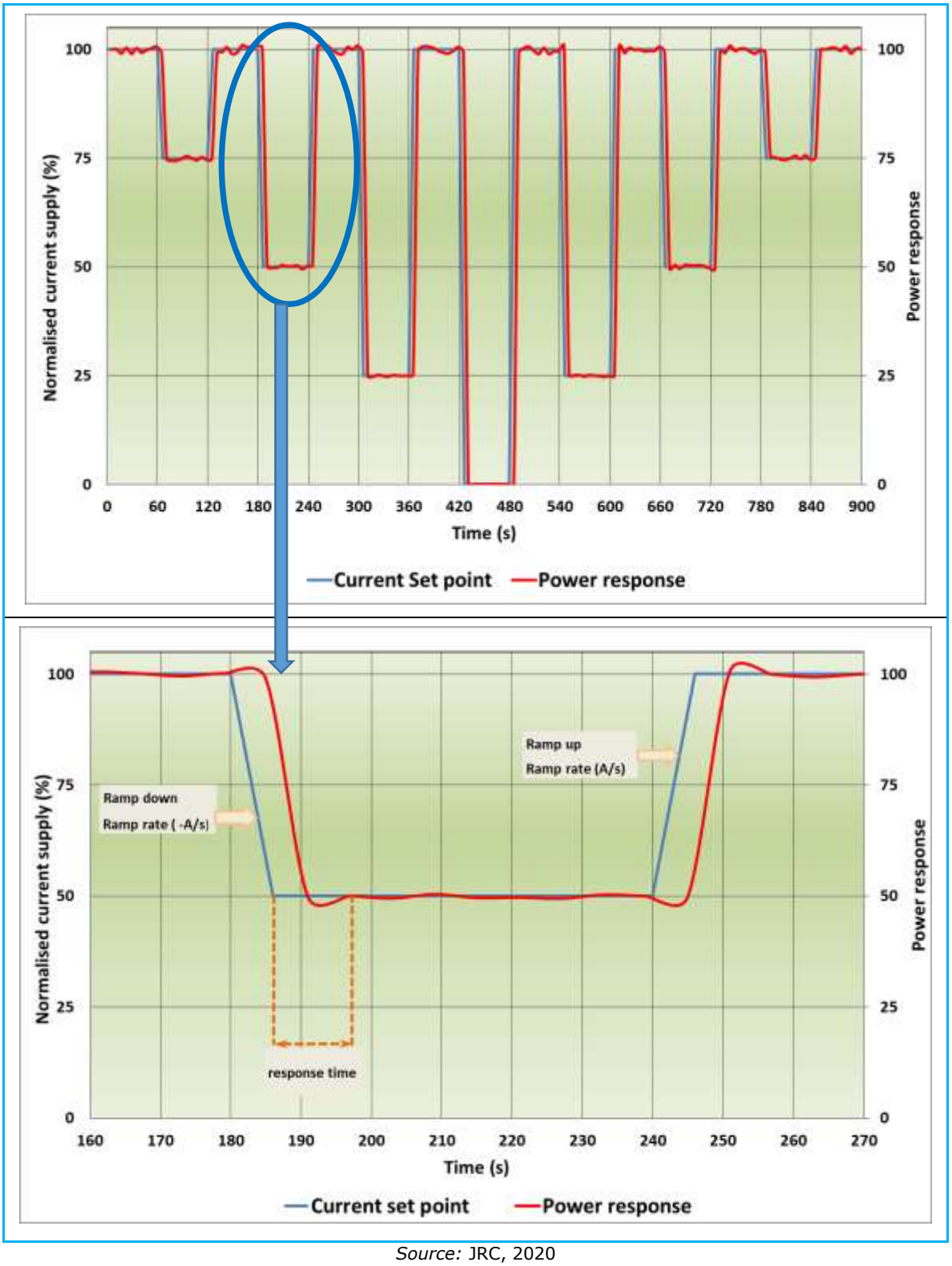

Source: JRC, 2020

When using the reactivity profile in AST according to the protocol described in Table 24, the variation of the power response (i.e. the product of the imposed current and the measured cell/stack cell voltage, right axis in Figures 25 and 26) shall be smaller than +/- 2 %.

The parameters to be determined from ALT using this profile and their derivation for each time the profile is imposed are the power response rate of change (in $\%\cdot s^{-1}$) and response time following the methodology described in Section 8.5.1.

The results of an AST test with the reactivity load profile are analysed and presented as described in Section 7.6.

8 Electrolyser system-level testing

An electrolyser is an energy conversion device which transforms electrical energy into chemical energy (H_2 and O_2). Its operation is bounded by constraints, both downstream (H_2 production demand) and upstream (availability and source of power input).

Downstream applications include production of hydrogen (and/or oxygen) as chemical feedstock for a range of process industries (PtX), generation of hydrogen for long-term (seasonal) storage, or for short-duration storage and subsequent use in transport (PtT) or re-electrification (PtP) (see Figure 1). These applications are characterised by different production volume versus time profiles reflecting the needs of the different customers, but because of economic considerations they are not expected to necessitate large and/or quick deviations from steady state electrolyser operation.

Next to these applications based upon the use of hydrogen, the provision of services to the power grid by acting as flexible electrical load (flexible demand) constitutes an increasingly interesting business case. However, in this case the necessity for the electrolyser to cope with transient and dynamic power inputs, decreasing as well as increasing (possibly exceeding maximum nominal power), at different rates and frequencies, is much more challenging for its performance and durability.

Upstream operation bounds are set by the availability of power to the electrolyser. Electrolyser systems operating off-grid that have to rely upon variable and intermittent renewable electricity from wind and/or solar, will be exposed to frequent start-ups from and shut-downs to various stand-by modes. Operations under such non-steady conditions pose challenges to performance and durability.

The downstream and upstream operation bounds have in common that they require the electrolyser system to be able to withstand a number of *load-versus-time* profiles with different levels of severity. This chapter establishes a set of agreed application-relevant load profiles and associated test protocols for assessing performance at system-level. Contrary to testing at cell/short stack level which includes both performance and durability characterisation (see Chapter 7), testing at system-level only covers evaluation of performance. However, as explained in Section 7.5, the load profiles used in durability tests at cell/short stack level (RWD load profiles) are directly derived from *load-versus-time* profiles described in this chapter, which are experienced by electrolyser systems in a number of service applications.

The chapter first presents an overall schematic for electrolyser system level testing considering the power sourcing and envisaged applications (Section 8.1). This is followed by an overview of grid support services (Section 8.2) and how electrolysers can provide these by acting as a flexible electric load (Section 8.3). Sections 8.4 and 8.5 subsequently deal with the establishment of agreed test protocols for assessing the capacity of electrolyser systems to meet the *load-versus-time* requirements imposed by the specific application of providing grid balancing services.

The content of this chapter is based on and builds upon efforts in the QualyGrids project in which PEMWE and AWE are considered [10].

8.1 System testing: overview

An electrolyser system is an assembly of various sub-systems including electrolysis stack, power supply, water conditioning, etc., each of which contains a number of components. The types and specifications of these components play an important role in the specification of the electrolyser system, in its overall performance in terms of efficiency, flexibility, responsiveness, durability, and in its capital expenditure and cost of ownership.

A general description of electrolyser system components is given in the document "EU harmonised terminology for low-temperature water electrolysis for energy-storage applications"[2]. Figure 28 presents a scheme of a PEM water electrolyser with a representation of its relevant components. Similar figures for the system configurations for AWE and AEMWE are included in [2].

Figure 28. PEM water electrolyser schematic

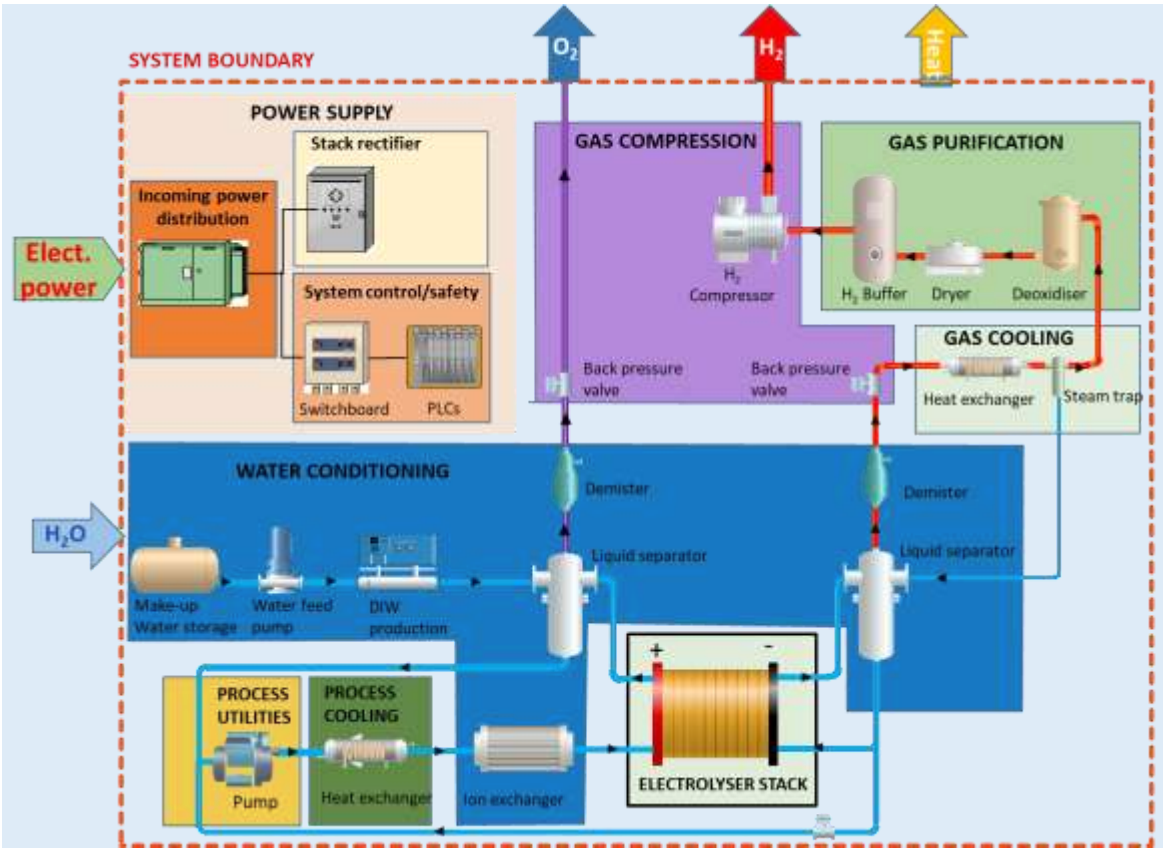

Source: JRC, 2020

As a first step in system testing, the various system components are tested because they impact the performance of the overall system. However, it is usually not possible to test individual system components independently. It is hence important for system-level testing to provide an adequate number of measuring instruments to monitor parameters such as electricity and water consumption, fluid flow rate and composition, pressures and temperatures, etc. at appropriate locations for getting an indication of the contribution of each component to overall system performance.

Subsequent aspects of system-level testing discussed in the following parts of this chapter address the envisaged applications of the electrolyser. This consists of multiple stages, as indicated in Figure 29.

For stationary mode testing the system should be tested at the reference conditions based upon system technology whenever possible, and to the supplier recommended nominal condition applying the methodology described in Section 7 to determine the indicators of Table 22 and in Section 8.7, Table 47.

For transient mode testing, in the first stage the basic performance characteristics of the system are checked by performing a number of simple "fit-for-purpose" screening tests for system use as a flexible electric load. Such tests, described in Section 8.4, can also provide an indication for which specific application a particular system is more suitable. Testing in the second stage aims at assessing performance in the light of the specific application, by incorporating system-level service-representative *load-versus-time* profiles (Section 8.5). The present report is limited to system-level testing aspects related to the use of electrolysers in conventional grid-connected applications (grey boxes in Figure 29). In future, applications for renewable electricity (distributed generation, remote off-grid) may be included (green boxes in Figure 29).

Figure 29. System testing schematic

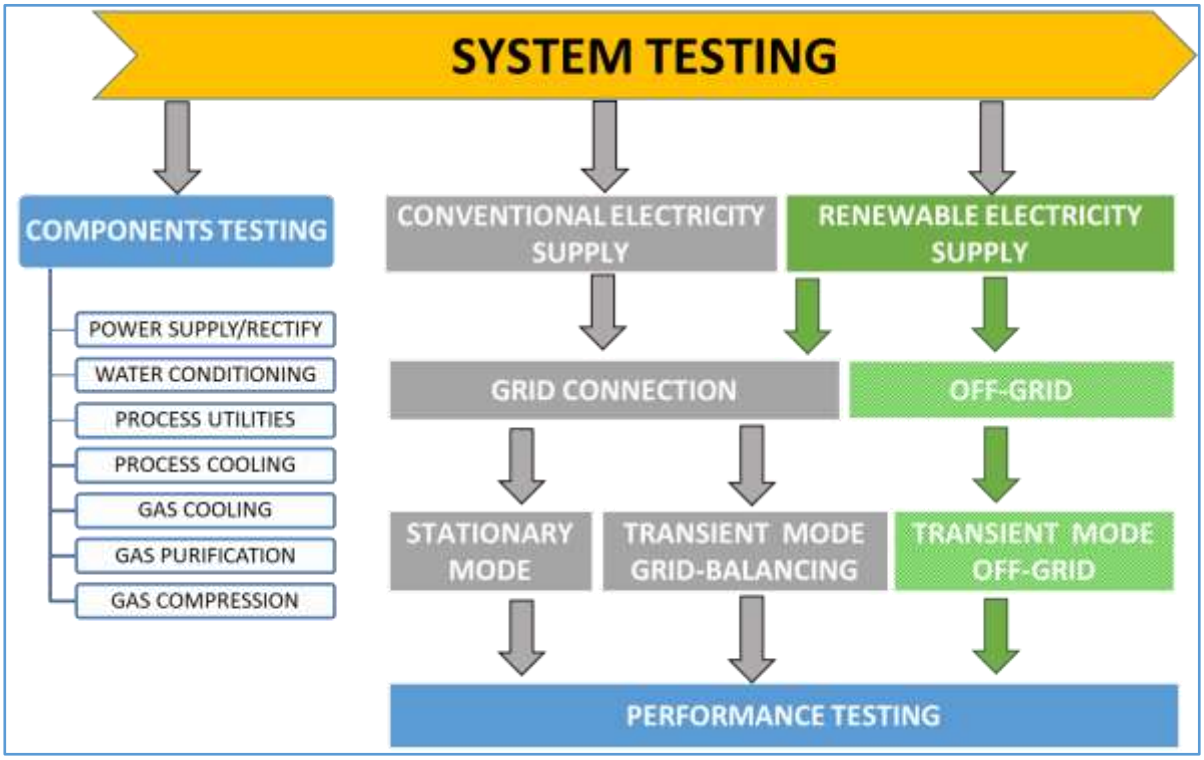

Source: JRC, 2020

8.2 Overview of grid services

Electricity grid services refer to a range of services needed to maintain a reliable and balanced electrical power system. Grid services are used to address imbalances between supply and demand, maintain a proper flow and direction of electricity, and help the system recover after a power system event. Conventionally, grid services are provided to the grid operators by big generation units and large-scale industrial loads, either as an obligation or through a service market. Small/medium scale units are usually excluded by grid operators because grid services have specific requirements on capacity, ramping, duration, location and auxiliary units for measurement, communication and control etc.

Grid services at the transmission level ("ancillary services") include frequency response (to maintain system frequency with automatic/manual active power reserves), voltage control (by reactive power support), capacity and congestion management (i.e. strategic reserves aimed at increasing security of supply by organizing adequate long-term peak and non-peak capacity), and redundancy support (providing emergency power, black-start capability and island capability) ([21]).

Increasing penetration of intermittent renewables and of distributed energy resources intensifies the demand for grid services to manage enhanced variability and uncertainty of generation at different voltage levels and to avoid or delay network reinforcement ([22]). At the same time, the importance of using different technologies, such as electrolysers, to provide grid service is increasingly recognized and facilitated by improved market designs and regulations.

8.2.1 Grid balancing services to address network frequency deviations

Due to the impossibility to store electricity, it is necessary to balance power generation and consumption at all times in the network. Any non-balance is manifested through a change in frequency of the alternating current: frequency increases when active power generation exceeds active power consumption and decreases in the opposite case.

The currently applicable EU Regulatory Framework on the provision of grid balancing services required to be deployed upon a frequency disturbance event, is summarised in Annex C. This section introduces the concepts which are relevant for electrolyser systems contributing to the provision of grid balance services.

When a frequency imbalance occurs, a series of actions involving three frequency control processes and related active power reserves are sequentially deployed, either automatically and/or manually, at varying time scales to return frequency to the nominal 50 Hz (see Table 29).

([21]) The electricity distribution grid also needs a number of support functions for its safe and reliable operation. These resemble to a large degree those at transmission level but are targeted to local issues at medium/low voltage levels. Therefore, frequency support is presently not needed at distribution level.

([22]) This may require ancillary grid services at distribution level in future.

Table 29. Types of reserves for grid balancing ([23])

Frequency Containment Reserve (FCR), (EU)2017/1485 art. 142, FCRs are automatically triggered within 15-30 s from a disturbance to prevent further frequency deviation and maintain frequency within a range centred around 50Hz ([1])
Frequency Restoration Reserve (FRR), (EU)2017/1485 art. 143, FRRs take over from the activated FCR and are deployed automatically (aFRR, fast ramping) or manually (mFRR, slower ramping) to bring the frequency back to 50 Hz
Replacement Reserve (RR), (EU)2017/1485 art. 144. RRs progressively restore the activated FRRs to be prepared for a further system imbalance and/or support the FRR activation

Source: JRC, 2020

(1) Different frequency bandwidths in different synchronous areas

Regulation (EU)2017/1485 stipulates that each TSO is responsible for establishing a pre-qualification process to assess a service provider's capability against the technical requirements for the intended services FCR, FRR and RR. These requirements are briefly described below ([24]).

8.2.2 Pre-qualification

The terms FCR, a/mFRR and RR which represent the fundamental principles for frequency control, are harmonized in the EU. However, due to structural differences among countries, actual implementation of frequency control and formulation of the corresponding requirements varies.

A service provider wanting to offer grid balancing services has to provide evidence of meeting a number of pre-qualification requirements. These include successfully passing acceptance criteria in dedicated tests established by the relevant transmission system operator (TSO). In such tests, the capability of meeting the performance required by the TSO in terms of capacity, speed of action, ability of ramping, and ability of offering a reliable dynamic/non-dynamic response over the designated service period is evaluated.

Load profiles by the TSOs ([25]) include both step signals and continuous signals, either practically measured (historical/real-time) or developed through simulations. Step signals are used to test performance characteristics such as accuracy, response delay, speed of response, ramping performance, etc., thereby offering an impression of the unit's technical performance. Continuous signals are used to test the unit's response within a longer time period. Currently, the total duration of pre-qualification tests varies from a few minutes up to two hours. Durability testing, as applied at cell/short stack level (see Section 7.5), to

([23]) Terminology still sometimes used classifies frequency reserves as Primary (FCR), Secondary (aFRR) and Tertiary Reserves (mFRR fast tertiary, RR slow tertiary)

([24]) In addition to prequalification requirements for grid balancing, grid operators also set technical requirements for limiting other network disturbances. These include electromagnetic compatibility requirements, avoidance of rapid voltage changes, harmonics, phase unbalances, reactive power compensation, ….

([25]) Regulation (EU)2017/1485 prescribes the minimum features that a pre-qualification load-versus-time must possess. (see Annex C).

assess the long-term performance and degradation of a service providing unit are not requested by grid operators during pre-qualification.

Assessment criteria for each performance characteristic are normally expressed in terms of permissible response ranges.

Because *load-versus-time* profiles included in the pre-qualification requirements of TSOs in the different member states are different for the three frequency control processes, it is useful to harmonise them into a single set of representative load profiles to be used for pre-qualification purposes ([26]).

8.3 Electrolysers for grid balancing support

The European Network of TSOs for the electricity grid (ENTSO-E) acknowledges that a range of technologies can serve grid balancing, such as power generators, batteries, flow batteries, electrolysers, etc. Which of these technologies is eligible depends on the conditions applicable in national reserve markets.

Because of their capacity to be connected/disconnected/regulated when requested to do so by grid operators, electrolysers can in principle act as flexible electrical loads (flexible demand) and thereby offer a variety of grid balancing services, provided that operation is technically and economically feasible. Because grid balancing is as a minimum in the MW range, at present only AWE and PEMWE technologies can deliver grid balancing services ([27]).

To qualify for providing grid balancing services, electrolysers must have an appropriate range of operational capacity and of dynamic characteristics. The most relevant dynamic characteristics are load flexibility and response time (reactivity) under fast load changes (up/down). Load flexibility refers to the capability of being operated under a broad range of load. The response time under fast load changes depends on the electrolyser status, namely in operation, at ambient conditions, or stand-by conditions (See Section 8.4).

Because of the aforementioned difference in pre-qualification requirements in Europe from service to service and from country to country, evaluating the suitability of an electrolyser system to offer grid balancing services would greatly benefit from an agreement on a set of representative *load-versus-time* profiles to assess electrolyser system load flexibility and response times. This is the objective of the QualyGridS project, and a selection of the harmonised set of load profiles developed in this project is summarised and presented in the subsequent sections of this report.

8.4 Fit-for-purpose testing

This set of tests aims at checking whether the electrolyser system is fit-for-purpose for use as flexible electric load and for which grid balancing service(s) it might in principle be suitable. The characteristics addressed are available power range and duration required for transients, as shown in Figure 46 of Annex C. Based upon the outcome of these "screening" tests, the testing protocols relevant for the specific grid service can then be applied in the next step (Section 8.5).

([26]) This is also in line with the recommendation to promote introduction of standard products to enhance competition between providers of balancing services(Network code on Electricity Balancing Article 31.6)

([27]) Water electrolysers in the kW range also have potential when many units are aggregated for providing balancing services.

The set of screening tests is listed in Table 30 and the different protocols taken from [10, Deliverable 2.5] are reported below. Some wording in protocols titles and tables has been adapted for the use in this document.

Table 30. FIT-for-Purpose test protocols QualyGridS

PROTOCOLS	
IDENTIFICATION OF SYSTEM POWER (SP) RANGE (1)	8.4.1
DETERMINATION OF MINIMUM-MAXIMUM SP DYNAMICS (RESPONSE TIME)	8.4.2
DETERMINATION OF NOMINAL TO MAXIMUM SP DYNAMICS (RESPONSE TIME)	8.4.3
RESPONSE TIME FROM NOMINAL SYSTEM POWER TO STAND BY (2)	8.4.4
TIME AT MAXIMUM SYSTEM POWER (3)	8.4.5
COLD START TIME TO NOMINAL POWER	8.4.6
START-UP TIME FROM STANDBY MODE	8.4.7

(1) Identified as "Protocol for identification of the power range available for grid services" in [10]
(2) Identified as "Protocol for determination of power down to standby time, etc." in [10]
(3) Identified as "Protocol for Determination of Duration of Maximum Power" in [10]

Source: JRC, 2020

As the electrical power input is a fundamental parameter for this series of tests it is important to define where to measure it. As described in Figure 28 the system boundary shall be considered and then the power shall be measured at the grid connection point of the incoming power distribution main switchboard/cabinet.

Moreover, measuring the electrical power supplied to the various BoPs will provide additional information for a detailed analysis of the system behaviour and efficiency.

8.4.1 Identification of system power range

This protocol aims at defining the minimum and maximum power for the system. The maximum power, $P_{max,}$ corresponds to generating the highest possible continuous output of hydrogen. The minimum power, $P_{min,}$ corresponds to the lowest continuous hydrogen output. The protocol is described in Table 31 and the test profile is schematically shown in Figure 30.

Table 31. System power range available for grid services test protocol

STEP	DESCRIPTION
1	Start system
2	Set system power for maximum possible continuous H_2 production output (Comment: for most systems this state will be the Nominal Operational Mode [2], P_{nom}, for systems with overload capability it might be higher than nominal power, P_{max})
3	Wait for power to stabilize *
4	Note the power $P_1 = P_{nom}$ or P_{max} system
5	Keep the state for 1 hour with power variation below ± 0.05·P_{nom} (or P_{max}) system
6	Set system at 0 % H_2 production output (or minimal continuously attainable output), respectively minimum rectifier power input
7	Wait for power to stabilize *
8	Note the power $P_2 = P_{min}$ system
9	Keep the state for 1 hour with power variation below ±0.05·P_{min} system
10	End of test
	* The system power is considered stable if the average power of two consecutive intervals of 60 seconds does not differ by more than (±2 %· P system)

Source: QualyGridS [10]

Figure 30. Example of system power range test profile

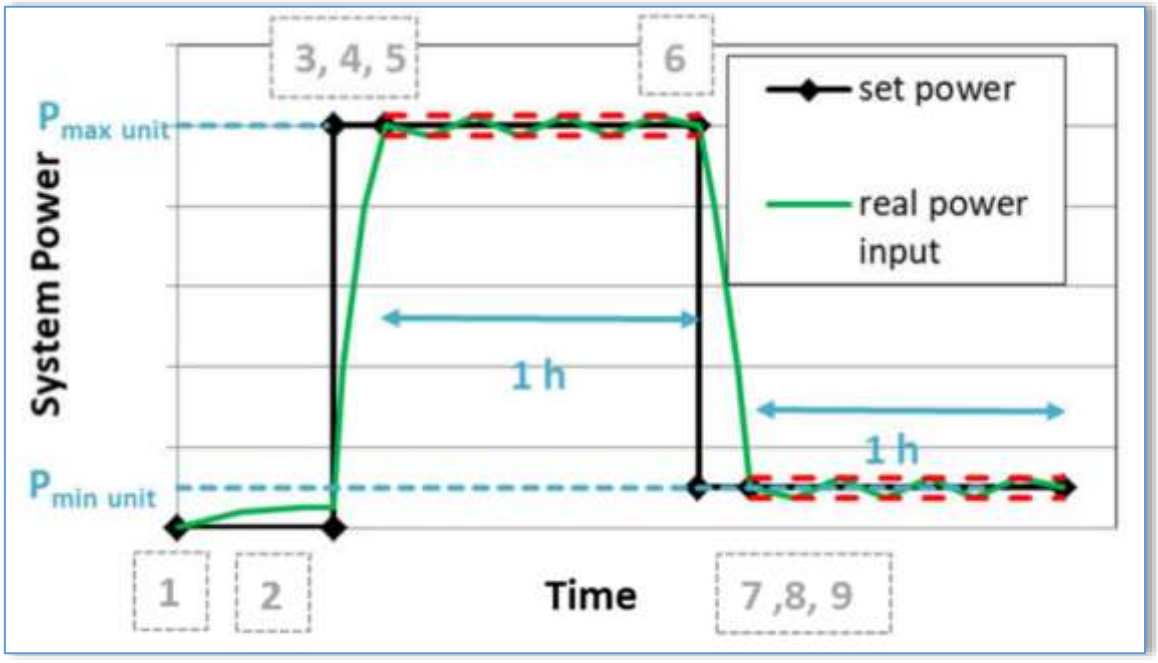

Source: QualyGridS [10]

- P_{nom} *or* P_{max} system is defined as the arithmetic average electrical power input in step 5.
- P_{min} system is defined as the arithmetic average electrical power input in step 9.

8.4.2 Determination of minimum-maximum sp dynamics (response time)

This protocol aims at identifying the times required for the system to switch from minimum to maximum power and vice-versa. The protocol is described in Table 32 and the test profile is schematically shown in Figure 31.

Table 32. Min-max dynamics (response time) test protocol

STEP	DESCRIPTION
1	Set system power at P_{min} system for 15 min
2	Set system power P_{max} system (as identified in 8.4.1)
3	Wait for system power to stabilize to ± 0.05·P_{max} system
4	Hold at P_{max} system for 15 min
5	Set system power at P_{min} system (as identified in 8.4.1)
6	Wait for system power to stabilize to ± 0.05·P_{min} system
7	Maintain system power at P_{min} system for 15 min

Source: QualyGridS [10]

Figure 31. Response times Min-Max test profile

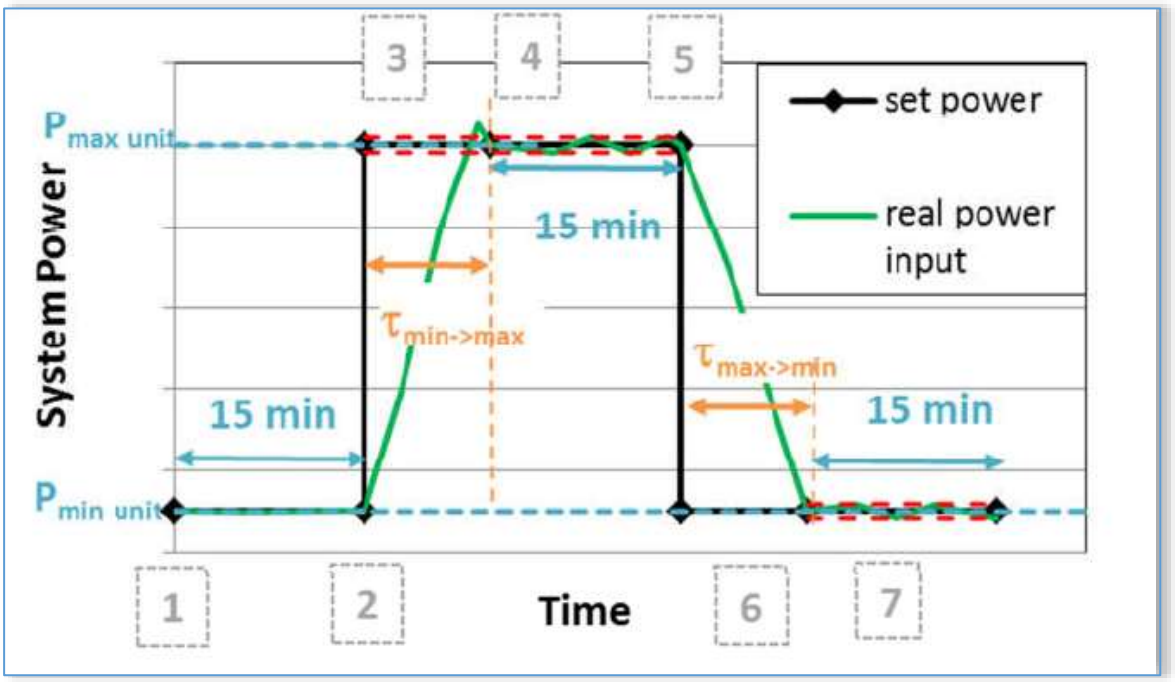

Source: QualyGridS [10]

- The response time minimum power to maximum power $\tau_{min->max}$ is defined as the time from beginning of step 2 to end of step 3.
- The response time maximum power to minimum power $\tau_{max->min}$ is defined as the time from beginning of step 5 to end of step 6.

8.4.3 Determination of nominal to maximum sp dynamics (response time)

This protocol is only relevant for systems which can be operated continuously for at least 15 minutes above nominal power. The protocol is described in Table 33 and the test profile is schematically shown in Figure 32.

Table 33. Nominal to maximum sp dynamics (response time) test protocol

STEP	DESCRIPTION
1	Set system operation at nominal power P_{nom} for 15 min
2	Set system power to P_{max} system (as identified in 8.4.1)
3	Wait for system power to stabilize to ± 0.05·P_{max} system
4	Hold at P_{max} system for 15 min
5	Set system at nominal system power P_{nom}
6	Wait for system power to stabilize to ± 0.05·P_{nom} system
7	Maintain system at nominal power, P_{nom}, for 15 min

Source: QualyGridS [10]

Figure 32. Example of Nominal-Maximum dynamics identification test profile

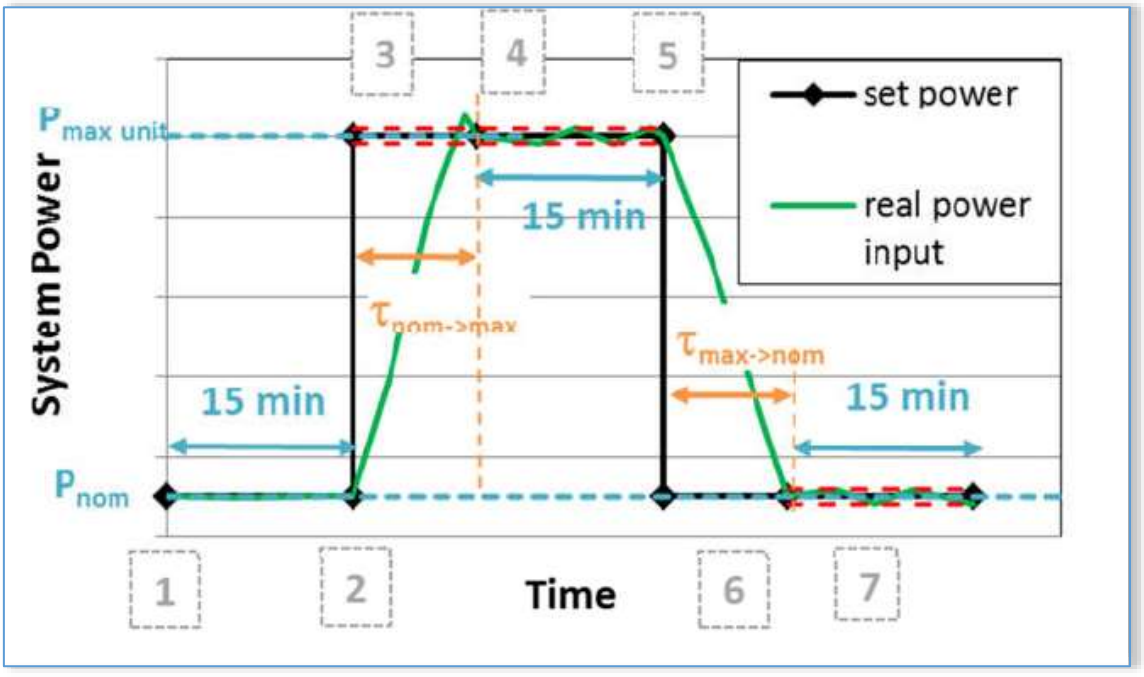

Source: QualyGridS [10]

- The response time nominal power to maximum power $\tau_{nom->max}$ is defined as the time from beginning of step 2 to end of step 3.
- The response time maximum power to nominal power $\tau_{max->nom}$ is defined as the time from beginning of step 5 to end of step 6.

8.4.4 Response time from nominal power to standy

This protocol aims at identifying the time required for the system to switch from nominal power to (one of) the stand-by condition(s) identified by the manufacturer. The protocol is described in Table 34.

Table 34. Response time from nominal power to standby and return to standby test protocol

STEP	DESCRIPTION
1	Set system operation at nominal power for 1 hour
2	Set system power at P_{min} system
3	When 0 % H_2 production or minimum continuously attainable output is reached switch the system to standby state as defined by the manufacturer
4	Wait for standby state to be reached
5	Start the system from standby state setting system power to nominal value P_{nom}
6	Wait for system power constant by ± 5% in a 15 min interval

Source: QualyGridS [10]

Identify the moment t_{down} during step 4 when the system power reaches the range $P_{standby}$± (5% Pmax system).

Time from nominal to standby state: $\tau_{down\_to\_standby}$=Time from start of Step 2 to end of Step 3.

The test should be repeated for each of the standby modes identified by the manufacturer.

τ_{stdby_up} is the time from standby state to Nominal Power calculated from start of step 5 to Step 6.

8.4.5 Time at maximum system power

This protocol is only relevant for systems which can be operated continuously for at least 15 minutes above nominal power. The protocol is described in Table 35 and the test profile is schematically shown in Figure 33.

Table 35. Time at maximum system power test protocol

STEP	DESCRIPTION
1	Set system operation at nominal power for 15 min
2	Set system power to P_{max} system
3	Wait for system power to stabilize to ±0.05·P_{max} system
4	Hold at P_{max} system for 4 hours or until system specifications require power reduction
5	Set system power at nominal value P_{nom}
6	Wait for system power to stabilize to ±0.05·P_{nom} system
7	Operate at nominal power for 15 min

Source: QualyGridS [10]

Figure 33. Example of time at maximum power test profile

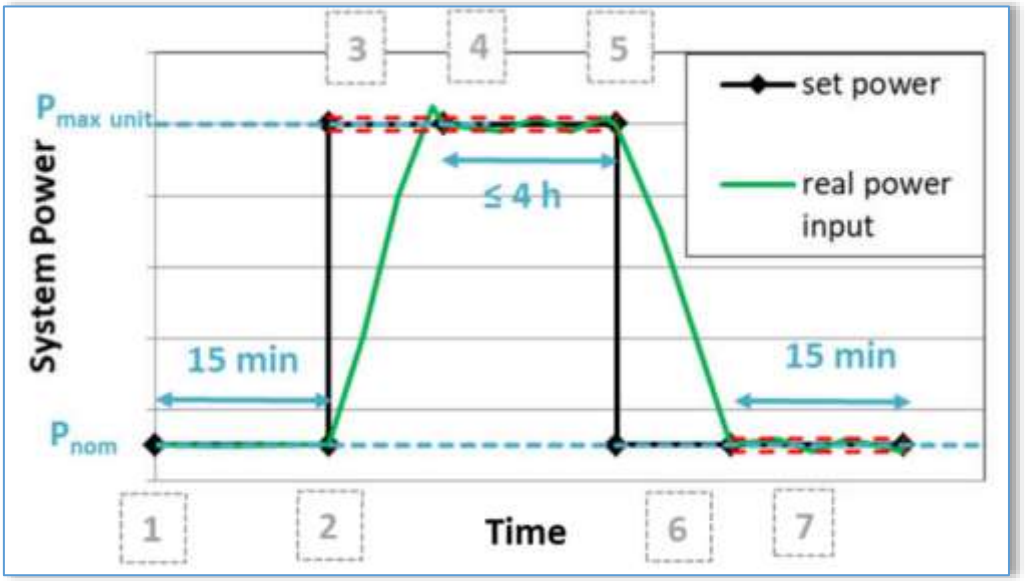

Source: QualyGridS [10]

The duration time of maximum power τ_{max} for which the system can remain in maximum power is determined by the duration of step 4.

8.4.6 Cold start time to nominal power test protocol

The cold start is intended as start-up when the device or system is at ambient temperature and pressure [26].

At the beginning of this test the system should have been in cold standby state [26] for at least 2 hours.

Table 36. Cold start time to nominal power test protocol

STEP	DESCRIPTION
1	Trigger the "start" button on the system
2	Wait for end of start-up protocol to reach nominal power
3	Wait for system power constant by ± 5 % in a 15 min interval

Source: start-up protocol,QualyGridS [10]

Cold Start Time to Nominal Power: τ_{cold} = Time from start of Step 1 to end of Step 3 minus 15 min.
In case the nominal power is not reached within 30 minutes, the test shall be considered failed. This implies that the system will not be able to perform the grid qualification tests.
The power needed to keep the system in standby state, $P_{cold\ standy}$, is given by the arithmetic average of power consumed during the last 30 minutes before step 1.

8.4.7 Start-up time from standy mode test protocol

At the beginning of this test the system should have been in standby state for at least 1 hour. For systems that have different types of standby modes the start-up time from standby mode should be determined for each of these states.

Table 37. Start-up time from standy mode test protocol

STEP	DESCRIPTION
1	Set the power of the system to nominal power P_{nom}
2	Wait for system power constant by ± 5% in a 15 min interval

Source: QualyGridS [10]

Start-up time from standby state to nominal electrical power input, $\tau_{start,standby}$ = time from start of step 1 to end of step 2 minus 15 min.
The arithmetic average of electrical power input of the system in standby state is $P_{standby}$

8.4.8 Fit for purpose test results and validity criteria

The result of the fit for purpose test can be summarised as follow:

1- The available power range for grid services depending on the selected lower power state is:

Power Range ΔP = $P_{max\ system}$ - $P_{Min\ system}$ or

$P_{max\ system}$ - $P_{standby}$ or

$P_{max\ system}$ - $P_{cold\text{-}standby}$

Minimum partial load operation = $P_{min\ system}$ / $P_{max\ system}$ %

2- The dynamics for increasing power depend on the selected lower and upper power state:

Time to power up τ_{up} = $\tau_{cold} + \tau_{nom\ ->max}$ or

$\tau_{start,standby} + \tau_{nom->max}$ or

$\tau_{min->max}$

3- The dynamics for decreasing power depend on the selected lower and upper power state:

Time to power down τ_{down} = $\tau_{max->min}$

$\tau_{down\_to\_standby} + \tau_{max->nom}$ or

$\tau_{down\_to\_cold} + \tau_{max->nom}$

minimum part load to full load is calculated as rate of load change (%) per second using $\tau_{min->max}$

full load to minimum part load is calculated as rate of load change (%) per second using $\tau_{max->min}$

8.4.9 Data measurement

- The recommended data sampling rate is 1 per second.
- Values for three or more measurements of the test input and output parameters shall be within the range of ±5 % of their average.

8.5 Load profiles for grid balancing

As indicated in Section 8.2.2, the actual implementation of frequency control and of the formulation of the corresponding requirements vary from country to country. In particular, load-versus-time profiles included in the pre-qualification requirements of TSOs in the different member states are different for the three grid balancing services identified in Regulation EU(2017)1485 (Table 29). It is therefore useful to harmonise the different load profiles into a single set of representative load profiles to be used for pre-qualification purposes of electrolysers. This is the main objective of the QualyGridS project which has formulated the set of 7 load profiles listed in Table 38, corresponding to the frequency control processes for grid balancing listed in Table 29. The set of harmonised load profiles is summarised and presented in this section.

Table 38. Load profiles for grid balancing

	LOAD PROFILES FOR GRID BALANCING	SECTION
1	**FREQUENCY CONTAINMENT RESERVE FCR**	**8.5.1**
	***AUTOMATED* FREQUENCY RESTORATION RESERVE aFRR**	**8.5.2**
2	➢ **aFRR Negative Control Power**	**8.5.2.1**
3	➢ **aFRR Positive Control Power**	**8.5.2.2**
	***MANUAL* FREQUENCY RESTORATION RESERVE mFRR**	**8.5.3**
4	➢ **mFRR Negative Control Power**	**8.5.3.1**
5	➢ **mFRR Positive Control Power**	**8.5.3.2**
	REPLACEMENT RESERVES RR	**8.5.4**
6	➢ **RR Negative (Upward) Control Power**	**8.5.4.1**
7	➢ **RR Positive (Downward) Control Power**	**8.5.4.2**

Source: JRC, 2020

The load profiles used by TSOs for pre-qualification purposes represent those in the intended grid balance application and have been referred to as system-level RWD load profiles (see Section 7.7). Hence the harmonised load profiles established by QualyGridS also represent system-level RWD. Individual load profiles from this set are therefore used for assessing degradation rate or durability under dynamic conditions in *in-situ* tests at cell/short stack level (see Section 7.7).

It is to be noted that the set of 7 harmonised load profiles simulating requirements for grid balancing services does not prevail over and does not intend to substitute the regulatory requirements regarding pre-qualification in different member states. Consequently, electrolyser system compliance with these load profiles described below does not imply meeting the pre-qualification requirements by TSOs.

8.5.1 Frequency containment reserves (FCR) test protocol

The load profile, depicted in Figure 34, aims at determining the electrolyser system response to positive and negative power steps, by assessing the characteristic duration times identified in FCR prequalification load profiles. The associated test protocol is described in Table 39. The parameters P_{up}, P_{low} and P_{med} are determined as described in Section 8.4.1 as, P_{max}, P_{min}, Pnom but they can be limited for grid servicing to a smaller power system interval. For this reason, in this section the terms P_{up}, P_{low} and P_{med} will be used. P_{med} is defined as $0.5 \cdot (P_{low} + P_{up})$. The same applies for all test protocols listed in Table 38.

Table 39. FCR test proocol

STEP	TEST TIME (S)	DESCRIPTION
1	0	Set the power set point to P_{med}. Measure the system electrical power input and the rectifier electrical power input vs. time.
2	3600	Set the power set point to P_{up}. Measure the system electrical power input and the rectifier electrical power input vs. time.
3	4530	Set the power set point to P_{med}. Measure the system electrical power input and the rectifier electrical power input vs. time.
4	5460	Set the power set point to P_{up}. Measure the system electrical power input and the rectifier electrical power input vs. time.
5	7290	Set the power set point to P_{med}. Measure the system electrical power input and the rectifier electrical power input vs. time.
6	8220	Set the power set point to P_{low}. Measure the system electrical power input and the rectifier electrical power input vs. time.
7	9150	Set the power set point to P_{med}. Measure the system electrical power input and the rectifier electrical power input vs. time.
8	10080	Set the power set point to P_{low}. Measure the system electrical power input and the rectifier electrical power input vs. time.
9	12010	Set the power set point to P_{med}. Measure the system electrical power input and the rectifier electrical power input vs. time.
10	12940	End of test.

Source: QualyGridS [10]

Figure 34. FCR profile, illustration of phases A-I for stability evaluation, allowed range for system power during these phases (marked with green dashed line) and steps 1-8

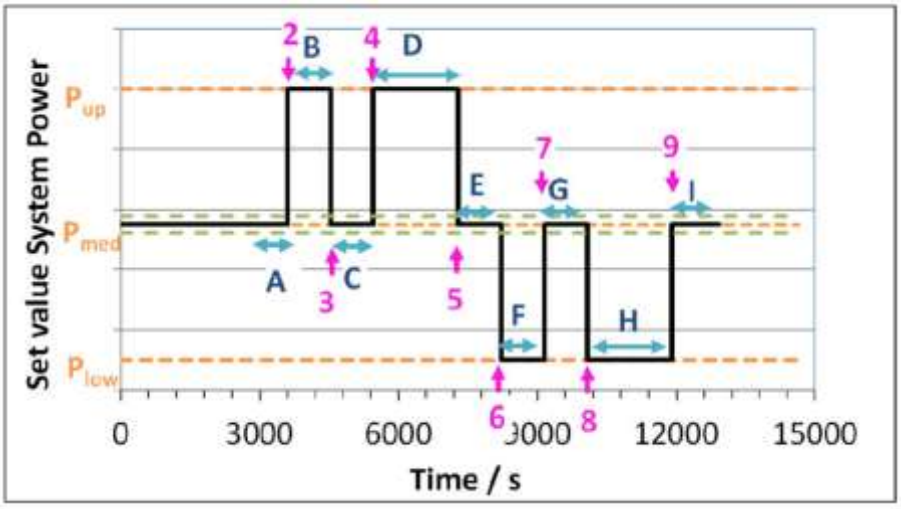

Source: QualyGridS [10]

The parameters to establish are related to the upward and downward ramps:

- **Ramps up duration (t_m; t_{full})**: upward ramps (2 and 4 (Figure 34)) are characterised by two characteristic times (Figure 35) which have to be determined for each of the ramps.

  t_m is the time from the start of the power increase to reach 50% of the value of the imposed step response, i.e. system power reaching $P_{med}+(0.5\cdot(P_{up} - P_{med}))$.

  t_{full} is the time from the start of the power increase to stabilise system power at P_{up}: In the following 15 min the system power must remain between P_{up} and (P_{up} ± $0.05\cdot(P_{up}-P_{med})$) for ramps 2 and 4 respectively between P_{med} and (P_{med} ± $0.05\cdot(P_{up}-P_{med})$) for steps 7 and 9.

Figure 35. FCR profile: illustration evaluation of ramps up. Black full line: power set points, green full line example of real system power

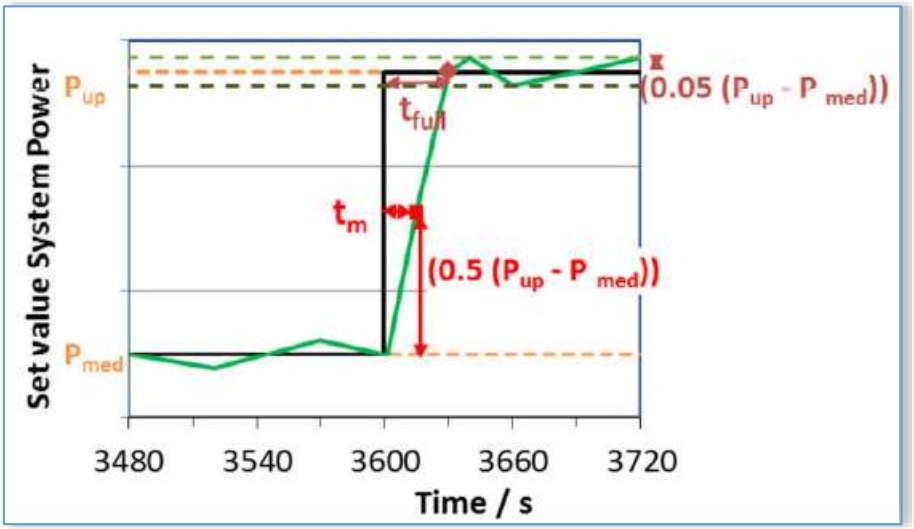

Source: QualyGridS [10]

- **Ramps down duration (t_m; t_{full}):** downward ramps 6 and 8, 3 and 5 (Figure 34) are characterised by two characteristic times (Figure 36) which have to be determined for each of the ramps:

  t_m is the time from the start of the power decrease to reach 50 % of the value of the set step response, i.e. system power reaching (P_{med} - 0.5 · (P_{med}– P_{low})) for ramps 6 and 8 respectively (P_{med} + 0.5 (P_{med} - P_{low} for ramps 3 and 5)

  t_{full} is the time from the start of the power decrease to stabilise system power at P_{low}: In the following 15 min the system power must remain between P_{low} and (P_{low} ± 0.05·(P_{up} - P_{med})) for ramps 6 and 8 respectively. P_{med} and (P_{med} ± 0.05· (P_{low} - P_{med})) for ramps 3 and 5.

Figure 36. FCR profile: Illustration evaluation of ramps down (for ramps 3 and 5). Black full line: power set points, green full line example of real system power

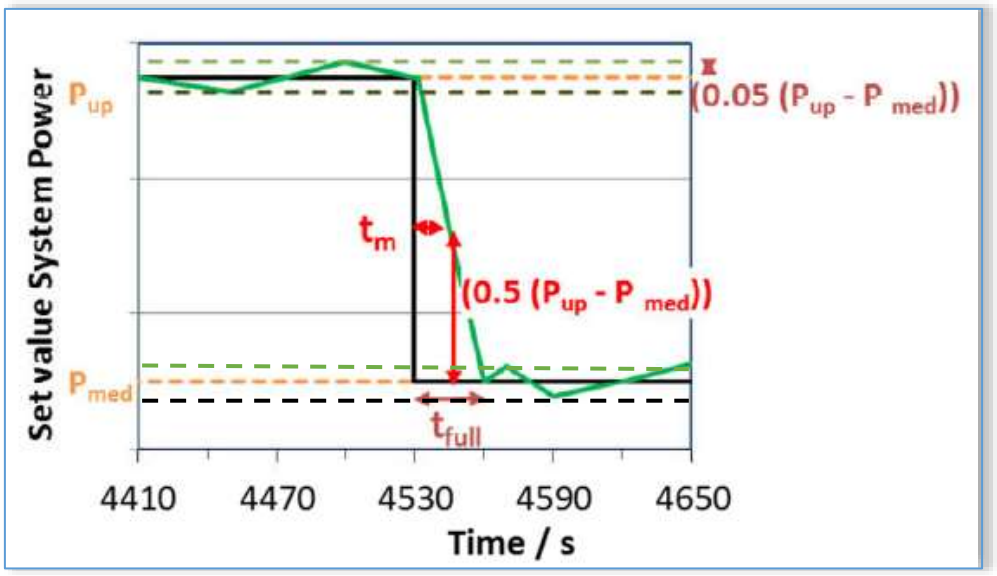

Source: QualyGridS [10]

Data analysis

- **Initial response time (t_{init}):** For steps 2, 4, 6 and 8 the time between the change of the power setpoint and the start of the system response is to be determined. For an upward ramp this is the time between the step request signal and the moment when the system power monotonically increases and has the value > P_{med}. For a downward ramp this is the time between the step request signal and the moment when the system power monotonically decreases and has the value < P_{med}.

KPI Initial response time: Maximum of t_{init} for ramps 2, 4, 6 and 8.

During all phases of constant power setpoint, power fluctuations must be limited to maximum 0.05·(P_{med} - P_{low}):

- Power setting at P_{med}: The maximum deviation from P_{med} during phases A, C, E, G and I (see Figure 34) shall be documented in the 15 min period before the respective imposed power step changes (2, 4, 6, 8) and before the end of test;
- Power setting at P_{up}: The maximum deviation from P_{up} during phases B and D (see Figure 34) shall be documented in the 15 min period following the first 30 s after

the imposed power step changes 2 and in the 30 min period following the first 30 after the imposed power step changes 4;

- Power setting at P_{low}: The maximum deviation from P_{low} during phases F and H (see Figure 34) shall be documented in the 15 min period following the first 30 s after the power step changes 6 and and in the 30 min period following the first 30 after the imposed power step changes 8.

The performance targets for the FCR test are listed in Table 40.

Table 40. FCR performance targets - KPIs

Indicator	Symbol	Target
Ramp duration	t_m	≤15 s
	t_{full}	≤ 30 s
Power stability: maximum deviation	ΔP_{max}	≤ 0.05 · (P_{med} - P_{low})
Initial response time	t_{init}	≤ 1.5 s

Source: QualyGridS [10]

8.5.2 Automated frequency restoration reserves (aFRR) testing protocol

This protocol aims at determining the electrolyser system response to power steps by assessing the characteristic duration times identified in aFRR prequalification load profiles. The protocol consists of two parts, with fast and medium ramp rates upwards and downwards, enabling separate evaluation of the services of negative and positive control power, respectively.

8.5.2.1 aFRR negative control power (electrolyser power increase upon request)

The load profile is depicted in Figure 37 and the associated test protocol is described in Table 41.

Table 41. aFRR negative control power protocol

STEP	DESCRIPTION
1	Set system at P_{low}
2	Wait for system power to stabilize*
3	Operate at this level for 1 hour
4	At $t=t_1$, initiate power ramp of power (+25% (P_{up} - P_{low})) in 800 seconds
5	$t=t_1$+800 seconds: end of the ramp
6	Keep set power for 5 minutes
7	Set system at P_{low} (the time the system needs to return to P_{low} is not Evaluated)
8	Wait for system power to stabilize *
9	At $t=t_2$, initiate power ramp of power (+50% (P_{up} - P_{low})) in 800 seconds
10	$t=t_2$+800 seconds: end of the ramp
11	Keep set power for 5 minutes
12	Set system at P_{low} (the time the system needs to return to P_{low} is not evaluated)
13	Wait for system power to stabilize *
14	At $t=t_3$, initiate power ramp of power (+75% (P_{up} - P_{low})) in 800 seconds
15	$t=t_3$+800 seconds: end of the ramp
16	Keep set power for 5 minutes
17	Set system at P_{low} (the time the system needs to return to P_{low} is not evaluated)
18	Wait for system power to stabilize *
19	At $t=t_4$, initiate power ramp of power (+100% (P_{up} - Pl_{ow})) in 800 seconds
20	$t=t_4$+800 seconds: end of the ramp
21	Keep set power for 15 minutes
22	At $t=t_5$, initiate power ramp of power (-100% (P_{up} - P_{low})) in 800 seconds
23	$t=t_5$+800 seconds: end of the ramp
24	Keep set power for 15 minutes
25	At $t=t_6$, initiate linear power ramp of power (+100% (P_{up} - Pl_{ow})) in 800 seconds
26	$t=t_6$+800 seconds: end of the ramp

STEP	DESCRIPTION
27	Keep set power for 15 minutes
28	At t=t_7, initiate power ramp of power (-100% (P_{up} - P_{low})) in 800 seconds
29	t=t_7+800 seconds: end of the ramp
30	Wait for system power to stabilize *
31	Operate at this level for 15 minutes
32	at=t_8, initiate linear power ramp of power (25% (P_{up} - P_{low})) in 133 seconds
33	t=t_8+133 seconds: end of the ramp
34	Keep set power for 5 minutes
35	Set system at P_{low} (the time the system needs to return to P_{low} is not evaluated)
36	Wait for system power to stabilize*
37	At t=t_9, initiate linear power ramp of power (+50% (P_{up} - P_{low})) in 133 seconds
38	t=t_9+133 seconds: end of the ramp
39	Keep set power for 5 minutes
40	Set system at P_{low} (the time the system needs to return to P_{low} is not evaluated)
41	Wait for system power to stabilize*
42	At t=t_{10}, initiate linear power ramp of power (+75% (P_{up} - P_{low})) in 133 seconds
43	t=t_{10}+133 seconds: end of the ramp
44	Keep set power for 5 minutes
45	Set system at P_{low} (the time the system needs to return to P_{low} is not evaluated)
46	Wait for system power to stabilize*
47	At t=t_{11}, initiate power ramp of power (+100% (P_{up} - P_{low})) in 300 seconds
48	t=t_{11}+300 seconds: end of the ramp
49	Keep set power for 15 minutes
50	At t=t_{12}, initiate linear power ramp of power (-100% (P_{up} - P_{low})) in 300 seconds
51	t=t_{12}+300 seconds: end of the ramp
52	Keep set power for 15 minutes
53	At t=t_{13}, initiate linear power ramp of power (+100% (P_{up} - P_{low})) in 300 seconds
54	t=t_{13}+300 seconds: end of the ramp
55	Keep set power for 15 minutes
56	At t=t_{14}, initiate linear power ramp of power (-100% (P_{up} - P_{low})) in 300 seconds
57	t=t_{14}+300 seconds: end of the ramp
58	Wait for system power to stabilize*
59	At t=t_{15}, initiate linear power ramp of power (+100% (P_{up} - P_{low})) in 133 seconds
60	t=t_{15}+133 seconds: end of the ramp
61	Keep set power for 15 minutes
62	At t=t_{16}, initiate linear power ramp of power (-100% (P_{up} - P_{low})) in 133 seconds

STEP	DESCRIPTION
63	Keep set power for 5 minutes
64	End of test

Source: QualyGridS [10], aFRR Upward ramp protocol from lower power level

*The system power is considered stable if the average power of two consecutive intervals of 60 seconds does not differ by more than (±0.05· (P_{up} - P_{low})).

Figure 37. aFRR profile with negative control power

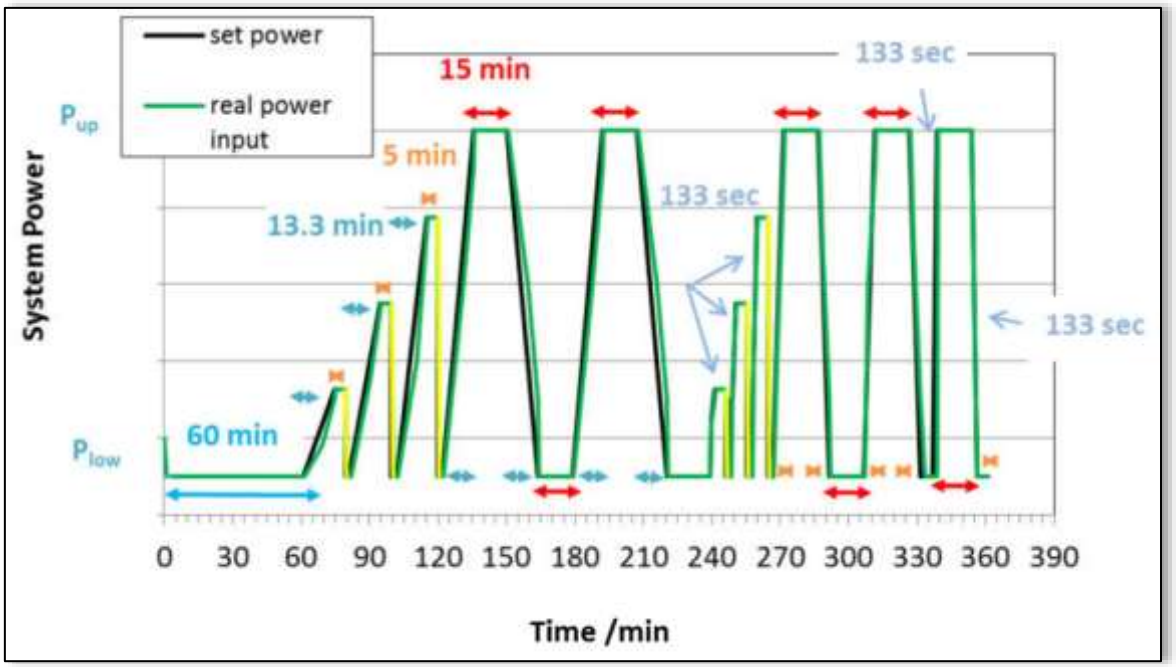

Source: QualyGridS [10]

8.5.2.2 aFRR positive control power (electrolyser power decrease upon request)

The load profile is depicted in Figure 38 and the associated test protocol is described in Table 42.

Table 42. aFRR positive control power protocol

STEP	DESCRIPTION
1	Set system at P_{up}
2	Wait for system power to stabilize*
3	Operate at this level for 1 hour
4	At $t=t_1$, initiate power ramp of power (-25% (P_{up} - P_{low})) in 800 seconds
5	$t=t_1$+800 seconds: end of the ramp
6	Keep set power for 5 minutes
7	Set system at P_{up} (the time the system needs to return to P_{up} is not evaluated)
8	Wait for system power to stabilize *

STEP	DESCRIPTION
9	At t=t_2, initiate power ramp of power (-50% (P_{up} - P_{low})) in 800 seconds
10	t=t_2+800 seconds: end of the ramp
11	Keep set power for 5 minutes
12	Set system at P_{up} (the time the system needs to return to P_{up} is not evaluated)
13	Wait for system power to stabilize *
14	At t=t_3, initiate power ramp of power (-75% (P_{up} - P_{low})) in 800 seconds
15	t=t_3+800 seconds: end of the ramp
16	Keep set power for 5 minutes
17	Set system at P_{up} (the time the system needs to return to P_{up} is not evaluated)
18	Wait for system power to stabilize *
19	At t=t_4, initiate power ramp of power (-100% (P_{up} - P_{low})) in 800 seconds
20	t=t_4+800 seconds: end of the ramp
21	Keep set power for 15 minutes
22	At t=t5, initiate power ramp of power (+100% (P_{up} - P_{low})) in 800 seconds
23	t=t_5+800 seconds: end of the ramp
24	Keep set power for 15 minutes
25	At t=t_6, initiate power ramp of power (-100% (P_{up} - P_{low})) in 800 seconds
26	t=t_6+800 seconds: end of the ramp
27	Keep set power for 15 minutes
28	At t=t_7, initiate power ramp of power (+100% (P_{up} - P_{low})) in 800 seconds
29	t=t_7+800 seconds: end of the ramp
30	Keep set power for 15 minutes
31	at=t_8, initiate power ramp of power (-25% (P_{up} - P_{low})) in 133 seconds
32	t=t_8+133 seconds: end of the ramp
33	Keep set power for 5 minutes
34	Set system at P_{up} (the time the system needs to return to P_{up} is not evaluated)
35	Wait for system power to stabilize*
36	At t=t_9, initiate power ramp of power (-50% (P_{up} - P_{low})) in 133 seconds
37	t=t_9+133 seconds: end of the ramp
38	Keep set power for 5 minutes
39	Set system at P_{up} (the time the system needs to return to P_{up} is not evaluated)
40	Wait for system power to stabilize*
41	At t=t_{10}, initiate power ramp of power (-75% (P_{up} - P_{low})) in 133 seconds
42	t=t_{10}+133 seconds: end of the ramp
43	Keep set power for 5 minutes
44	Set system at P_{up} (the time the system needs to return to P_{up} is not evaluated)
45	Wait for system power to stabilize*
46	At t=t_{11}, initiate power ramp of power (-100% (P_{up} - P_{low})) in 300 seconds
47	t=t_{11}+300 seconds: end of the ramp

STEP	DESCRIPTION
48	Keep set power for 15 minutes
49	At t=t_{12}, initiate power ramp of power (+100% (P_{up} - P_{low})) in 300 seconds
50	t=t_{12}+300 seconds: end of the ramp
51	Keep set power for 15 minutes
52	At t=t_{13}, initiate power ramp of power (-100% (P_{up} - P_{low})) in 300 seconds
53	t=t_{13}+300 seconds: end of the ramp
54	Keep set power for 15 minutes
55	At t=t_{14}, initiate power ramp of power (+100% (P_{up} - P_{low})) in 300 seconds
56	t=t_{14}+300 seconds: end of the ramp
57	Wait for system power to stabilize*
58	At t=t_{15}, initiate power ramp of power (-100% (P_{up} - P_{low})) in 300 seconds
59	t=t_{15}+133 seconds: end of the ramp
60	Keep set power for 15 minutes
61	At t=t_{16}, initiate power ramp of power (+100% (P_{up} - P_{low})) in 133 seconds
62	Keep set power for 5 minutes
63	End of test

Source: QualyGridS [10], aFRR downward ramp protocol from upper power level

*The system power is considered stable if the average power of two consecutive intervals of 60 seconds does not differ by more than (±0.05 · (P_{up}-P_{low}))

Figure 38. aFRR profile with positive control power

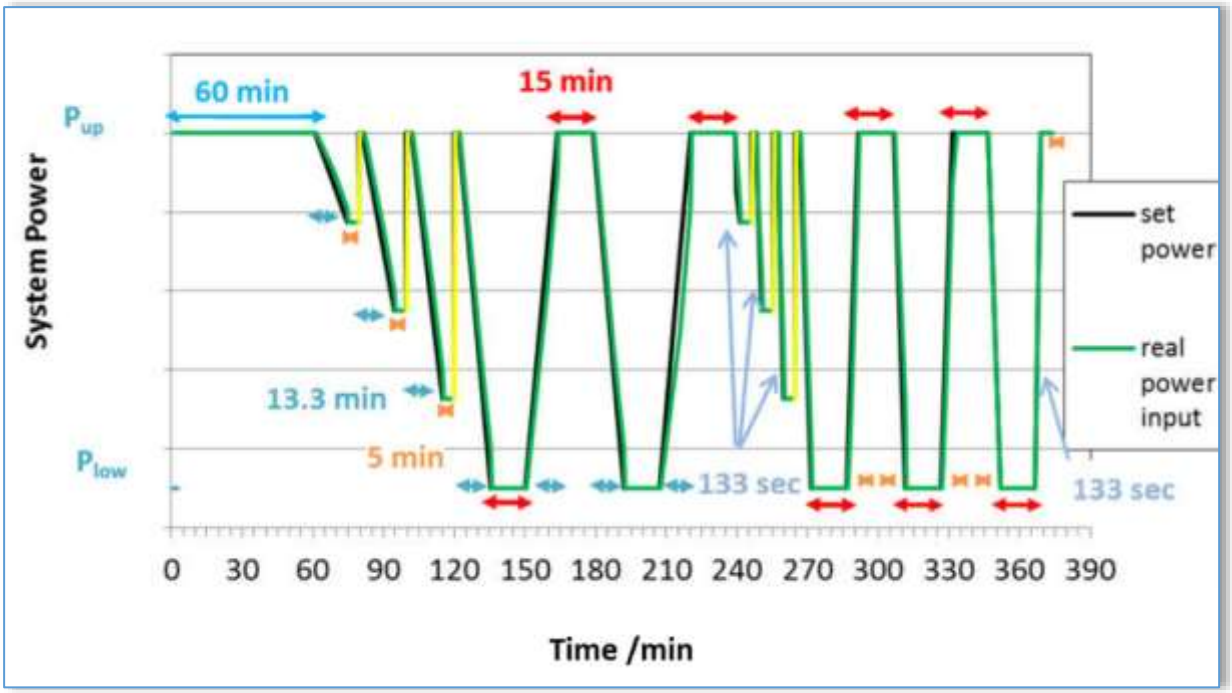

Source: QualyGridS [10]

Data evaluation and validation for aFRR

The following conditions and limit as depicted in Figure must be met:

- The power difference $\Delta P=2P_r$ measured at the end of the ramp must correspond to the target.
- During the periods of constant power request the real system power must be in the range ($\pm 0.05 \cdot (P_{up} - P_{low})$) around the requested power.
- The actual power of the system must remain 95% of the time in the bracket [$P_{tol} - \varepsilon_v$; $P_c + \varepsilon_v$] in case of a positive ramp, and [$P_c - \varepsilon_v$; $P_{tol} + \varepsilon_v$] for a negative ramp, with:
  - P_0: initial power level of the system at the beginning of the ramp (see Fig. 39)
  - Pr: absolute value at the half the ramp power amplitude
  - N: parameter going from 0 at t=0 to +2 at the end of the ramp in case of ramp up, and 0 to -2 in case of negative ramp
  - $P_c = P_0 + N \cdot Pr$
  - $P_{tol} = P_c \cdot$ (t-20 second): set power at t-20 seconds
  - ε_v : 2.5% of the full ramp power ($P_{up} - P_{low}$)

Analysis of the test results: the percentage of data points with deviation from the requested ranges during :

- the period of constant power,
- the ramps (800 s, 300 s, 133 s ramp duration type)

are the subject of this evaluation with a maximum acceptance limit of 5% for each type.

Figure 39. Positive and negative ramp acceptance limits

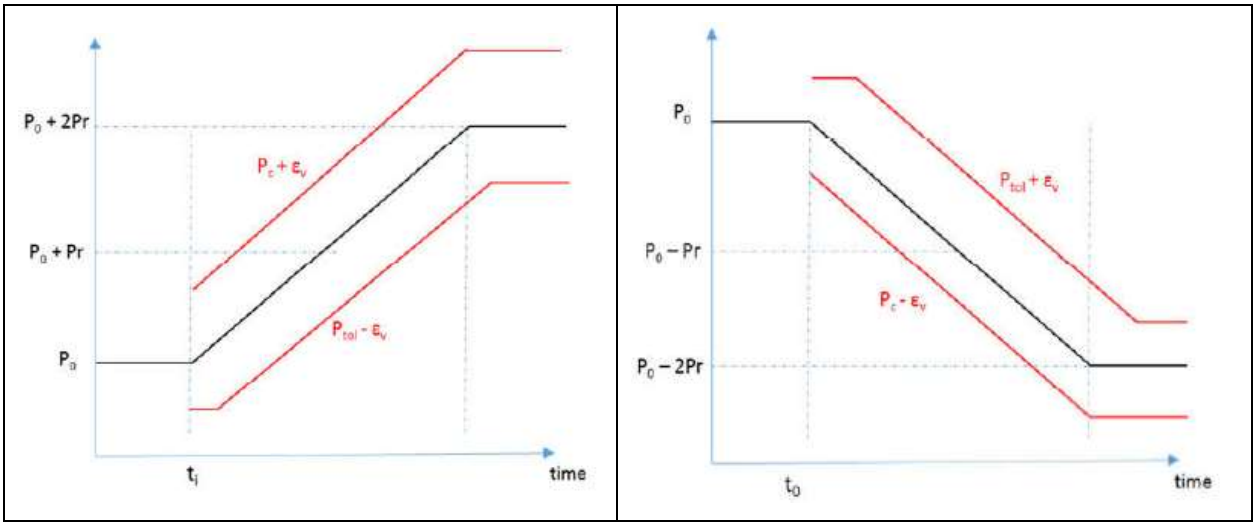

Source: QualyGridS [10]

8.5.3 Manual frequency restoration reserves (mFRR) testing protocol

This protocol aims at determining the electrolyser system response to power steps by assessing the characteristic duration times identified in mFRR prequalification load profiles. The protocol consists of two parts, with fast and medium ramp rates upwards and downwards, enabling separate evaluation of the services of negative and positive control power, respectively.

As the aFRR profile the mFRR profile contains ramps between a power level P_{low} and a power level P_{up} as well as fractions of the range. The ramp rates in mFRR are lower than for aFRR.

8.5.3.1 mFRR negative control power (electrolyser power increase upon request)

The load profile is depicted in Figure 40 and the associated test protocol is described in Table 43.

Table 43. mFRR negative control power

STEP	DESCRIPTION
1	Set system at P_{low}
2	Wait for system power to stabilize*
3	Operate at this level for 1 hour
4	At $t=t_1$, initiate power ramp of power (25% (P_{up} - P_{low})) in 10 minutes
5	$t=t_1$+600 seconds: end of the ramp
6	Keep set power for 5 minutes
7	Set system at P_{low} (the time the system needs to return to P_{low} is not Evaluated)
8	Wait for system power to stabilize *
9	At $t=t_2$, initiate power ramp of power (50% (P_{up} - P_{low})) in 10 minutes
10	$t=t_2$+600 seconds: end of the ramp
11	Keep set power for 5 minutes
12	Set system at P_{low} (the time the system needs to return to P_{low} is not evaluated)
13	Wait for system power to stabilize *
14	At $t=t_3$, initiate power ramp of power (75% (P_{up} - P_{low})) in 10 minutes
15	$t=t_3$+600 seconds: end of the ramp
16	Keep set power for 5 minutes
17	Set system at P_{low} (the time the system needs to return to P_{low} is not evaluated)
18	Wait for system power to stabilize *
19	At $t=t_4$, initiate power ramp of power (100% (P_{up} - P_{low})) in 10 minutes
20	$t=t_4$+600 seconds: end of the ramp
21	Keep set power for 60 minutes
22	At t=t5, initiate linear power ramp of power (-100% (P_{up} - P_{low})) in 10 minutes
23	$t=t_5$+600 seconds: end of the ramp

STEP	DESCRIPTION
24	Keep set power for 15 minutes
25	At $t=t_6$, initiate power ramp of power (+100% (P_{up} - Pl_{ow})) in 10 minutes
26	$t=t_6$+600 seconds: end of the ramp
27	Keep set power for 60 minutes
28	At $t=t_7$, initiate power ramp of power (-100% (P_{up} - P_{low})) in 10 minutes
29	$t=t_7$+600 seconds: end of the ramp
30	Wait for system power to stabilize*
31	End of test

Source: QualyGridS [10], mFRR upward ramp protocol from lower power level

*The system power is considered stable if the average power of two consecutive intervals of 60 seconds does not differ by more than (±0.05 (P_{up} - P_{low})).

Figure 40. mFRR profile with negative control power

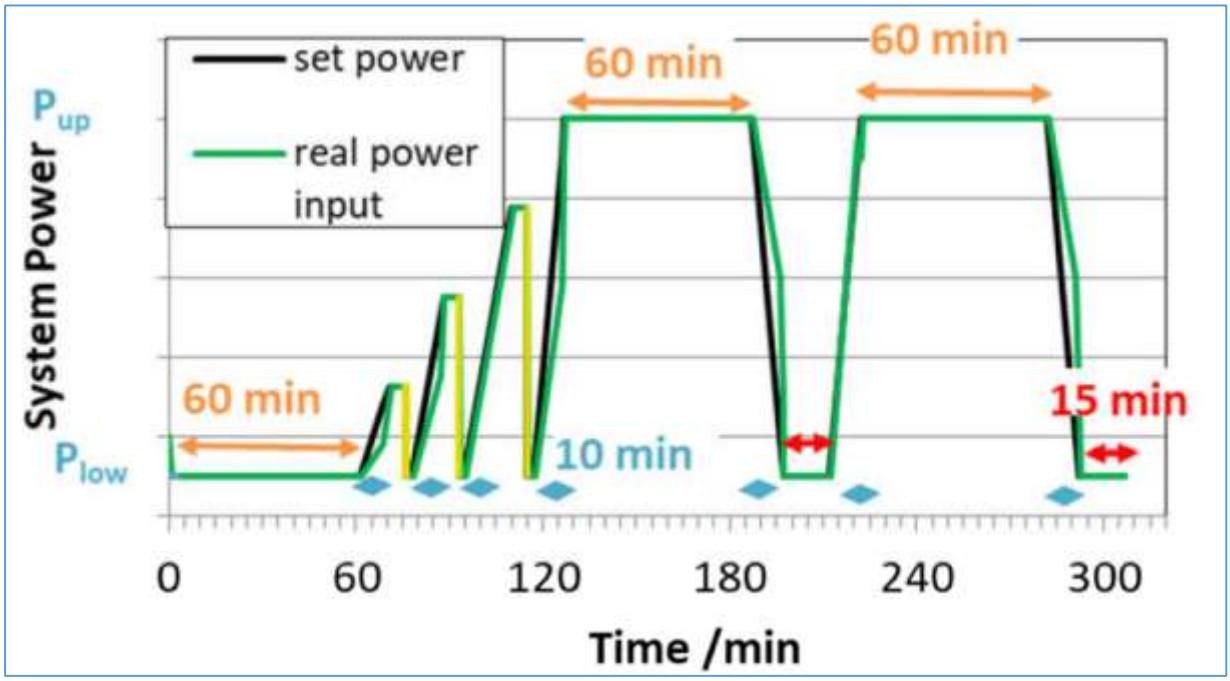

Source: QualyGridS [10]

8.5.3.2 mFRR positive control power (electrolyser power decrease upon request)

The load profile is depicted in Figure 41 and the associated test protocol is described inTable 44.

Table 44. mFRR positive control power protocol

STEP	DESCRIPTION
1	Set system at P_{up}
2	Wait for system power to stabilize*
3	Operate at this level for 1 hour
4	At $t=t_1$, initiate power ramp of power (-25% (P_{up} - P_{low})) in 10 minutes
5	$t=t_1$+600 seconds: end of the ramp
6	Keep set power for 5 minutes
7	Set system at P_{up} (the time the system needs to return to P_{up} is not Evaluated)
8	Wait for system power to stabilize *
9	At $t=t_2$, initiate power ramp of power (-50% (P_{up} - P_{low})) in 10 minutes
10	$t=t_2$+600 seconds: end of the ramp
11	Keep set power for 5 minutes
12	Set system at P_{up} (the time the system needs to return to P_{low} is not evaluated)
13	Wait for system power to stabilize *
14	At $t=t_3$, initiate power ramp of power (-75% (P_{up} - P_{low})) in 10 minutes
15	$t=t_3$+600 seconds: end of the ramp
16	Keep set power for 5 minutes
17	Set system at P_{up} (the time the system needs to return to P_{up} is not evaluated)
18	Wait for system power to stabilize *
19	At $t=t_4$, initiate power ramp of power (-100% (P_{up} - Pl_{ow})) in 10 minutes
20	$t=t_4$+600 seconds: end of the ramp
21	Keep set power for 60 minutes
22	At t=t5, initiate power ramp of power (+100% (P_{up} - P_{low})) in 10 minutes
23	$t=t_5$+600 seconds: end of the ramp
24	Keep set power for 15 minutes
25	At $t=t_6$, initiate linear power ramp of power (-100% (P_{up} - Pl_{ow})) in 10 minutes
26	$t=t_6$+600 seconds: end of the ramp
27	Keep set power for 60 minutes
28	At $t=t_7$, initiate power ramp of power (+100% (P_{up} - P_{low})) in 10 minutes
29	$t=t_7$+600 seconds: end of the ramp
30	Keep set power for 15 minutes
31	End of test

Source: QualyGridS [10], mFRR downward ramp protocol from upper power level

*The system power is considered stable if the average power of two consecutive intervals of 60 seconds does not differ by more than (±0.05 · (Pup-Plow)).

Figure 41. mFRR profile with positive control power

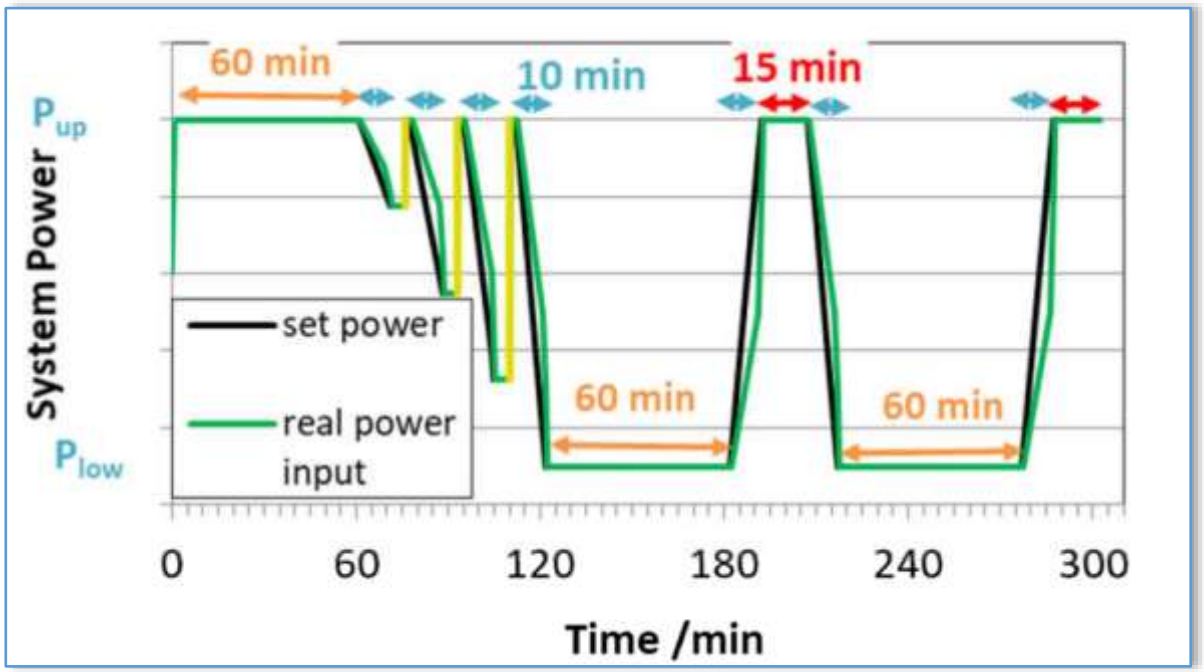

Source: QualyGridS [10]

Data evaluation and validation for mFRR

The following conditions and limit as depicted in Figure 42 must be met:

- The power difference $\Delta P=2P_r$ measured at the end of the ramp must correspond to the target.
- During the periods of constant power request the real system power must be in the range ($\pm 0.05 \cdot (P_{up}-P_{low})$) around the requested power. This condition is valid as soon as the power enters the interval ($P_0+2\ P_r \pm 5\%\ (P_{up}-P_{low})$) for positive ramp and ($P_0-2\ P_r \pm 5\%\ (P_{up}-P_{low})$) for negative ramp.
- The actual power of the system must remain 95% of the time in the bracket $[P_{tol} - \varepsilon_v;\ P_c + \varepsilon_v]$ in case of a positive ramp, and $[P_c - \varepsilon_v;\ P_{tol} + \varepsilon_v]$ for a negative ramp, with:
  - P_0: initial power level of the system at the beginning of the ramp (see Fig. 42)
  - Pr: absolute value at the half the ramp power amplitude
  - N: parameter going from 0 at t=0 to +2 in the end of the ramp in case of positive ramp, and 0 to -2 in case of negative ramp
  - $P_c = P_0 + N \cdot Pr$
  - $P_{tol} = P_c \cdot$ (t-20 second): set power at t-20 seconds
  - ε_v: 2.5% of the full ramp power (P_{up} - P_{low}).

Analysis of test results: the percentage of data points with deviation from the requested ranges during :

- the period of constant power,
- the ramps

are the subject of this evaluation with a maximum acceptance limit of 5% for each type.

Figure 42. Positive and negative ramp acceptance limits

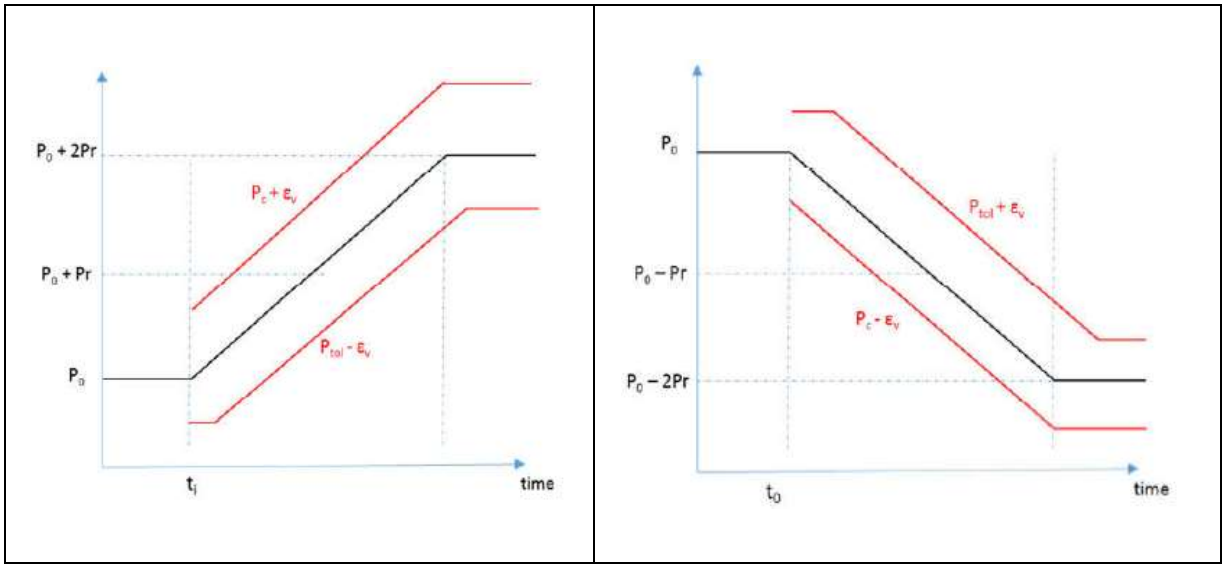

Source: QualyGridS [10]

8.5.4 Replacement reserves (RR) testing protocol

This protocol aims at checking the agreement between consumption based on setpoint and real consumption over time intervals of selected duration. The services of positive and negative control power are considered separately.

8.5.4.1 RR negative control power (electrolyser power increase upon request)

The load profile is depicted in Figure 43 and the associated test protocol is described in Table 45.

Table 45. RR negative control power protocol

STEP	DESCRIPTION
1	Set system at P_{low}
2	Wait for system power to stabilize*
3	Operate at this level for 1 hour
4	At $t=t_1$, set system power to P_{low} + 25 %(P_{up} - P_{low})
5	Wait until $t=t_1$+15 minutes
6	Keep set power for 5 minutes
7	Set system at P_{low}
8	Wait for system power to stabilize *
9	At $t=t_2$, set system power to P_{low} + 50 %(P_{up} - P_{low})
10	Wait until $t=t_2$+15 minutes
11	Keep set power for 5 minutes
12	Set system at P_{low}
13	Wait for system power to stabilize *
14	At $t=t_3$, set system power to P_{low}+75 %(P_{up} - P_{low})
15	Wait until $t=t_3$+15 minutes
16	Keep set power for 5 minutes
17	Set system at P_{low}
18	Wait for system power to stabilize *
19	At $t=t_4$, set system power to P_{up}
20	Wait until $t=t_4$+15 minutes
21	Keep set power for 60 minutes
22	At $t=t_5$, set system power to P_{low}
23	Wait until $t=t_5$+15 minutes
24	Keep set power for 15 minutes
25	At $t=t_6$, set system power to P_{up}
26	Wait until $t=t_6$+15 minutes
27	Keep set power for 60 minutes
28	At $t=t_7$ set power to P_{low}
29	Wait until $t=t_7$+15 minutes

STEP	DESCRIPTION
30	Wait for system power to stabilize*
31	End of test

Source: QualyGridS [10], RR upward power conformity protocol from lower power level

*The system power is considered stable if the average power of two consecutive intervals of 60 seconds does not differ by more than ($\pm 0.05 \cdot (P_{up}-P_{low})$).

Figure 43. RR profile with upward control power

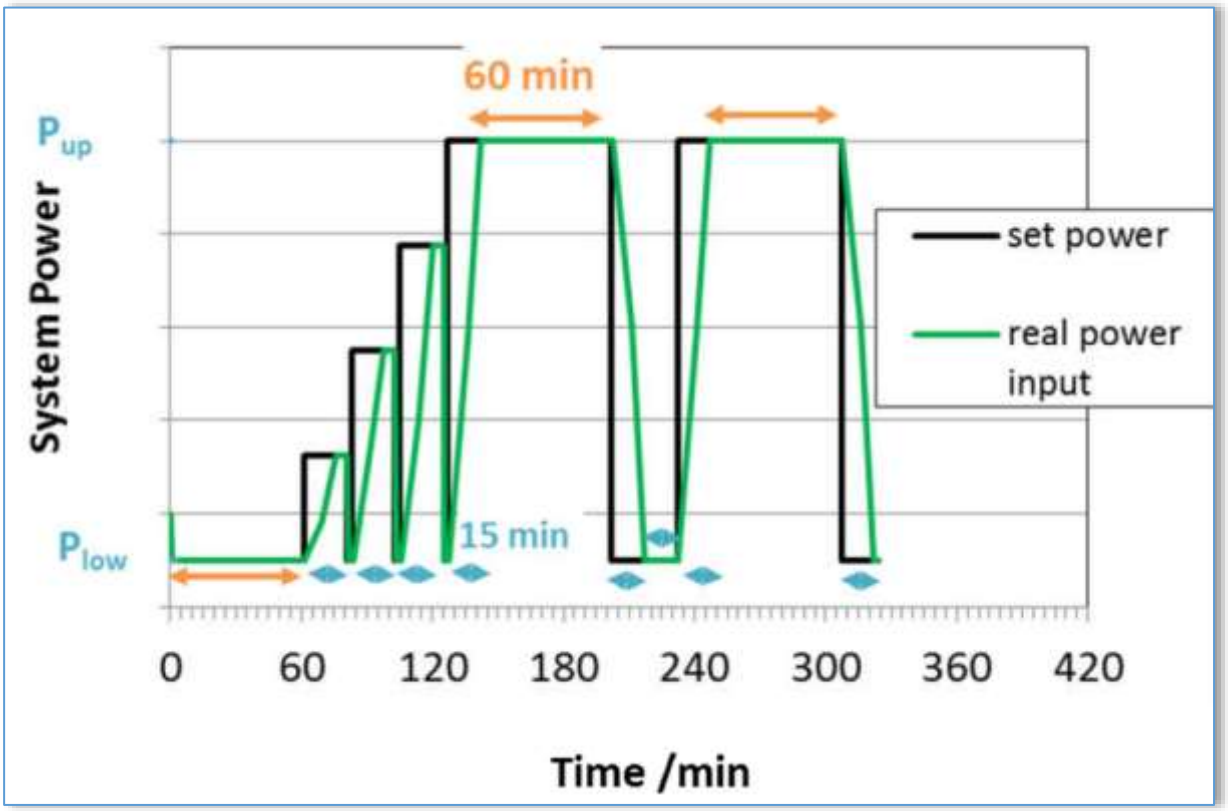

Source: QualyGridS [10]

8.5.4.2 RR positive control power (electrolyser power decrease upon request)

The load profile is depicted in Figure 44 and the associated test protocol is described in Table 46.

Table 46. RR positive control power protocol

STEP	DESCRIPTION
1	Set system at P_{UP}
2	Wait for system power to stabilize*
3	Operate at this level for 1 hour
4	At $t=t_1$, set system power to P_{up} - 25% (P_{up} - P_{low})
5	Wait until $t=t_1$+15 minutes
6	Keep set power for 5 minutes
7	Set system at P_{up}
8	Wait for system power to stabilize *
9	At $t=t_2$, set system power to P_{up}-50% (P_{up} - P_{low})
10	Wait until $t=t_2$+15 minutes
11	Keep set power for 5 minutes
12	Set system at P_{up}
13	Wait for system power to stabilize *
14	At $t=t_3$, set system power to P_{up}-75% (P_{up} - P_{low})
15	Wait until $t=t_3$+15 minutes
16	Keep set power for 5 minutes
17	Set system at P_{up}
18	Wait for system power to stabilize *
19	At $t=t_4$, set system power to P_{low}
20	Wait until $t=t_4$+15 minutes
21	Keep set power for 60 minutes
22	At $t=t_5$, set system power to P_{up}
23	Wait until $t=t_5$+15 minutes
24	Keep set power for 15 minutes
25	At t=t6, set system power to P_{low}
26	Wait until $t=t_6$+15 minutes
27	Keep set power for 60 minutes
28	At $t=t_7$ set power to P_{up}
29	Wait until $t=t_7$+15 minutes
30	Wait for system power to stabilize*
31	End of test

Source: QualyGridS [10], RR downward power conformity protocol from upper power level

*The system power is considered stable if the average power of two consecutive intervals of 60 seconds does not differ by more than ($\pm 0.05 \cdot (P_{up}-P_{low})$).

Figure 44. RR profile with downward control power

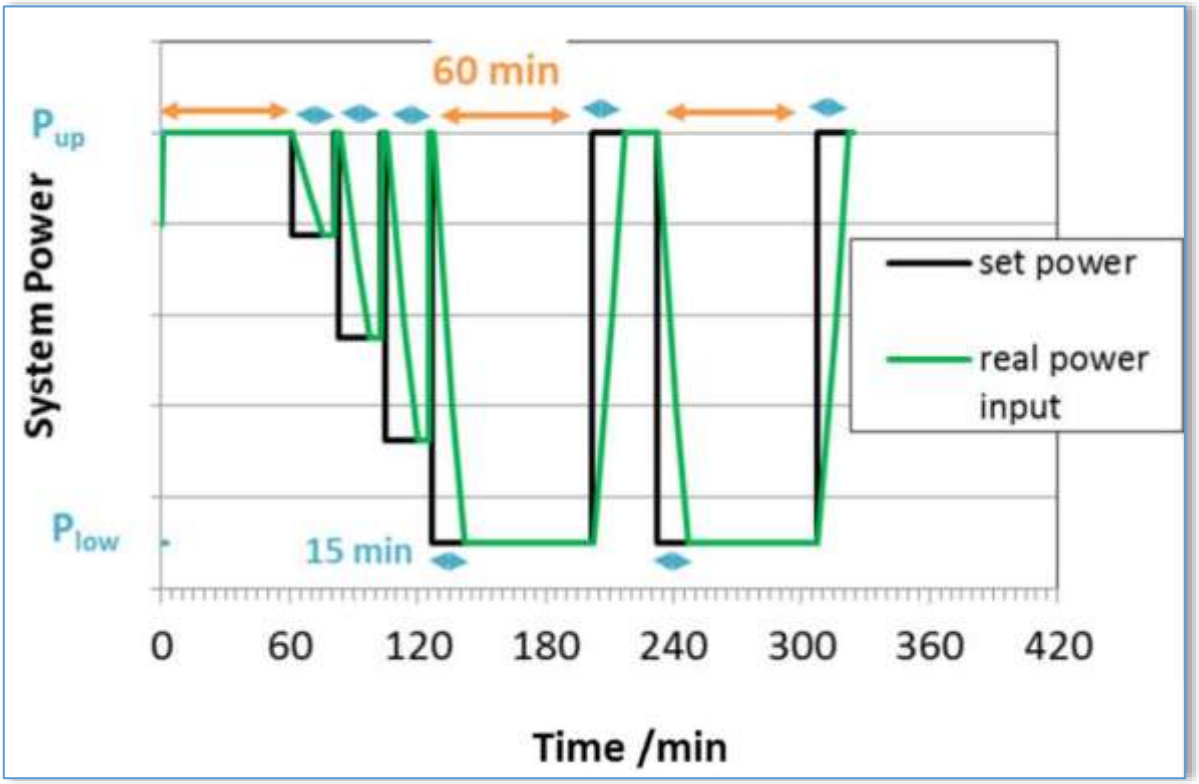

Source: QualyGridS [10]

Acceptance criteria

For each step response, the test is considered successful when the measured power is equal to the target power. The target power must be reached after no more than 900 seconds.

During the activation the power should remain in an interval of P_{up} (±5% (P_{up}-P_{low})) for negative control power and P_{low} (±5% (P_{up}-P_{low})) for positive control power.

8.6 Efficiency at system level

To determine efficiency at system level, the energy consumption of ancillary equipment has to be accounted for. The latter heavily depends on the system boundaries. Within these boundaries, the total energy input to be considered consists of the sum of the electricity and of heat provided to the electrolyser itself and to the BoP components.

Similarly, as for the approach described in Section 7.2.4 at cell level, efficiency at system level is defined as the ratio between the flow rate of the produced hydrogen, $\dot{n}_{H_2}$, multiplied by its energy content, and the total electric and thermal power supplied to the system:

$$\epsilon_{system}^{HHV\ or\ LHV} = \frac{HHV\ or\ LHV}{P_{elec} + P_{therm} + P_{aux}} \cdot \dot{n}_{H_2} \qquad \text{[Eq. 8.1]}$$

where P_{aux} takes into account of all the power related to auxiliary equipment (heat exchangers, pumps, etc.).

As described in Section 7.2.4, the selection of HHV or of LHV matters and should therefore be explicitly mentioned when providing efficiency values.

HHV or LHV are expressed in J.mol^{-1}, but via some unit conversion the value can be expressed in kWh.kg^{-1}. In this case the HHV value is equivalent to 39.40 kWh.kg^{-1}, and represents the minimum amount of energy needed to produce 1 kg of hydrogen. Therefore the specific energy consumption is defined as the electrolyser system total energy supplied, in kWh, to produce 1 kg of hydrogen.

By integration of Eq. 8.1 on a time interval Δt, it is possible to express the energy efficiency at system level in terms of the total energy provided:

$$W_{total} = \int_0^{\Delta t} \varepsilon_{system}\,(P_{elec} + P_{therm} + P_{aux})\,dt = \Delta H^{HHV\ or\ LHV} \times \Delta N_{H_2}$$

so for a given interval of time under stationary conditions:

$$\varepsilon_{system}^{HHV\ (or\ LHV)} = \frac{HHV\ (or\ LHV)\dot{n}_{H_2}\Delta t}{W_{elec} + \Delta Q_{rev} + \Delta Q_{H2O}} = \frac{HHV\ (or\ LHV)\ \Delta N_{H_2}}{W_{elec} + \Delta Q_{rev} + \Delta Q_{H2O}} =$$

$$= \frac{\Delta H_{rev}\,\Delta N_{H_2}}{W_{irrev}} = \frac{N\,U_{tn}(T,p)\,N_{H_2}}{W_{irrev}} \qquad \text{[Eq. 8.2]}$$

with ΔQ_{H20} the thermal energy input supplied externally.

Rather than in terms of hydrogen production rate, some authors prefer expressing system efficiency in terms of voltage ratio corrected by an AC/DC conversion coefficient:

$$\varepsilon_{system} = \frac{N \cdot U_{tn}(T,p)\,N_{H_2}}{W_{irrev}} \left(\frac{\eta_{AC/DC}}{1+\xi}\right) \qquad \text{[Eq. 8.3]}$$

with $W_{irrev} = W_{elec} + \Delta Q_{rev} + \Delta Q_{H2O} = 2F\,[U_{stack} + N\,(U_{tn} - U_{rev})] + \Delta Q_{H2O}$,

$\eta_{AC/DC}$ the efficiency of the AC/DC converter and

ξ the ratio between parasitic power due to energy consumption by auxiliary equipment and net power consumed by the electrolyser.

8.7 System: data analysis for performance assessment

System Performance is assessed on the basis of the indicators listed in the following table.

Table 47. System Performance Criteria

	CRITERIA	unit	Ref.
1	System (stack) Voltage	V	
2	System (stack) Current	A	
3	Current density	$A.cm^{-2}$	
4	Hydrogen production rate	$kg.h^{-1}$	
5	System outlet hydrogen pressure	MPa or Bar	
6	Hydrogen Quality	%	
7	System Efficiency as $\eta^{(HHV\ or\ LHV)}$	%	Eq 8.1
8	System Efficiency as ε_{system}	%	Eq. 8.2
9	System Efficiency with AC/DC conversion as ε_{system}	%	Eq. 8.3
10	Specific energy consumption	$kWh.kg^{-1}$	§ 8.6
11	Response time	s	Table 40
12	Minimum partial load operation	%	§ 8.4.9
13	Start-up time (cold) to nominal power load	s	§ 8.4.6
14	Minimum part load to full load rate	$\%.s^{-1}$	§ 8.4.9
15	Full load to minimum part load rate	$\%.s^{-1}$	§ 8.4.9

Source: JRC, 2020

Determination of the system performance indicators at different moments in time between BoL and EoL can provide an indication of the change of performance of the electrolysis system. This change of system performance with time is often referred to as "system durability". This approach of assessing durability at system level is directly comparable to the first method described for cell/short stack level in Section 7.6 and a spider graph similar to the one given in Figure 23 can be used to illustrate system-level performance at a given moment in time and compare it to the initial performance at the normal operation set point.

9 Conclusive remarks and recommendations

This report is based upon a state-of-the-art knowledge and upon results available today. Along with the development of water electrolysis technologies, we expect a need for updating and improving some of the protocols presented. Particularly in the area of accelerated testing and the grid-electrolyser coupling mode, ongoing FCH2JU projects and the installation in Europe of high-power electrolyser systems will produce new evidences and identify new testing requirements. The LTWE Working Group will then work on an update of the present report.

The testing protocols provided in this report can be adopted by Research and Innovation (R&I) funding agencies, and in particular by the FCH2JU, to assess quantitatively the progress reached towards their programme objectives and targets. To achieve this, it is necessary that the related projects are committed to apply the harmonised test protocols and to report in a consistent way the results. The adoption of the protocols by FCH2JU projects could also enable their utilisation in a broader scientific community by offering a methodological approach suitable for use in peer-reviewed scientific publications. Finally, the approaches and outcomes of this report are believed to offer a workable basis for future European and international standardisations.

Symbols

Table 48. Definition of Symbols

Symbol	Unit	Description
A	m^2, cm^2	Active surface area of the cell
C	C	Electric charge, Coulomb
c	%, $Mol.L^{-1}$	Concentration
c_p	$J.g^{-1}.K^{-1}$	Specific Heat capacity under standard conditions ($c_{p(H2O)}$ = 4.186 $J.g^{-1}.K^{-1}$)
E	V	Electrical potential
F	$C.mol^{-1}$	Faraday's constant (F = 96485.3328959 C mol^{-1})
G	$J.mol^{-1}$	Gibbs free energy
H	$J.mol^{-1}$	Molar enthalpy
j	$A.m^{-2}$, $A.cm^{-2}$	Current density (j = I / A)
I	A	Electrical current
I_{max}	A	Maximum current
J	J	Energy unit (Joules)
m	g	Mass
M	$g.mol^{-1}$	Molar mass
N		Number of objects
n	$Mol.L^{-1}$	molarity
$\dot{n}$	$Mol.s^{-1}$	Molar flow rate
p	Pa, bar, atm	Pressure
p^{θ}	Pa, bar	Reference pressure
p^{A}	Pa, bar	Anodic pressure
p^{C}	Pa, bar	Cathodic pressure
P	W	Power
Q	$J.mol^{-1}$	Heat
R	$J.mol^{-1}.K^{-1}$	Universal gas constant (R = 8.31446 $J.mol^{-1}.K^{-1}$)
S	$J.mol^{-1}.K^{-1}$	Entropy
t	s, h	Time (second, hour)

Symbol	Unit	Description
T	K, °C	Temperature (Kelvin, degree Celsius)
$T_{x, y}$	K, °C	Temperature of cell fluid *x* at cell location *y* (inlet = in or outlet = out)
T_{env}	K, °C	Ambient temperature
T_{ehs}	K, °C	Temperature of an external heat source
T_c	K, °C	Cell temperature
U	V	Voltage
U_{irrev}	V	Irreversible voltage
U_{rev}	V	Reversible voltage
U_{tn}	V	Thermoneutral cell voltage (U_{tn}= 1.48V at SATP conditions)
$\dot{U}$	$\mu V.h^{-1}$	Voltage degradation
W	$J.mol^{-1}$	Work, electrical energy needed to transform 1 mole of reactant
z		Number of electrons exchanged in red-ox reaction
Greek symbols		
Δ		Quantity variation (finite)
ε		Energy efficiency, dimensionless
η_I		Current efficiency, dimensionless
η_ω		Total efficiency, dimensionless
η^{HHV}		Hydrogen production efficiency
ξ		Ratio between parasitic power and net power consumed by the electrolyser due to the energy consumption by the auxiliaries, dimensionless
ρ	$g.cm^{-3}$	Density
Λ		Flow coefficient
τ		Response time

References

[1] FUEL CELLS AND HYDROGEN JOINT UNDERTAKING (FCH2JU); https://www.fch.europa.eu/projects/knowledge-management

[2] Tsotridis G. and Pilenga A., EU harmonised terminology for low-temperature water electrolysis for energy-storage applications, EUR 29300 EN, Publications Office of the European Union, Luxembourg, 2018, ISBN 978-92-79-90387-8, doi:10.2760/138987, JRC112082

[3] Lettenmeier, P., Wang, R., Abouatallah, R. et al. Low-Cost and Durable Bipolar Plates for Proton Exchange Membrane Electrolyzers. Sci Rep 7, 44035 (2017) doi:10.1038/srep44035

[4] Hany A. El-Sayed, Alexandra Weiß, Lorenz F. Olbrich, Garin P. Putro, and Hubert A. Gasteiger "OER Catalyst Stability Investigation Using RDE Technique: A Stability Measure or an Artifact?", J. Electrochem. Soc., 2019 volume 166, issue 8, F458-F464

[5] A. Villagra, P. Millet, An analysis of PEM water electrolysis cells operating at elevated current densities, Int. J. Hydrogen Energy, 44(20) (2019) 9708-9717. DOI: https://doi.org/10.1016/j.ijhydene.2018.11.179

[6] V. Schroeder, K. Holtappels, "Explosion characteristic of hydrogen-air and hydrogen-oxygen mixtures at elevated pressures", BAM.http://conference.ing.unipi.it/ichs2005/Papers/120001.pdf

[7] T. Malkow, A. Pilenga, G. Tsotridis, and G. De Marco, EU harmonised polarisation curve test method for low-temperature water electrolysis, EUR 29182 EN, Publications Office of the European Union, Luxembourg, 2018, ISBN 978-92-79-81992-6, doi:10.2760/324006, JRC104045.

[8] T. Malkow, G. De Marco, G. Tsotridis, EU harmonised cyclic voltammetry test method for low-temperature water electrolysis single cells, EUR 29285 EN, Publications Office of the European Union, Luxembourg, 2018, ISBN 978-92-79-89871-6, doi:10.2760/140687, JRC111151

[9] T. Malkow, A. Pilenga, G. Tsotridis, EU harmonised test procedure: electrochemical impedance spectroscopy for water electrolysis cells, EUR 29267 EN, Publications Office of the European Union, Luxembourg, 2018, ISBN 978-92-79-88739-0, doi:10.2760/8984, JRC107053

[10] Deliverable reports "Testing protocols for electrolyser qualification " D2.4 and D2.5 v.1f (03.07.2020) – Project FCH2JU 735485.
DOI: https://doi.org/10.5281/zenodo.3937273

[11] ENTSO-E Network Code on Load-Frequency Control and Reserves (28.06.2013)

[12] ENTSO-E Supporting Document for the Network Code on Load-Frequency Control and Reserves (28.06.2013)

[13] Deliverable report "Standardized qualifying tests of electrolysers for grid services Electrical grid service catalogue for water electrolyser" D1.1 (27.1.2017)
Project FCHJU 735485 – QualyGridS http://www.qualygrids.eu/

[14] Deliverable report "Protocols for characterisation of active components" D2.1 Project FCHJU 300081 Electrohypem

[15] P. Lettenmeier, Efficiency – Electrolysis, January 2019, Article No. SICM-T10001-00-7400

[16] C. Rozain, P. Millet, Electrochimica Acta 131 (2014) 160-167

[17] Schroeder, V., Sicherheitstechnische Untersuchungen fur die Hochdruck-wasserelektrolyse zur Speicherung regenerative Energie, Report No. VH2226, BAM Berlin, 2002]

[18] 3M, Lewinski KA, van der Vliet D, Luopa SM. NSTF advances for PEM electrolysis - the effect of alloying on activity of NSTF electrolyzer catalysts and performance of NSTF based PEM electrolyzers. ECS Trans 69 (17) (2015) 893–917

[19] Ayers K. E., Anderson E. B., Capuano C., Carter B., Dalton L., Hanlon G., et al. Research advances towards low cost, high efficiency PEM electrolysis. ECS Trans 33 (2010) 3–15

[20] ACS Appl. Energy Mater., 2019, 2, 7903-7912

[21] J.M. Taylor, Thermoplastic composites for polymer electrolyte membrane fuel cell bipolar plates, in Chemical engineering. 2006, Waterloo: Waterloo.

[22] Pollet B.G., Let's not ignore the ultrasonic effects on the preparation of fuel cell materials, 2014, Electrocatalysis, 5, 4, 330, 343

[23] Pollet B.G., Goh J.T.E., The importance of ultrasonic parameters in the preparation of fuel cell catalyst inks, 2014, Electrochimica Acta, 128, 292, 303

[24] M. Wang, J.H. Park, S. Kabir, K.C. Neyerlin, N.N. Kariuki, H. Lv, V.R. Stamenkovic, D.J. Myers, M. Ulsh, S.A. Mauger, Impact of Catalyst Ink Dispersing Methodology on Fuel Cell Performance Using in-Situ X-ray Scattering, ACS Appl. Energy Mater.2 (2019) 6417–6427. doi:10.1021/acsaem.9b01037

[25] Noga Ziv, Dario R. Deckel, A practical method for measuring the true hydroxide conductivity of anion exchange membranes, Electrochemistry Communications 88 (2018) 109-113

[26] Malkow K T, Pilenga A, Blagoeva D; EU harmonised terminology for hydrogen generated by electrolysis; EUR 30324 EN; Publications Office of the European Union, Luxembourg, 2020; ISBN 978-92-76-21041-2; doi:10.2760/293538; JRC120120.

[27] C. I. Bernäcker et al, Powder Metallurgy Route to Produce Raney®-Nickel Electrodes for Alkaline Water Electrolysis, 2019 J. Electrochem. Soc. 166 F357A, https://doi.org/10.1149/2.0851904jes

[28] C. Lamy, P. Millet "A critical review on the definitions used to calculate the energy efficiency coefficients of water electrolysis cells working under near ambient temperature conditions", Journal of Power Sources, 447 (2020) 227350; https://doi.org/10.1016/j.jpowsour.2019.227350

ANIONE project website https://anione.eu/

CHANNEL project website https://www.sintef.no/projectweb/channel-fch/

ELYGRID project website http://www.elygrid.com/

ELYNTEGRATION project website http://elyntegration.eu/

HPEM2GAS project website https://hpem2gas.eu/

NEPTUNE project website https://www.neptune-pem.eu/en/

NEXPEL project website https://www.sintef.no/projectweb/nexpel/

NOVEL project website https://www.sintef.no/projectweb/novel/

NEWELY project website https://newely.eu/project/fch-ju/

A. S. Aricò, V. Baglio, N. Briguglio, G. Maggio and S. Siracusano "Proton Exchange Membrane Water Electrolysis" in "Fuel Cells : Data, Facts and Figures" D. Stolten,R. C. Samsun and N. Garland Editors, 2016 Wiley-VCH Verlag GmbH & Co. KGaA.

A. S. Aricò, S. Siracusano, N. Briguglio, V. Baglio, A. Di Blasi, V. Antonucci, "Polymer electrolyte membrane water electrolysis: status of technologies and potential applications in combination with renewable power sources" Journal of Applied Electrochemistry, 2013, 43, 107-118.

I. Vincent, D. Bessarabov; "Low-cost hydrogen production by anion exchange membrane electrolysis: A review "Renewable and Sustainable Energy Reviews 81 (2018) 1690–1704; http://dx.doi.org/10.1016/j.rser.2017.05.258

Maximilian Schalenbach et al "Acidic or Alkaline? Towards a New Perspective on the Efficiency of Water Electrolysis " 2016, J. Electrochem. Soc. 163 F3197

Ganley, J. C. (2009). "High temperature and pressure alkaline electrolysis" International Journal of Hydrogen Energy, 34(9), 3604–3611

Varcoe J.R., Slade R.C.T. and How Yee E.L. (2006) "An Alkaline Polymer Electrochemical Interface: A breakthrough in application of alkaline anion-exchange membranes in fuel cells", Chem. Commun., 1428

R.L. LeRoy, C.T. Bowen, D.J. Leroy "The Thermodynamics of Aqueous Water Electrolysis", J. Electrochem. Soc., 127 (1980) 1954

R. Hanke-Rauschenbach, B. Bensmann, P. Millet "Compendium of Hydrogen Energy", Volume 1: Hydrogen Production and Purification, Chapter 7: Hydrogen production using high-pressure electrolyzers, Woodhead, 2015

Allidieres L et al., "On the ability of PEM water electrolysers to provide power grid services", International Journal of Hydrogen Energy, https://doi.org/10.1016/j.ijhydene.2018.11.186

Supporting Document on Technical Requirements for Frequency Containment Reserve Provision in the Nordic Synchronous Area, 2017, ENTSO-E AISBL

D. Bessarabov, H. Wand, H. Li, N. Zhao "PEM water Electrolysis for hydrogen production: Principles and Applications", CRC Press (2015)

PEM Water Electrolysis, Volume 1, D. Bessarabov & P. Millet, 2018, Hydrogen Energy and Fuel Cells Primers, Ed. B.G. Pollet, Elsevier Academic Press, ISBN: 9780128111451.

PEM Water Electrolysis, Volume 2, D. Bessarabov & P. Millet, 2018, Hydrogen Energy and Fuel Cells Primers, Ed. B.G. Pollet, Elsevier Academic Press, ISBN: 9780081028308.

S. Siracusano, V. Baglio, N. Van Dijk, L. Merlo, A. S. Aricò, Appl Energy (2016), http://dx.doi.org/10.1016/j.apenergy.2016.09.011

Electricity balancing: COMMISSION REGULATION (EU) 2017/2195 of 23 November 2017 https://www.entsoe.eu/network_codes/eb/

Emergency and restoration: COMMISSION REGULATION (EU) 2017/2196 of 24 November 2017. https://www.entsoe.eu/network_codes/er/

Establishing a guideline on electricity transmission system operation: Commission Regulation (EU) 2017/1485 of 2 August 2017

https://www.cobaltinstitute.org/critical-raw-material.html

'Test protocol for accelerated *in situ* degradation of alkaline water electrolysis under dynamic operation conditions', presentation 15.03.2018, EHEC 2018

F.N. Büchi, 'Cell Performance Determining Parameters in High Pressure Water Electrolysis'. http://dx.doi.org/10.1016/j.electacta.2016.06.120

K.W. Harrison, R. Remick, and G.D. Martin, A. Hoskin "Hydrogen Production: Fundamentals and Case Study Summaries".
https://www.nrel.gov/docs/fy10osti/47302.pdf

T.G. Douglas, A. Cruden, D. Infield "Development of an ambient temperature alkaline electrolyser for dynamic operation with renewable energy sources", international journal of hydrogen energy 38 (2013) 723 -739,
http://dx.doi.org/10.1016/j.ijhydene.2012.10.071

H. A. Miller, K. Bouzek, J. Hnat, S. Loos, C. I. Bernäcker, T. Weißgärber, L. Röntzsch and J. Meier-Haack, "Green hydrogen from anion exchange membrane water electrolysis: a review of recent developments in critical materials and operating conditions". Sustainable Energy Fuels, 2020, 4, 2114. DOI: 10.1039/C9SE01240K

Zhenye Kang, Gaoqiang Yang, Jingke Mo, Shule Yu, David A. Cullen, Scott T. Retterer, Todd J. Toops, Michael P. Brady, Guido Bender, Bryan S. Pivovar, Johney B. Green, Feng-Yuan Zhang, "Developing titanium micro/nano porous layers on planar thin/tunable LGDLs for high-efficiency hydrogen production", International Journal of Hydrogen Energy, Volume 43, Issue 31, 2018, Pages 14618-14628, https://doi.org/10.1016/j.ijhydene.2018.05.139

Effect of flow-field pattern and flow configuration on the performance of a polymer-electrolyte membrane water electrolyzer at high temperature,
https://doi.org/10.1016/j.ijhydene.2018.02.171

Source: Mathematical modeling of high-pressure PEM water electrolysis,
https://doi.org/10.1007/s10800-009-0031-z

Effect of flow regime of circulating water on a proton exchange membrane electrolyzer,
https://doi.org/10.1016/j.ijhydene.2010.06.103

List of abbreviations and definitions

AC	Alternating Current
AEM	Anion Exchange Membrane
AES	Atomic Emission Spectroscopy
AFM	Atomic Force Microscopy
ALT	Accelerated Life Tests
AST	Accelerated Stress Test
ASTM	American Society for Testing and Materials International
Avg	Average
BET	Brunauer-Emmett-Teller surface area measurement
BPP	BiPolar Plate
BoP	Balance of Plant
BoT	Beginning of Test
BoL	Beginning of Life
Bpp	Bubble point pressure
CCM	Catalyst Coated Membrane
CCE	Catalyst Coated Electrode
CV	Cyclic Voltammetry
DC	Direct Current
DMA	Dynamic Mechanical Analysis
ECSA	Electrochemical Surface Area
EDX	Energy dispersive X-ray spectroscopy
EIS	Electrochemical Impedance Spectroscopy
EoT	End of Test
EoL	End of Life
EW	Equivalent Weight
EXAFS	Extended X-ray Absorption Fine Structure
FEG SEM-EDX	Field Emission Gun-Scanning Electron Microscope Energy Dispersive X-Ray Analysis
FCH2JU	Fuel Cell and Hydrogen Joint Undertaking
FTIR	Fourier Transformed Infrared Analysis
HER	Hydrogen Evolution Reaction
HFR	High Frequency Resistance
HHV	Higher Heating Value, expressed in $J.mol^{-1}$
HW	Hardware
ICP-MS	Inductively Coupled Plasma Mass Spectrometry

IEC	Ion Exchange Capacity
KPI	Key Performance Indicator
LHV	Lower Heating Value, expressed in $J.mol^{-1}$
LEL	Lower Explosive Limit, expressed in %
LWD	Laboratory-World Degradation
MEA	Membrane Electrode Assembly
MD	Machine Direction
MS	Mass spectrometry
Micro-CT	X-ray micro computed tomography
NT	Neutron Transmission
OCP	Open Circuit Potential
OEM	Original Equipment Manufacturer
OER	Oxygen Evolution Reaction
PEM	Proton Exchange Membrane
PFSA	Perfluorosulphonic Acid
PGM	Platinum Group Metal
PSA	Pressure Swing Absorption
PTL	Porous Transport Layer
PtP	Power to Power
PtT	Power to Transport
PtX	Power to chemical feedstock
RDE	Rotating Disk Electrode
RES	Renewable Energy Sources
RH	Relative Humidity
RWD	Real-World Degradation
SATP	Standard Ambient Temperature and Pressure conditions ($T = 298.15$ K and $p = 10^5$ Pa)
SEC	Specific Energy Consumption
SEM	Scanning Electron Microscopy
SHE	Standard Hydrogen Electrode
SIMS	Secondary Ion Mass Spectroscopy
SF	Stability Factor
SP	System Power
TC	Thermal Conductivity
tn	Thermo neutral
TEM	Transmission Electron Microscope

Tg	Glass Transition Temperature
TGA-DSC	Thermogravimetric-Differential Scanning Calorimetry
TIP	Test Input Parameter
TM	Transition Metals
TOP	Test Output Parameter
TSA	Temperature Swing Absorption
TSO	Transmission System Operator
UEL	Upper Explosion Limit
UF_w	Water Utilization factor
XANES	X-ray Absorption Near-Edge Structure
XPS	X-ray Photoelectron Spectroscopy
XRD	X-ray Diffraction
XRF	X-ray Fluorescence

List of boxes

List of figures

List of tables

Annex A. *Ex-situ* analysis additional information

Ex-situ physico-chemical analysis pre- and post-operation by XRD, XRF, TEM, and SEM-EDX may be carried out to elucidate structural, chemical, surface and morphology changes in the catalysts.

physico-chemical analyses are carried out by:

- X-ray diffraction (XRD) to determine structural and crystallite size changes: catalysts are scraped from the catalyst coated membrane assembly and corresponding powders are distributed over an amorphous sample holder. Crystalline phases are identified vs. the JPDS cards; crystallite size changes are determined from the peak broadening using the Levenberg–Marquardt algorithm for peak fitting and the Debye–Scherrer equation for quantification.

Crystallite size is reported as d_{XRD} / nm.

- X-ray fluorescence (XRF) is carried out to determine chemical modifications, e.g. in the IrRuOx composition (elemental analysis). The catalyst can be analysed after it is scraped from the CCM.

Chemical formulas are reported as "at. %" content of the elements

- Transmission electron microscopy (TEM) is carried out to determine any change in the mean particle size and particle size distribution (e.g. due to Ostwald ripening effects such as dissolution and reprecipitation): catalysts are scraped from the catalyst coated membrane assembly and powders are dispersed in isopropanol under ultrasonic agitation in a temperature controlled ultrasonic bath for very short periods of time to avoid catalyst deterioration (see [22-24. A few drops are deposited on Cu grid sample holders and analysed. At least 200 particles are counted in different regions.

Crystallite size is reported as d_{TEM} / nm.

- Scanning electron microscopy and energy dispersive analysis (FEG SEM-EDX) is carried out on the MEA without any further treatment to investigate morphological changes and chemical modifications, e.g. inclusion of catalyst particles in the membrane, Ostwald ripening effects (dissolution and re-precipitation), membrane thinning, catalytic layer thinning, particle agglomeration etc.

Annex B. Examples of *ex-situ* test procedures

This annex presents the testing procedures for **PEMWE membrane** from deliverable 2.1 Electrohypem [14]

REF	TESTS
B1	Measurement of Membrane Ion Exchange Capacity and Equivalent Weight
B2	Membrane Hydrolytic Stability Test
B3	Membrane Chemical Stability Fenton's test
B4	In-Plane ionic Conductivity and/or Through Plane
B5	Measurement of Membrane Thickness and Uniformity
B6	Water Uptake and Linear Expansion
B7	Membrane Permeability to Hydrogen Gas
B8	Thermo-Gravimetric Testing
B9	Tensile testing

B1: Measurement of membrane ion-exchange capacity and equivalent weight

Summary

A base titration is used to obtain the number of equivalent moles of sulfonic acid groups within the polymer and the results used to calculate the ion-exchange capacity and equivalent weight of the membrane.

MEMBRANE CONDITIONING	1	Treat samples with 0.1M sulphuric acid for 1 hr, at 30 °C.
	2	Rinse the samples thoroughly with water and then soak in water for 1 hr, at 30 °C.
	3	Dry the samples in a vacuum oven for 4 hrs, at 50 °C.
TEST CONDITIONS		Approximately 0.5 g of dried sample is required for the test.
	1	Weigh the dried sample and record the mass to 4 decimal points.
	2	Place the sample into 100 ml of 0.01M potassium hydrogen carbonate (aq) solution and leave to soak for 16 hrs, at room temperature.
	3	Titrate the potassium hydrogen carbonate soak solution against 0.01M hydrochloric acid and record the volume of hydrochloric acid required to neutralize the potassium hydrogen carbonate soak solution.
	4	Based upon at least three runs, determine the average volume of hydrochloric acid required to neutralize the potassium hydrogen carbonate soak solution.
	5	Calculate the concentration of the potassium hydrogen carbonate soak solution following contact with the membrane.
	6	Calculate the difference between the concentrations of the potassium hydrogen carbonate solution before and after contact with the membrane, to obtain the equivalent number of moles of sulfonic acid groups in the membrane
	7	Using the number of moles of sulfonic acid groups in the membrane and the mass of the dry membrane, calculate the ion exchange capacity and equivalent weight of the membrane

B2: Membrane hydrolytic stability test

Summary

A section of the membrane is held in water at 95°C for 24 hours and the mass loss is determined from a comparison of dry mass before and after the test. The IEC of the specimen is then measured and compared to the standard value for the membrane.

MEMBRANE HYDROLYTIC TABILITY TEST		
Membrane Conditioning		Measurements are performed with **membrane conditioned at 23 °C, 50 % RH**.
Specimen size		4 cm x 4 cm
Test Conditions		Immersed 24 hr in 50 ml Type 1 (ASTM D1193-91 Type II Standard) water. Water at 95 °C
		Dried in a vacuum oven at 50 °C for 4hr.
		Membrane mass measured before and after
Number of repeats		5

METRIC	FREQUENCY	TARGET
Mass Loss	After 24 hours	No target for monitoring
IEC change	After 24 hours	No target for monitoring

B3: Membrane chemical stability – Fenton's test

Summary

This test provides an indication of the oxidative chemical stability of the membrane. A section of the membrane is held in an aqueous solution of 3% H_2O_2 and 4ppm Fe^{2+} at 80 °C for 2 hours and the mass loss is determined from a comparison of dry mass before and after the test.

MEMBRANE HYDROLYTHIC STABILITY TEST		
Membrane Conditioning		Hydrate membrane according to standard hydration procedure, take sample from central area, dry gently under vacuum (500 ^{0}C for 4 hrs) and measure the mass
Specimen size		4 cm x 4 cm
Concentration of Hydrogen peroxide		3 % by weight
Concentration of Fe^{2+}		4 ppm by weight
Test Conditions-Volume		50ml
Test Conditions-Temperature		80 °C
Test Conditions-Time		2 hrs
Test Conditions		Wash the membrane throughout in Type 1 water (ASTM D1193-91 Type II Standard), before drying the membrane under vacuum at 500 °C for 4 hrs. Measure the mass.
Mass loss formula		Mass loss (%) = {($mass_{initial}$ – $mass_{after}$) / mass } x 100
Number of repeats		3

METRIC	CONDITIONS	TARGET
Mass Loss	Average of readings of mass loss to 4	No target for monitoring

B4: Measurement of in-plane ionic conductivity

Summary

Using a four-electrode conductivity clamp (e.g. the Bekk Tech BT-110 Conductivity Clamp) in-plane conductivity can be determined by applying a specific current across a linear strip of membrane and measuring the resulting voltage. Four electrodes are used in order to separate voltage drop due to ion transport from that due to any electrochemical reactions.

MEASUREMENT OF IN PLANE CONDUCTIVITY		
Pre-Conditioning		Membrane must be cleaned and hydrated prior the measurement and the conductivity clamp immersed in a beaker of Type 1 (ASTM D1193-91 Type II Standard) water.
Measurement technique ([1])		Four-electrode chronopotentiometry
Membrane sample size		At least 20 mm long and less than 17 mm wide
Water temperature		Controlled and recorded
Current		Appropriate current such that the voltage is between 0.01 and 1.0 V
Technique	1	To test whether the electrodes are making good electrical contact with the membrane and to determine the appropriate current:
	2	Apply a linear voltage sweep across the two outer electrodes
	3	Then in the four-electrode mode, apply the predetermined appropriate current for one minute to outer contacts or until a constant voltage is achieved, whichever is longer
	4	Measure voltage difference across inner electrodes
	5	Using the applied current and resulting voltage, the resistance of the sample of membrane can be calculated $R = V/I$
	6	From the resistance of the membrane sample and the known dimension of the sample, resistivity and conductivity can also be calculated

([1]) An alternative methode utilise electrochemical impedance spectroscopy (EIS) with an AC amplitude of 5 – 100 mV between the sense electrodes and under zero DC current (PEM) or under a certain DC current, e.g. 100 µA (AEM). AEM ionic conductivity measurements require a constant DC current to regenerate the AEM HO- conductivity of the poisoning effect of CO2 in air [25].

B5: Measurement of membrane thickness and uniformity

Summary

The thickness of a membrane specimen in dry, humidified or hydrated state is the arithmetic mean of the values obtained from at least three-dimensions measurements (see table for recommended number of measurements) taken at different points across a membrane specimen, using a calibrated micrometer screw gauge capable of measurement to the nearest 2.5 µm. The uniformity of a membrane specimen is indicated by the maximum and minimum of the range of the dimension measurements.

MEASUREMENT OF MEMBRANE THICKNESS AND UNIFORMITY		
Membrane Conditioning	1	Dry state: 23 °C ±2 °C, 50 % relative humidity
	2	Humidified state: As appropriate should be recorded
	3	Hydrated state: As appropriate should be recorded
Test Method	1	Prepare and condition each specimen as appropriate.
	2	Close the micrometer on an area of the specimen that has a similar dimension to the one to be measured, but is not one of the measurement positions.
	3	Observe this reading, and then open the micrometer approximately 100 µm beyond the expected reading and move the specimen to the measurement position.
	4	Close the micrometer at such a rate that the scale divisions may be counted easily as they pass the reference mark. This rate is approximately 50 µm/s.
	5	Continue the closing motion until contact with the specimen surface is just made as evidenced by the initial development of frictional resistance to movement of the micrometer screw. If using a micrometer fitted with a calibrated ratchet or friction thimble, continue the closing motion until the ratchet clicks three times or the friction thimble slips. Observe the indicated dimension.
	6	If required, correct the observed indicated dimension using a calibration chart and record the corrected dimension value.
	7	Move the specimen to another measurement position and repeat steps 2 -6.
	8	Make and record at least three-dimension measurements on each specimen (see table below for recommended measurements). **The arithmetic mean of all dimension values is the thickness of the specimen**

Specimen Dimensions (cm)	Specimen Area (cm^2)	Recommended Number of Measurements
5 x 5	25	5
10 x 10	100	9
15 x 15	225	16
20 x 20	400	25

FUNCTIONAL PROPERTIES	FREQUENCY	TARGET
Membrane Thickness (µm)	As required	No target for monitoring
Membrane Uniformity (µm)	As required	+/-10 % of the mean thickness

B6: Water uptake and linear expansion

Summary

The hydration of membranes could be characterised by comparing the weight and size of dry samples with that of hydrated samples. From these measurements, water uptake and dimensional change can be calculated.

WATER UPATKE and LINEAR EXPANSION		
Pre-Conditioning		The membrane should be dried in an oven to constant weight.
Measurement technique		A balance capable of measuring to 0.0001 g Calipers capable of measuring 0.01 mm
Membrane sample size		Approximately 20 mm x 10 mm.
Hydration temperature		30 °C, 60 °C and 90 °C
Technique	1	A minimum of three samples should be used for each test.
	2	The size and weight of pre-conditioned samples are determined
	3	The samples are then place in containers of deionised water and placed in an oven at the appropriate temperature for 24 hours
	4	After 24 hrs, the samples are removed from the oven and measurements of length and weight are taken
Analysis	5	% Water Update = {(hydrated mass – dry mass) / dry mass} x 100
	6	% Linear Expansion = {(hydration length – dry length) / dry length} x 100

FUNCTIONAL PROPERTIES	FREQUENCY	TARGET
Water Uptake	As required	No target for monitoring
Linear Expansion	As required	No target for monitoring

B7: Membrane permeability to hydrogen gas

Summary

The hydrogen crossover rate through the membrane is assessed via an electrochemical method at relevant temperatures and pressures. The membrane is assembled in a standard test cell with hydrogen flowing on one side of the membrane and water on the other side. A potentiostat is used to sweep the potential. The current resulting from the oxidation of molecular hydrogen is measured and used to calculate the hydrogen crossover rate.

MEMBRANE PERMEABILITY to HYDROGEN GAS		
Membrane Conditioning		Hydrate according to standard method
Temperature		Set as required, must be recorded and reported
Pressure		Set as required, must be recorded and reported
Voltage Range		100 mV to 400 mV
Scan Rate		2 mV/s
Test Method	1	Assemble the cell with potentiostat to control voltage and measure current. The anode acts as the reference and counter electrode and the cathode acts as the working electrode.
	2	Set the temperature and pressure as required
	3	Flow 100% of humidified hydrogen on anode (equiv. of 1.5 stoichiometry at 1 A/cm2) and de-aerated water on cathode (5 ml/min) to keep the membrane hydrated
	4	Sweep cathode potential from rest potential from 100 mV to 400 mV against anode at 2 mV/s
	6	Report crossover at 300 mV

FUNCTIONAL PROPERTIES	FREQUENCY	TARGET
Hydrogen crossover current	As required	<1.0 A/cm^2
Hydrogen crossover rate	As required	<0.07 ml/min/cm^2 hydrogen

There is also a potential step method which can be faster and more reliable – by interest see:
Evaluation of Hydrogen Crossover through Fuel Cell Membranes (wiley.com)

B8: Thermogravimetric testing

Summary

This test gives an indication of the chemical and thermal stability of the membrane

Thermogravimetric/DSC Testing		
Membrane Conditioning		Hydrate according to standard hydration procedure
Equipment		TA Instruments Q2000 DSC, Q500 TGA or similar
Atmosphere		Nitrogen / Air
Temperature range		25 °C to 900 °C
Heating ramp		2 °C/min
Logging Frequency		1 Hz
Number of repeats		3

FUNCTIONAL PROPERTIES	temperature	TARGET
Start of Thermal decomposition		No target for monitoring

Thermogravimetric/DSC Testing		
Membrane Conditioning		Hydrate according to standard hydration procedure
Equipment		TA Instruments Q800 DMA or similar
Atmosphere		Air
Temperature range		25 °C to 400 °C
Heating ramp		2 °C/min
Logging Frequency		1 Hz
Number of repeats		3

FUNCTIONAL PROPERTIES	temperature	TARGET
Glass Transition Temperature Tg		No target for monitoring

B9: Tensile Testing

Summary

This test gives an indication of the mechanical properties of the membrane and it is based on ASTM D882 - 09 Tensile Properties of Thin Plastic Sheeting. As the machine does not have an environmental chamber, the test will be performed submerged in a water bath.

MEMBRANE HYDROLYTIC TABILITY TEST		
Membrane Conditioning		Hydrate membrane according to standard hydration procedure
Equipment		Instron 3344 or similar
Stamp size		Dumbell shaped stamp similar to Type IV in ASTM D638-10. Width of narrow section = 6 mm Length of narrow section = 33 mm Gauge length = 25 mm Distance between the tabs = 65 mm Length overall = 115 mm Radius of fillet = 14 mm Outer radius = 25 mm
Initial Grip Separation		60 mm
Initial Strain Rate		0.5 mm/mm.min
Rate of Grip Separation		30 mm/min (Rate of Grip Separation = Initial Strain Rate x Initial Grip Separation)
Load cell		Suitable for material tested
Water bath temperature		23 °C ± 1°C
Number of repeats		5 (in each direction if the sample is anisotropic)

METRIC	FREQUENCY	TARGET
UTS (MPa to 3 significant figures)	As required	No target for monitoring
Elongation at break (% to 2 significant figures)	As required	No target for monitoring
Young's Modulus (MPa to 3 significant figures)	As required	No target for monitoring

Annex C. EU regulatory framework for equipment providing grid balancing services

The following legislative documents which touch upon the provision of grid balancing services as part of frequency control measures, are relevant for this report:

- Directive (EU) 2019/944, Directive on common rules for internal market for electricity
- Regulation (EU) 2019/943, Regulation on the internal market for electricity
- Commission Regulation (EU) 2017/1485: Establishing a guideline on electricity transmission system operation
- Commission Regulation (EU) 2017/2195: "establishing a guideline on electricity balancing"
- Network Code on Load-Frequency Control and reserves [12] developed by the European Commission, the Agency for the Cooperation of Energy Regulators (ACER), the European Network of Transmission System Operators for Electricity (ENTSO-E) and market participants
- ENTSO-E, "Supporting Document for the Network Code on Load-Frequency Control and Reserves", 2013, accessed Aug. 2017 http://www.acer.europa.eu/Official_documents/Acts_of_the_Agency/Annexes/ENTSO-E%E2%80%99s%20supporting%20document%20to%20the%20submitted%20Network%20Code%20on%20Load-Frequency%20Control%20and%20Reserves.pdf

LOAD FREQUENCY CONTROL PROCESS

Art 139.1 of Commission Regulation (EU) 2017/1485, points out that "*All TSOs of each synchronous area shall specify the load-frequency-control structure for the synchronous area [….]. Each TSO shall be responsible for implementing the load-frequency-control structure of its synchronous area and operating in accordance with it*".

The parameters defining the Frequency Quality art. 19 [11] are illustrated in Figure 45. The figure shows a disturbance event that generates a system imbalance reflected by a frequency change, the different action activation limits and the deployment over time of the different types of reserves, FCR, FRR, and RR. Regulatory requirements on frequency correction actions include frequency ranges as well as time durations in which the respective ranges should be reached. Limits on range and duration are therefore included in the pre-qualification requirements by the TSOs.

Figure 45. Frequency control parameters and cascade actions following a disturbance event

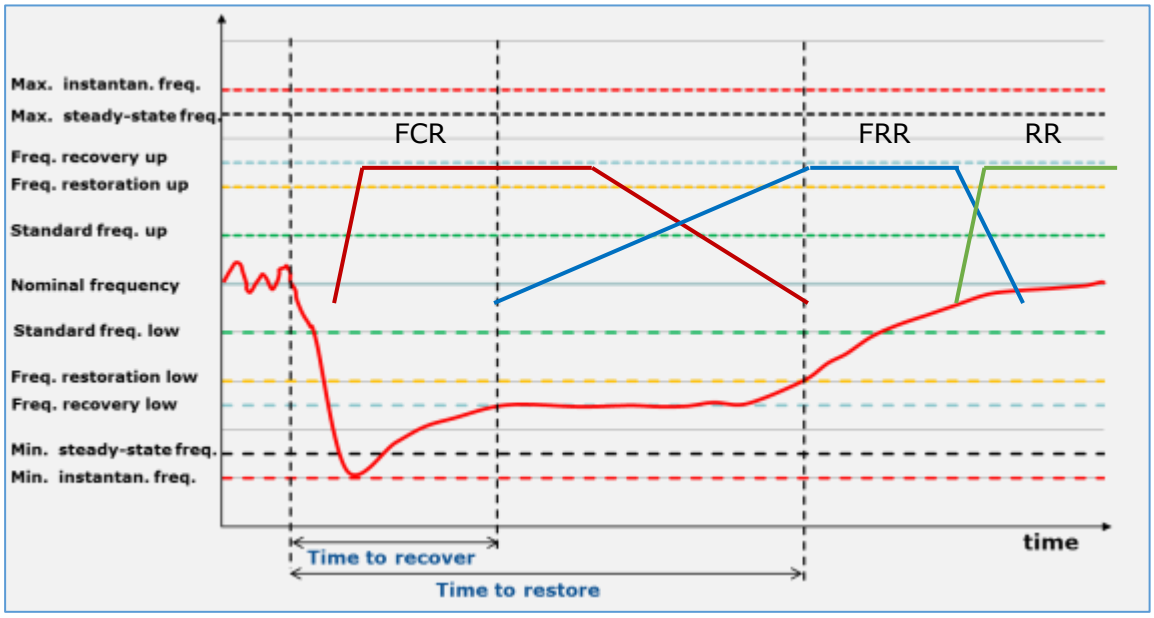

Source: JRC, 2020

The Network Code Electricity Balancing article 29.5 [11] provides common requirements for equipment to be used for frequency control service. These include capacity, speed of action, ability of ramping, and ability of offering a reliable dynamic/non-dynamic response over designated service periods. Figure 46 shows a generic profile applicable to the operation of the three types of frequency control reserves FCR, FRR and RR. Whereas the Figure 46 shows reserve activation through a positive ramp, negative ramp activation may also be needed.

Figure 46. Standard description of any balancing equipment

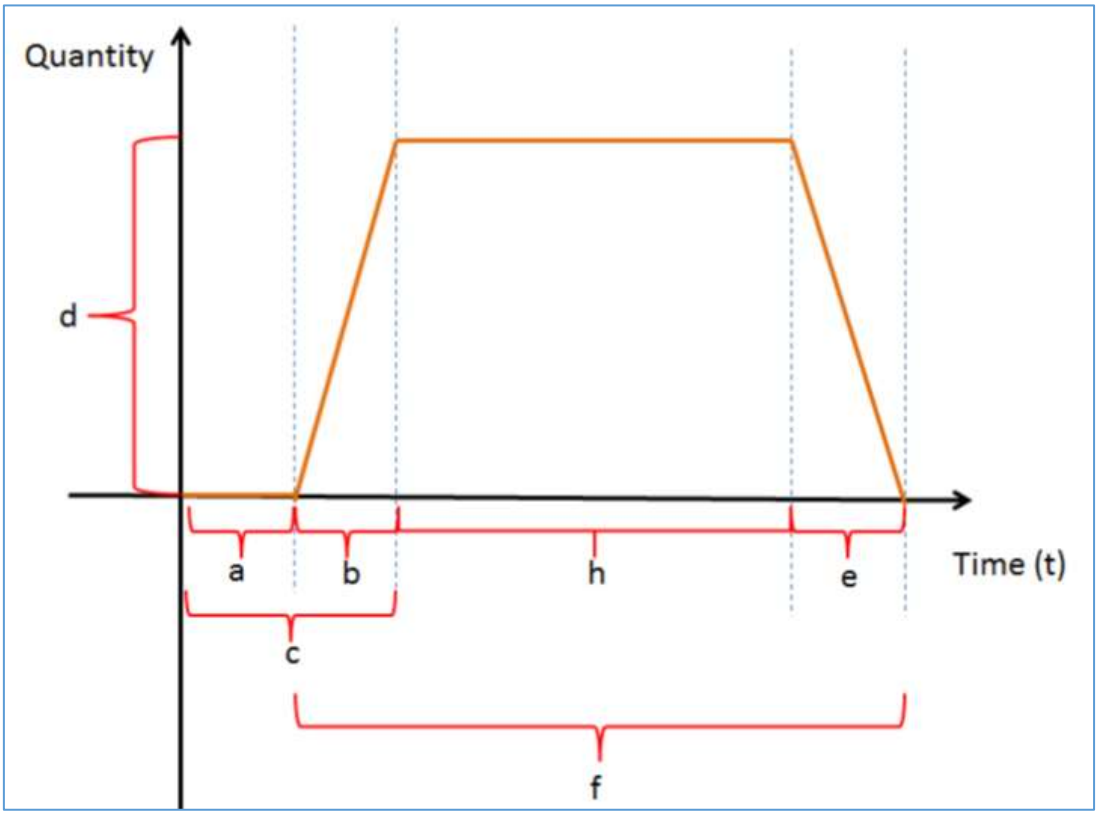

Source: QualyGgridS, [13]

(a) preparation period; (b) ramping period;(c) = (a)+(b) full activation time;(d) minimum and maximum quantity;(e) deactivation period; (f) = (b)+(h)+(e) full delivery period; (h) minimum and maximum duration of delivery period

GETTING IN TOUCH WITH THE EU

In person

All over the European Union there are hundreds of Europe Direct information centres. You can find the address of the centre nearest you at: https://europa.eu/european-union/contact_en

On the phone or by email

Europe Direct is a service that answers your questions about the European Union. You can contact this service:

- by freephone: 00 800 6 7 8 9 10 11 (certain operators may charge for these calls),

- at the following standard number: +32 22999696, or

- by electronic mail via: https://europa.eu/european-union/contact_en

FINDING INFORMATION ABOUT THE EU

Online

Information about the European Union in all the official languages of the EU is available on the Europa website at: https://europa.eu/european-union/index_en

EU publications
You can download or order free and priced EU publications from EU Bookshop at: https://publications.europa.eu/en/publications. Multiple copies of free publications may be obtained by contacting Europe Direct or your local information centre (see https://europa.eu/european-union/contact_en).

KJ-NA-30752-EN-N

The European Commission's science and knowledge service

Joint Research Centre

JRC Mission

As the science and knowledge service of the European Commission, the Joint Research Centre's mission is to support EU policies with independent evidence throughout the whole policy cycle.

EU Science Hub
ec.europa.eu/jrc

@EU_ScienceHub

EU Science Hub - Joint Research Centre

EU Science, Research and Innovation

EU Science Hub

Publications Office of the European Union

doi:10.2760/58880

ISBN 978-92-76-39266-8